NOVA SCHOOL OF SCIENCE & TECHNOLOGY

DEPARTMENT OF PHYSICS

LUÍS ABÍLIO DE SOUSA FONSECA MACHADO E CUNHA

BSc in Biomedical Engineering

USING MUSCULOSKELETAL MODELING TO ASSESS MUSCLE FUNCTION AND GAIT ASYMMETRY AFTER A STRAYER PROCEDURE APPLIED TO A CHILD WITH CEREBRAL PALSY

NOVA University Lisbon
March, 2023

NOVA SCHOOL OF SCIENCE & TECHNOLOGY

DEPARTMENT OF PHYSICS

USING MUSCULOSKELETAL MODELING TO ASSESS MUSCLE FUNCTION AND GAIT ASYMMETRY AFTER A STRAYER PROCEDURE APPLIED TO A CHILD WITH CEREBRAL PALSY

LUÍS ABÍLIO DE SOUSA FONSECA MACHADO E CUNHA

BSc in Biomedical Engineering

Adviser: António Veloso
Full Professor, University of Lisbon

Co-adviser: Cláudia Quaresma
Assistant Professor, NOVA University Lisbon

NOVA University Lisbon
March, 2023

Using musculoskeletal modeling to assess muscle function and gait asymmetry after a Strayer procedure applied to a child with cerebral palsy

This document was created with the (pdf/Xe/Lua)LaTeX processor and the NOVAthesis template (v6.9.5) [92].

Agradecimentos

Em primeiro lugar, gostaría de agradecer ao Professor Doutor António Veloso pela oportunidade de realizar a tese sobre a sua orientação, o que me proporcionou uma ótima experiência de aprendizagem. Em segundo lugar, queria agradecer à professora Cláudia Quaresma pela disponibilidade e atenção que sempre demonstrou.

Um agradecimento muito especial ao Doutor Basílio Gonçalves e Engenheiro Rodrigo Mateus pelo acompanhamento que fizeram ao longo deste último ano. Agradeço toda a disponibilidade, boa disposição, e partilha de conhecimento que se revelou fundamental para o sucesso e concretização desta tese.

A finalização desta dissertação marca o final de 5 cinco anos de vivências, aprendizagens e crescimento no campus da Faculdade de Ciências e Tecnologia. Agradeço a todos os professores e colegas que me marcaram e fizeram desta uma experiência inesquecível.

Aos meus amigos agradeço por toda a amizade, carinho e apoio precioso que me deram ao longo da minha vida académica. Ao meu "irmão de tese" João Ortiz, um especial obrigado por todos momentos de cumplicidade partilhados. Aos meus colegas de casa, Rui André, João Silva e António Dias, agradeço todos os momentos de brincadeira, amizade e histórias por contar ao longo destes 5 anos. Para as minhas madrinhas de faculdade, Inês e Maria Inês, um enorme obrigado por serem os meus pilares e por me guiarem durante o meu percurso académico. Para os meus afilhados, Luís, Marta, Miguel e Catarina, foi e sempre será um orgulho ser vosso padrinho.

Por último, o meu maior agradecimento vai para a minha família que sempre me incentivou e apoiou ao longo deste percurso. Gostaria de dedicar esta tese aos meus pais, que me apoiaram incondicionalmente por todas as peripécias e por celebrarem ao meu lado cada conquista e etada superada.

Abstract

Cerebral palsy (CP) is a common group of neuromotor disorders with symptoms appearing during childhood. Children with CP often undergo orthopedic surgeries and treatment plans depending on the gait pattern and its severity. Jump gait is a gait pattern present in bilateral spastic CP and is characterized by a combination of ankle equinus, accentuated hip and knee flexion, lumbar lordosis, and anterior pelvis tilt. The modified Strayer procedure is a surgical intervention to treat equinus in ambulatory children with CP and is often accompanied by botulinum toxin type A (BTX) injections to aid in spasticity reduction. Musculoskeletal modeling is a promising approach to indirectly estimate muscle function, including muscle force, and muscle induced accelerations. Gait asymmetry is often studied as it is associated with pathological gait. This study aimed to analyze the improvements in gait function in one child with CP following corrective surgery for jump gait. Gait asymmetry, muscle forces and contributions to the center of mass accelerations during walking were assessed before, one and two years after surgery. Furthermore, comparison with typically developed children was also performed. Three-dimensional marker coordinates and ground reaction forces (GRF) during walking were recorded and used as input for musculoskeletal simulations using OpenSim. Two years post-surgery, gait asymmetry reduced to levels similar to or lower than unimpaired gait. Overall joint kinematics improved, although the increase in dorsiflexion was not enough to achieve heel strike at first contact in the lower limb submitted to surgery. Estimates of muscle forces showed the child with CP relied more on proximal muscles to walk, mainly the vasti and hamstrings, before and after surgery. Soleus muscle forces increased following surgery, becoming the primary contributor to vertical support from the plantarflexors. Suggestions were made for treatment plans and for maintaining surgical improvements, such as strengthening of weakened muscles.

Keywords: Jump gait, Cerebral palsy, Strayer procedure, Musculoskeletal modeling, Computed Muscle Control, Induced Acceleration Analysis

Resumo

Paralisia cerebral (PC) é um grupo de perturbações neuromotoras cujos sintomas aparecem durante a infância. Crianças com PC são regularmente submetidas a cirurgias ortopédicas e planos de tratamento de acordo com o padrão de marcha e grau de severidade. Marcha em salto é um padrão de marcha presente em PC espástica bilateral caracterizada por pé equino, flexão acentuada do joelho e anca, lordose lombar, e inclinação pélvica anterior. O procedimento modificado de Strayer é uma cirurgia comum para tratar pé equino em crianças com PC em contexto ambulatório e é normalmente acompanhada por injeções de toxina botulínica. Modelação musculoesquelética é uma abordagem que permite estimar, indiretamente, as forças e acelerações induzidas musculares. Assimetria na marcha é frequentemente estudada por estar associada a uma marcha patológica. O objetivo deste trabalho consiste em estudar as melhorias na marcha de uma criança com PC após cirurgia. Assimetria da marcha, forças e contribuições musculares para a aceleração do centro de massa foram avaliadas antes, um e dois anos após cirurgia. Além disso, foi feita a comparação com marcha saudável. Foram gravadas as coordenadas tridimensionais dos marcadores e forças de reação do solo para as simulações musculoesqueléticas através do OpenSim. Dois anos após cirurgia, a assimetria melhorou para níveis semelhantes ou inferiores aos da marcha saudável. Em termo gerais, a cinemática melhorou, porém, apesar da capacidade de dorsiflexão ter aumentado, o calcanhar não estabelece o primeiro contacto no membro inferior submetido a cirurgia. Resultados das forças musculares mostram uma maior dependência em músculos proximais na criança com PC, principalmente o vasto e os isquiotibiais, antes e após cirurgia. As forças musculares do solear aumentaram após cirurgia, tornando-se o principal plantarflexor a contribuir para o suporte. Fortalecimento de músculos enfraquecidos foi um dos planos de tratamento sugeridos para preservação das melhorias obtidas pela cirurgia.

Palavras-chave: Marcha em salto, Paralisia cerebral, Procedimento de Strayer, Modelação musculoesquelética, Otimização dinâmica, Análise de acelerações induzidas

Contents

List of Figures

List of Tables

Glossary

agonist Main muscle that contracts to promote movement. 10

antagonist Muscles that produce an opposing movement to the agonist muscle. 10

athetosis Movement dysfunction. It's characterized by involuntary writhing movements. 10

clonus Involuntary and rhythmic muscle contractions. 9

dysarthria Muscles used for speech are weak and control over them becomes difficult. 10

dystonia Movement disorder in which muscles contract involuntarily, causing twisting or repetitive movements. 10, 12

hyperreflexia Overactive or overresponsive reflexes. 9

osteotomy Surgical procedure involving the cutting and re-positioning of a bone 12

spasticity Abnormal muscle tightness due to prolonged muscle contraction. 9

Abbreviations

AFO Ankle Foot Orthosis 15, 16

BOPS Batch OpenSim Processing Scripts 36
BTX Botulinum toxin type A iv, 2, 3, 11, 15, 69, 70, 72, 73, 75

CMC Computed Muscle Control viii, x–xii, 36, 43–45, 55, 56, 60, 69, 76, 105–112
COM Center of mass ix, x, 3, 5, 7, 13, 18, 38, 60–68, 71–73, 75, 114, 115
CP Cerebral Palsy iv, viii–x, 1–7, 9–12, 14–17, 19, 32, 33, 47–53, 55, 56, 59–61, 68–77, 113

DBS Deep brain stimulation 12
DOF Degree of freedom ix, 8, 37, 41, 47, 49, 52–55, 71

EMG Electromyography x, 4, 6, 32–35, 45, 60, 69, 76, 111, 112

GGA Global Gait Asymmetry ix, 8, 47, 52, 53, 71
GMFCS Gross Motor Functioning Classification System 10, 12, 32
GRF Ground Reaction Forces iv, x, 4, 32–35, 41, 45, 46, 54, 60, 68, 72, 76, 112

IAA Induced Acceleration Analysis viii, x, 5, 36, 45–47, 60, 112
ID Inverse Dynamics xi, 40, 41, 43, 49, 96–98
IK Inverse Kinematics 40–42, 49

MOToNMS matlab MOtion data elaboration TOolbox for NeuroMusculoSkeletal applications 36
MRI Magnetic Resonance Imaging 7, 39

PC Paralisia cerebral v

RRA Residual Reduction Algorithm viii, xi, 36, 41–43, 45, 53, 55, 96–104

SDR Selective dorsal rhizotomy 11, 12, 16

SEMLS Single-event Multilevel Surgery 12, 16

1 Introduction

The research work described in this dissertation was carried out in accordance with the norms established in the ethics code of Universidade Nova de Lisboa. The work described and the material presented in this dissertation, with the exceptions clearly indicated, constitute original work carried out by the author.

1.1 Motivation

The ability to move and exercise autonomously depends on appropriate psychological, physiological, and immunological functions [99]. Freedom of movement is especially important in the younger age groups due to their high activity, which makes movement disorders, such as CP, have a negative impact on the overall physical and social development of children. CP encompasses a variety of permanent disorders that affect posture and movement, caused by non-progressive injury to the infant or fetal brain [58]. The incurable damage to the developing brain often leads to secondary musculoskeletal problems along with disturbances in communication, cognition, perception, and others [58]. CP is the most common chronic physical disability in childhood, being present in every 2-3 out of 1000 live births worldwide [25]. However, there is a variety of risk factors that can increase the probability of CP development in infants, such as low birth weight and premature birth [140], [73]. Despite CP severity having a major impact on life expectancy, the majority of children with CP are expected to live well into adulthood [73].

Gait abnormalities are often present in different syndromes of CP, increasing the need for improved diagnosis and treatment techniques [76]. In order to study gait deviations, gait analysis is used to provide quantitative data regarding the degree of functional restrictions, their development over time, and the most efficient rehabilitation plan [26]. Gait analysis implementation in a clinical environment has been growing over the last decades and has been included in CP management and surgical decision-making, proving to be a valuable asset [82]. A relevant parameter to assess through gait analysis is gait symmetry. The presence of asymmetry in the lower limbs during gait is a common trait in CP and is often associated with pathological gait due to being more unstable, less effective

and increased likelihood of musculoskeletal lesion [56]. On that account, an increase in gait symmetry can be seen as an indicator of successful treatment or intervention.

Protocols of gait analysis often use motion capture procedures and force platforms to obtain kinematic data and calculate net joint moments. However, external measurements such as angles and net moments do not supply information regarding internal forces, such as muscle and joint reaction forces [91]. Therefore, computational approaches, such as musculoskeletal modeling, are continuously being developed to provide the necessary tools to make these estimates in an accurate manner [2]. Although direct methods could also estimate internal forces, these involve impractical and highly invasive measurement techniques, such as surgical procedures to place measurement devices [83], favoring indirect and non-invasive methods, such as musculoskeletal modeling. Therefore, the implementation of models capable of reproducing the structure and dynamics of the musculoskeletal system, is a dependable and promising way to provide insight into the effects of surgical interventions regarding muscle function and coordination.

Jump gait is a common gait pattern in patients with diplegic CP. This gait pattern is defined by ankle equinus, excessive hip and knee flexion, increased anterior pelvis tilt and accentuated lumbar lordosis [8]. Moreover, jump gait is associated with spasticity in the hip flexors, hamstrings, and triceps surae [141]. Jump gait management in children varies according to their age and includes treatments for spasticity and contractures. In the setting of this work, injections of BTX for spasticity management, and the modified Strayer procedure for equinus correction have a central role. It is important to note that, for ambulatory CP children, equinus is the most common deviation [123]. The modified Strayer is a very popular procedure for equinus management and consists of the complete release of the gastrocnemius alongside the lengthening of the soleus fascia. While most children submitted to these interventions have positive and successful outcomes, there are cases where overcorrection and recurring equinus contracture occur, which might lead to foot deformities, other patterns of CP gaits, and revision surgery [165], [47]. To the author's knowledge, the use of musculoskeletal modeling to assess muscle function after a modified Strayer procedure together with BTX injections has not been used.

In order to understand gait deviations in pathological gait, a common approach is to compare with data from healthy subjects with unimpaired gait. This is because surgical interventions aim to normalize muscle function. Furthermore, comparing pathological and healthy gait patterns provides insight into discerning gait deviations as they are a combination of neurological injury (i.e., primary deviations), abnormal growth as consequences from these injuries (i.e., secondary deviations), and other compensations (i.e., tertiary deviations) [50]. A full understanding of these factors is crucial for the clinician to provide the correct CP management.

1.2 Objectives and contributions

The present work aimed to use musculoskeletal modeling to compare the muscle function and gait asymmetry during the single support phase of walking of a child diagnosed with spastic CP from before to one and two years after it underwent a modified Strayer procedure and BTX injections. Furthermore, a secondary purpose of this dissertation was to compare the CP results with those of typically developed children.

The work was divided into three main objectives. The first objective was to use a musculoskeletal model linearly scaled to the child's dimensions to estimate muscle forces and contributions to the center of mass (COM) accelerations before and after surgical intervention and compare it to what was expected from the literature. The second goal was to employ an asymmetry index to analyze the evolution of the pathological gait through the kinematic results. The last step was to compare the results from the first and second objectives with data from healthy children and understand if gait asymmetry and muscle function improved through the surgical procedure and what compensation mechanisms were possible to identify. Ultimately, this work aims to contribute to the demonstration of the potential application of musculoskeletal modeling in the clinical setting, which is yet to be fully accepted in clinical practice, by assisting in providing a more precise diagnostic, surgical decision-making, and treatment of children with jump gait.

The main limitation that this work tackles is the lack of studies that have explored musculoskeletal modeling regarding muscle function of jump gait in the aftermath of the Strayer procedure and BTX injections.

2

State of the Art

The analysis of human gait is a broadly used assessment tool in a wide range of fields (e.g., clinical diagnosis, sports, and rehabilitation) that encompasses procedures with the goal to record, study, and improve our understanding of human locomotion [136]. In the clinical setting, pathological gaits are not always apparent through visual observation alone. Therefore, gait analysis is often used to provide diagnostic information and to assist clinical decision-making in a large variety of neuromuscular and musculoskeletal diseases that affect gait (e.g., multiple sclerosis, stroke, and CP) [86].

In historical context [10], the first record of the analysis of human walking was written by Aristotle in the fourth century BC. Gaston Carlet was the first to publish a correct description of human gait in 1872, through the recording of ground reaction forces by pressure transducers placed in the shoe sole. Also in the 19th century, the study of equine gait even encouraged the development of video with Eadweard Muybridge creating a system that took multiple images. The creation of video camera systems, which evolved into having direct connections to computers, lead to the development of faster and more efficient gait analysis procedures [155]. Motion capture uses video cameras and mathematical models to record and reconstruct human motion. Marker-based gait analysis is very popular and uses motion capture to collect positions of reflective markers placed on body segments. Once reconstructed, maker trajectories allow the investigator to represent the human body through rigid segments with joints connecting them, which are used to calculate the kinematics of the motion task. Furthermore, motion capture can be supplemented with recordings of GRF via force platforms and incorporation of electromyography (EMG) sensors to gain assess to muscle activity [54]. Some disadvantages include soft tissue artifacts due to marker displacement during the motion task, incorrect positioning of markers in anatomical landmarks, and expensive equipment [139]. More accessible technologies of gait analysis include the implementation of wearable inertial sensors, such as accelerometers, gyroscopes, and magnetometers which measure acceleration, angular velocity, and magnetic field, respectively. This is a novel approach and allows for the detection of gait abnormality without the need for laboratory equipment [87]. Inertial sensors have also been incorporated with machine learning in order

to estimate foot trajectories during gait, providing a robust approach to reduce errors in spatiotemporal gait analysis [59]. Even though these technologies exist, the current thesis will be focused on marker-based approaches.

The quantitative information obtained from motion capture and force platforms allows the kinematics and kinetics of body segments to be calculated. However, external measures obtained through joint kinematics and kinetics provide limited explanation of how the musculoskeletal and neuromuscular systems work together to achieve gait patterns [109]. Computational musculoskeletal modeling has been widely used to provide further insights into muscle forces, joint reaction forces, and muscle induced accelerations. Furthermore, computational musculoskeletal models also incorporate optimization methods to overcome the problem of muscle redundancy, which refers to the infinite combinations of muscle forces that result in the same net joint moments, making muscle force calculation a challenging procedure [168], [29]. These methods paved the way for several studies to analyze a variety of motion tasks with greater detail in sports performance (e.g., such as sprinting [149] and running [62]) and in the clinical environment, including pathological gait [31], [135]. However, even with the potential displayed, the application of musculoskeletal modeling is yet to be part of routine clinical assessment. The quality of modeling approaches for muscle force estimation has been explored and, despite a general consensus about the muscle activation sequence in the gait cycle, a significant variation in force magnitude and peak timing, among the methods used, was evident. The cause remains unknown, making the selection of the most accurate approach challenging [147].

Despite CP being the subject of several research studies using musculoskeletal modeling, few have explored jump gait, even though it is one of the most common gait patterns associated with this neuromuscular disorder. Correa et al. [28] compared lower limb muscle function between children with jump, crouch, and typically developed gait. By using a scaled generic model, the kinematics and kinetics of the hip, knee, and ankle were obtained. Furthermore, the potential of lower limb muscles to accelerate the COM in fore-aft, vertical, and mediolateral direction during the stance phase was estimated using an induced acceleration analysis (IAA). Findings included a statistically significant difference in potential acceleration between jump and healthy gait, and between crouch and healthy gait for almost all muscles. The gluteus medius had a lesser contribution to hip extension in both pathological gaits compared with healthy children. Regarding different gait patterns, contributions of the soleus to vertical COM acceleration (against gravity) were greater in jump gait and contributions of the gluteus maximus to posterior COM acceleration were greater in crouch gait. Due to the differences in ankle motion, it was hypothesized that gastrocnemius would have different contributions between crouch and jump, however, that was not the case.

Lin et al. [88], compared the joint angles, moments, powers and muscle activations during walking between children with spastic diplegia with jump, crouch, recurvatum, and healthy gait. This study found abnormal joint powers at initial stance of the ankle and

knee in jump gait. Moreover, this paper demonstrated that jump gait had an abnormal knee and ankle power generation during initial stance, which contributed to upward support. Increased EMG activity from the eccentric contraction of the hamstrings was also noted, which could be due to accentuated knee extensor moment.

The study of neurologically intact subjects imitating a pathological gait and compare it with healthy gait is a common approach to understanding gait deviations and compensation mechanisms. Rezgui et al. [119] asked healthy adults to imitate jump and crouch gait patterns to understand and distinguish primary from secondary deviations of CP in clinical diagnostic. Similarly to Lin et al. [88], kinematics, kinetics and EMG envelopes data were collected and calculated. This work concluded that healthy subjects could only simulate the principal characteristics of crouch and jump gait. Another aspect of jump gait studied through comparison with healthy subjects were the equinus and toe-walking gait. Hampton et al. [64], wanted to test the theory that plantarflexor weakness leads to a compensatory equinus posture. Therefore, it analyzed plantarfexor strength in able-bodied children simulating equinus and heel-toe gait in a progressive manner and CP gait. The results showed plantarflexor force diminished with higher levels of equinus suggesting that weakness of the plantarflexors complemented equinus posture. Sasali et al. [126] studied the compensatory mechanism of toe-walking in able-bodied subjects. It was found that, in early stance, plantarflexor power was increased to maintain equinus posture, reducing contributions of the vasti, gluteus maximus and hamstrings muscles to support, and the vasti for braking. In late stance, the hamstrings were found to show a continuous contribution in single support period. Thus, compensatory mechanisms have a main role in toe walking, and they should be taken into account to lead to a more efficient treatment of equinus gait.

Children with CP often undergo surgical procedures to regulate muscle functions through lengthening muscles, correcting lever-arms and spasticity reduction [127]. Musculoskeletal modeling shows a promising non-invasive approach to analyze the outcome of these interventions. Kainz et al. [77] aimed to investigate the variation in muscle forces after a selective dorsal rhizotomy, which is a procedure that decreases activation levels of motor neurons. Using motion capture and generic scaled musculoskeletal models, joint kinematics, joint kinetics, and muscle forces were estimated throughout the gait cycle. Static optimization and EMG-informed methods were employed to assess muscle forces. Both techniques concluded that muscle forces became closer to those of unimpaired gait and non-spastic muscle contributions were not diminished.

Brierty et al. [17] investigated the effects of calf-lengthening in the muscle belly region to understand how gait was affected by this procedure. This work is used to treat equinus gait in children with CP and idiophatic toe-walkers (i.e., healthy children that walk and run in their toes for no known reason). Joint kinematics and kinetics, and muscle-tendon lengths were obtained. Ankle dorsiflexion improved in the majority of subjects, lengths in the modeled muscle-tendon actuators increased in all patients with CP, and power development remained the same during push-off. These results support the effectiveness

of calf-lengthening in the muscle belly in CP and idiophatic toe-walkers subjects.

A study by Mansouri [93] aimed to simulate a biarticular rectus femoris transfer through a musculoskeletal model to understand how this intervention influenced the balance recovery of CP children with mild and moderate crouch. This surgery is often chosen to treat stiff-knee gait (i.e., reduced toe-clearance during swing phase), turning the rectus femoris muscle into a knee flexor instead of a knee extensor. The distal tendon of the rectus femoris, which is originally attached to the patella, is reattached to the insertion of the sartorius on the tibia in the musculoskeletal model. Results of magnetic resonance imaging (MRI) of CP subjects served as base for the tendon attachments and muscle paths. Neuromuscular controllers were used to estimate muscle excitations so that a forward dynamics could replicate experimental joint movement. Balance was estimated by calculating the smallest distance between the COM and the base of support while taking into account the shortest time for the extrapolated COM to reach the limit of the base of support. This work concluded that balance recovery of CP children is affected by rectus femoris tendon transfer.

Delp et al. [35] developed models to simulate muscle contracture and the outcome of the gastrocnemius and Achilles tendon lengthening procedure. Patients who have undergone such interventions sometimes reported loss of plantarflexion strength. The model included the triceps surae complex along with the main ankle dorsiflexors and other plantarflexors. The results of the simulations suggest that individual lengthening of the gastrocnemius and soleus, instead of their common tendon, may prove to be more successful in keeping plantar flexor strength and rehabilitating range of motion.

The relevance of musculoskeletal modeling also encompasses sports recovery after surgical intervention to ensure the best rehabilitation program. For example, Mateus et al. [97] conducted a study to understand the primary muscle contributions in a variety of tasks (e.g., drop jump tasks, and bilateral and unilateral countermovement) to evaluate if an athlete was ready to return to regular activity after an anterior cruciate ligament injury and reconstruction. Results showed the quadriceps were the main contributors to the acceleration of the COM in the anterior-posterior direction, and, together with soleus and gastrocnemii, contributed to oppose gravity in the vertical direction. Since these muscles are closely related to the loading of the anterior cruciate ligament, the authors emphasize the importance of including these tasks in rehabilitation plans. The mentioning of this article serves to show the versatility of musculoskeletal modeling whose techniques can be used in contexts other than the clinical setting.

One of the objectives of this thesis was to study gait asymmetry in children with jump gait. Although gait asymmetry can be present in healthy population [16], pathological gait is often associated with higher levels of asymmetry in the lower limbs, making this feature frequently reported, especially in subjects with conditions or disorders that primarily affect one of the lower limbs, such as hemiplegic CP. Therefore, symmetrical execution of motions, such as walking, running, and cycling are seen as a healthy aspect of a subject's physiology and should be a treatment goal. At the present day, there are several symmetry

indices, although a standard index has not been accepted. Siebers et al. [132] conducted a study where three symmetry indices for lower limb joint angles were analyzed and the results compared. The first index was introduced by Robinson et al. [121] and is one of the most commonly used due to its sensitivity to spatiotemporal parameters in the clinical setting. However, this index is not suitable to analyze joint angles throughout a full gait cycle, as it presents extreme artificial values when in zero-crossing zones. To overcome this drawback, Gouwanda et al. [57] developed and validated a normalized symmetry index, which implemented a min-max normalization of the angular velocities. This approach avoided zero-crossings situations by having as output only positive values making this index suited for a complete gait cycle examination. The third index was presented by Nigg et al. [105] and is expressed through an integral over the complete gait cycle according to the symmetry function. Lastly, Queen et al. [117] created another symmetry index, in which the normalization takes into consideration all trials instead of a single one, while also considering the maximum range of values of the variable being tested. The output varies between 0% (full symmetry) and 100% (full asymmetry). Another index worth mentioning is the global gait asymmetry (GGA) index developed by Cabral et al. [20]. The authors applied their symmetry score by testing if it could be used as a metric for biofeedback gait retraining. This was achieved by comparing the outcome of the index between three types of footwear. The first one was custom-made footwear, the second one with soles of different sizes to induce gait asymmetry, and the third one with standard footwear. The mathematical approach consists of time normalizing the gait cycles on both sides and obtaining the sum of the vectors resulting from subtracting the values of both sides for each angular variable. The score results of the three situations were significantly different from each other, implying that the GGA index is capable of detecting different levels of asymmetry. This index avoids the limitations mentioned in the symmetry index developed by Robinson et al. and allows the analysis of asymmetry in each degree of freedom (DOF). For these reasons, the GGA index was the one used for this work.

3

Theoretical Concepts

3.1 Cerebral palsy

CP is defined as a group of permanent neuromotor disorders that compromise a person's physical autonomy by limiting their ability to move, maintain posture, and balance. These traits are caused by nonprogressive injuries in the developing brain, which may lead to a variety of secondary musculoskeletal disorders over time, further compromising functional skills. Moreover, motor impairments are frequently accompanied by epilepsy and changes in sensation, perception, cognition, communication, and behavior [1], [112], [148].

There is a multitude of factors that can cause CP. A more detailed look into this condition's etiology reveals brain malformations on preterm white matter injury, pre, peri, or postnatal stroke, genetic disorders, infections or inflammations of the central nervous system, and early traumatic brain injury. However, up to 50% of cases of CP do not have a defined etiology [76]. The main risk factors for CP include low birth weight, and multiple gestations, with preterm birth being the leading factor [112], [58]. As the gestational age at delivery decreases, risk of CP development slowly rises, with it being apparent as early as 38 weeks of pregnancy. In comparison to full-term pregnancies, the risk for children delivered before 28 weeks of gestation is almost 50 times higher [58].

3.2 Classification

According to [60], the syndromes of CP are classified by type and distribution of motor abnormalities. Three of the most common syndromes of CP are spastic, dyskinetic, and ataxic.

- **Spastic CP**: This form of CP is the most common one and patients with this syndrome show signs of upper motor neuron lesions such as spasticity, clonus, hyperreflexia, and extensor plantar response [150]. These symptoms result in stiffer muscles and lesser control of voluntary movement. Some forms of spastic CP are:

  - **Spastic hemiplegia**: Children diagnosed with spastic hemiplegia have either the right or left half of the body affected, and often have more severe motor limitations in the arm when compared to the leg. Moreover, complications associated with behavioral problems (such as anxiety and specific phobias), visual problems, intellectual impairment, and athetosis are commonly present.
  - **Spastic diplegia**: Normally, a child with spastic diplegia has increased muscle stiffness predominantly in the lower limbs while maintaining fine motor skills in the upper limbs. While this subtype of CP doesn't usually affect speech and intelligence, some children have visual impairments.
  - **Spastic quadriplegia**: Spastic quadriplegia is considered the most severe syndrome of CP and is associated with acute motor impairments, in both upper and lower limbs. Most children affected by spastic quadriplegia have visual and feeding difficulties, undeveloped speaking abilities, and epilepsy. These symptoms are normally caused by extensive brain damage.

- **Dyskinetic CP**: Dyskinetic CP is often characterized by the existence of more than one form of involuntary movement. Children with this type of syndrome show increased muscle stiffness while attempting to perform a movement or a display of emotion. Some complications caused by Dyskinetic CP consist of hearing, breathing, drooling, and speaking problems. Clinical features include dystonia, dysarthria, and intellectual disability. Dyskinetic CP includes:
  - **Choreo-athetoid**: This form of CP can be identified by the presence of unpredictable contractions of muscles groups located in the face, bulbar muscles, proximal extremities, and digits.
  - **Dystonic**: The repetitive contractions of both antagonist and agonist muscles occurs in Dystonic CP, often resulting in dysarthria.

- **Ataxic CP**: Ataxic CP is the rarest form of CP (5-10%) and is normally caused by malformations to the cerebellum [58], which is responsible for coordination and precise movements, leading to difficulty in tasks such as writing or buttoning a shirt.

In cases where the patient shows characteristics of more than one syndrome, it is diagnosed as a mixed syndrome.

Classification of motor function in CP children is widely used in the clinical environment. Palisano et al. [107] created the Gross Motor Function Classification System (GMFCS), which allows for an easy understanding of the child's motor restrictions. This system is commonly used and is divided into 5 levels (Figure 3.1). A higher level translates into a decrease in motor function and activity ability, such as running, jumping or even walking. This method of classification has been expanded and revised and its validity has been verified [108].

Gross Motor Function Classification System				
Level 1	Level 2	Level 3	Level 4	Level 5
No limitations in walking ability. Capacity to execute gross motor skills like running and jumping. However, speed, balance, and coordination are restricted.	Ability to walk without assistive devices. Children walk in most settings and climb stairs holding onto a railing. Gross motor skills, such as running and jumping very limited.	Need for an assistive device when walking. Children climb stairs holding onto a railing and require wheeled mobility for long distances.	Need for physical assistance or powered mobility in most settings. Although, for short periods, children can stand with assistive devices.	Voluntary control of movement is severely restricted even with assistive devices. Limitations in their ability to maintain antigravity, head and trunk postures, and control leg and arm movements.

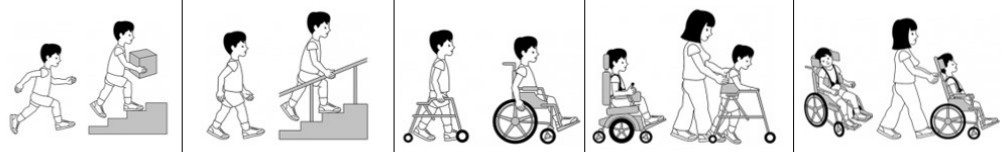

Figure 3.1: Gross motor function classification system. Adapted from [107], [72].

3.3 Treatments

In the present day, there is not a cure for CP. Due to the range of different symptoms and impairments that can occur, there isn't a standard treatment for every individual. However, a variety of treatments are available in the clinical environment to weaken the severity of CP's symptoms, allowing for a more personalized medical assistance. A few examples are physical, occupational, and speech therapy, as well as oral medications, such as oral antispasticity agents, being the most common diazepam, baclofen, and tizanidine. Pharmacological treatment includes targeted injections of intrathecal baclofen, which actuates like oral baclofen, although is administered directly to the central nervous system at the spinal level, with the aim to treat severe spasticity [24]. BTX is an effective and widely used pharmacological treatment for local spasticity to increase range of motion while avoiding side effects of oral medications, such as muscle weakness and sedation [24],[81]. However, the duration of muscle tone reduction due to these injections appear to be ambigous [142], [45]. It also includes the possibility of muscle atrophy [102]. Another treatment that almost all CP patients are submitted to is physical therapy. This treatment emphasizes physical exercises that manage function and movement, in order to promote, preserve, and restore physical, psychological, and social wellbeing [7]. However, a recent study by Das and Ganesh [30] points out the modest outcomes of this therapy, reporting moderate effectiveness in gait speed, focal/functional, and upper-limb training, conflicting evidence for the results of strength and cardiorespiratory training, and even the inefficacy of some interventions, such as neurodevelopmental training. There is a wide range of surgical interventions in the CP landscape. As a last example, the three main procedures are briefly explained:

- **Selective dorsal rhizotomy (SDR)**

The main objective of SDR is to reduce spasticity by severing selected nerves of the deep tendon reflex. This procedure is mainly used in the lower limbs and provides better results in children with spastic diplegia. It is applied when all other treatments options have been unsuccessful [25].

- **Deep brain stimulation (DBS)**

  The procedure for DBS consists of the implantation of electrodes in gray structures located deep within the brain. This method enables control over stimulation which is caused by a generator implanted subcutaneously in the upper chest region. DBS has shown great results for patients with the DYT1 gene, which is one of the most common genetic causes of dystonia [25], [79].

- **Orthopedic surgery**

  In order to treat the secondary musculoskeletal deviations that children with CP often experience over time, surgical orthopedic procedures are frequently used. Due to muscle overactivity, most children with spastic CP eventually require tendon lengthening surgery to prevent and correct contractures. Another relevant surgical procedure, with the aim to restore muscle balance, consists of the transfer of tendons. Finally, when the patient reveals torsional deformities, or spine, hip, and/or foot destabilization, rotational osteotomy is a commonly used surgical procedure. To prevent multiple hospitalizations, single-event multilevel surgery (SEMLS) is often the chosen medical procedure, where multiple joints are operated in a single surgery [25]. SEMLS is shown to be an effective procedure to improve mobility of children and adolescents with CP [51]. The efficacy of the applied treatment is often classified according to the GMFCS.

3.4 Gait

Human gait is a complex ability acquired through the continuous process of learning, allowing our centre of gravity to be propelled in a forward motion while maintaining stability [128]. Gait is defined as a manner of walking or moving on foot, encompassing a broader meaning than walking. In order to analyse pathological gait, a complete understanding of the gait cycle is first required.

3.4.1 Gait cycle

One of the most essential aspects to understand in human gait is its cycle. A healthy gait cycle is defined by seven major events [156], which are represented in Figure 3.2. A complete gait cycle occurs when a successive repetition of one of those events takes place. Normally, the initial contact is the event used as reference to mark the begging and end of the gait cycle. The gait cycle is also divided in the swing phase and the stance phase. The swing phase, which lasts 40% of the cycle, is when the foot is in a forward motion in

the air and the stance phase, which lasts 60% of the cycle, is when the foot is placed on the ground. The gait cycle is composed of these two phases, being the initial contact and the toe off the events that divide them [156]. The initial contact is the moment when the foot starts to contact the ground and the toe off is when it stops.

Since the nomenclature of the gait cycle has some variations in literature, alternative gait terminology is further explained. During the gait cycle, there are two phases where both legs are in contact with the ground, denominated the double support periods, and two phases where one of the legs is swinging, which are denominated single support periods. Both double support periods and the single support period are part of the stance phase, while the remaining gait cycle is part of the swing phase [8]. The first double support period is referred to as early stance, and the last one pre-swing. The single support phases are divided equally in the mid-stance and terminal or late stance [104].

The position of the ankle during the stance period is divided into three phases denominated as rockers. The first rocker is the heel rocker, which begins at the heel strike and ends at flat foot position, and is responsible for decelerating the trunk. The second rocker is the ankle rocker, which includes the change from the initial plantarflexion position to dorsiflexion and finishes with a heel lift, allowing the shank (i.e., tibia and fibula) to rotate forward upon the ankle and lead to the COM's progression. The last rocker is the forefoot rocker, which starts with a heel lift and accelerates the body before toe-off and swing phase [18].

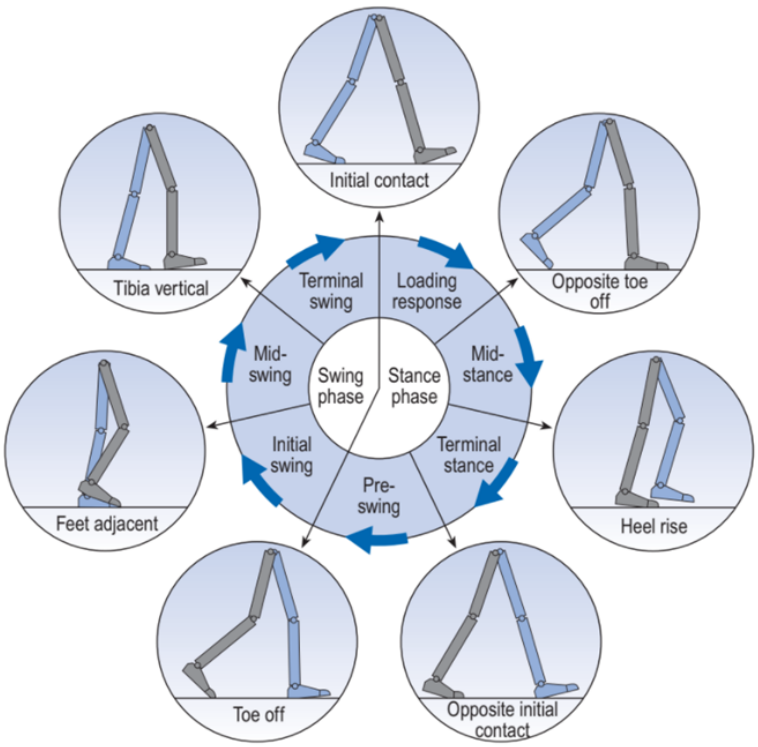

Figure 3.2: Gait cycle according to right leg (gray) with the various events and gait phases. From [156].

3.4.2 Gait deviations

The classification of gait deviations allows for better identification and understanding of what causes pathological gait in CP. These deviations are divided into primary, secondary, and tertiary categories according to their biomechanical or pathophysiological etiology [50]. The primary deviations are caused by injuries in the central nervous system, which may result in spastic and muscular weakness, as well as compromised selective muscle control. This abnormal activity of the nervous system leads to asymmetric growth of the musculoskeletal system, making these deviations secondary. Examples include muscle contractures and bone deformities. The final deviation occurs as a compensatory response to the primary and secondary deviations, and can result in excess use of energy and anatomical damage over long periods of time. For example, in the presence of ankle plantar flexion or weakness in the quadriceps, knee hyperflexion might occur and lead to the deterioration of the knee joint [33].

3.4.3 Gait patterns

Gait pattern classification is normally differentiated between unilateral (i.e. spastic hemipligia) and bilateral spastic (i.e. spastic diplegia and quadriplegia) CP. Winters et al. [163] developed the most commonly used classification of spastic hemiplegia, establishing four gait patterns according to kinematics of the sagittal plane (Figure 3.3).

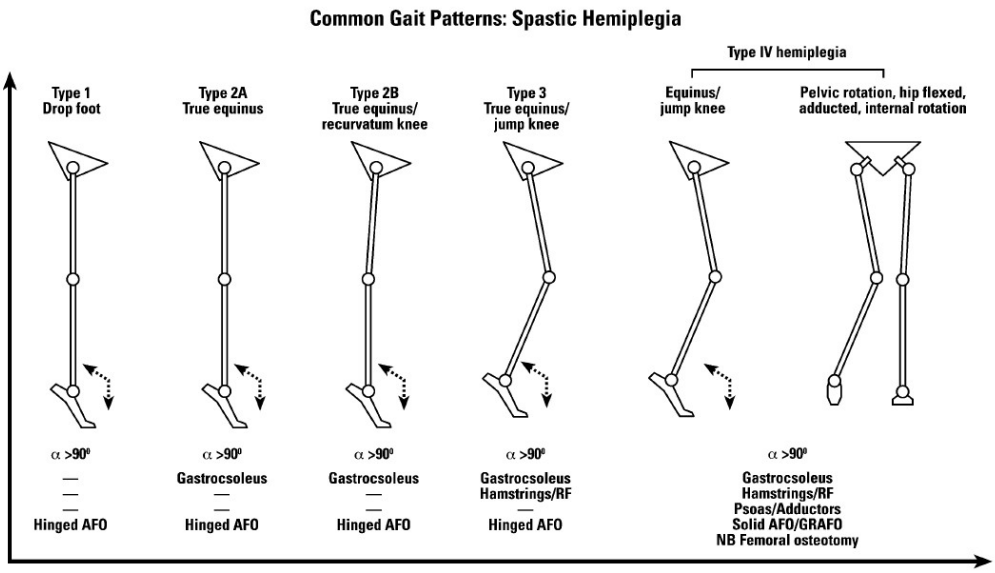

Figure 3.3: Gait patterns in unilateral spastic CP. From [122].

The most relevant gait patterns in subjects with bilateral spastic CP were established according to Rodda and Graham [122]. This classification contains four types (Figure 3.4) and is based on the sagittal plane kinematics of the pelvis, hip, knee and ankle as a whole.

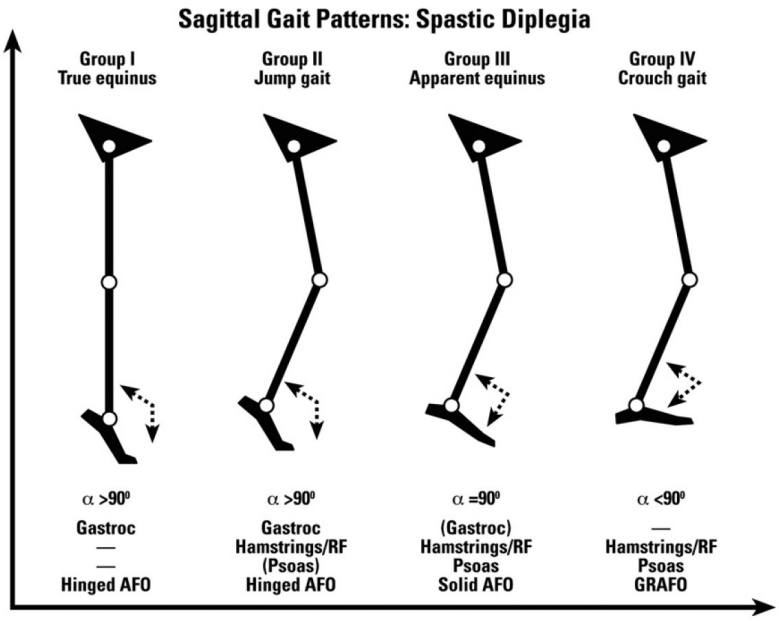

Figure 3.4: Gait patterns in bilateral spastic CP. From [166].

It is important to note that these gait patterns are defined according to the postures shown during the gait cycle. These postures vary depending on the gait phase and are more clearly observed during the mid and end of the stance phase [122].

3.5 Jump gait

A common gait pattern in children with spastic diplegia is jump gait. This gait is characterized by spastic hip flexors, hamstrings, and triceps surae. Furthermore, it presents certain traits such as ankle equinus, excessive hip and knee flexion, anterior pelvis tilt, and accentuated lumbar lordosis [122]. Other features include the absence of heel strike at initial contact, with toe contact incorporated during the stance phase, and the often presence of stiff knee (i.e. excessive knee extension) during the swing phase on account of rectus femoris prolonged activity [33] , [141].

In children with jump gait, the absence of heel strike compromises the shock absorption, which is done with the forefoot [32]. Moreover, the foot never reaches a flat position, hindering the forward rotation of the tibia (i.e., second rocker). The absence of these rockers leads to compensatory motions by other joints, such as the accentuated knee flexion or extension depending on the gait pattern [3], [100]. The presence of the first rocker is a prime indicator of healthy gait and is often absent in CP. Thus, the main goal of equinus gait treatment is to restore the first rocker [100].

Depending on the age of the child, different treatments are implemented [122]. Injections of BTX in the gastrocnemius and hamstrings are applied, as well as the use of ankle foot orthoses (AFO), when it comes to younger children. However, Gough et al. [55] advises cautious application of BTX injections, especially in spastic diplegic CP, due to lack of long-term understanding of the effects of denervation atrophy. Relative to AFO, Smith

et al. [134] reported that AFO have shown to improve mediolateral stability during stance phase by restricting ankle and subtalar mobility as well as facilitating toe clearance during swing phase and heel strike at first contact. Furthermore, they studied the results of hinged and dynamic braces in children with jump gait pattern and concluded their equal effectiveness in the improvement of ankle kinematics and kinetics. Moreover, the implementation of the SDR procedure might be necessary to permanently reduce muscle tone. Older children are submitted to SEMLS with muscle-tendon lengthening of muscles that present contractures, such as the gastrocnemius, hamstrings, and ilipsoas, together with a tendon transfer of the rectus femoris to semitendinosus to treat knee co-contraction. To correct equinus in children with spastic CP, a lengthening of the gastrocsoleus complex is required depending on the lack of capacity to perform ankle dorsiflexion [123].

Out of all the treatment approaches mentioned, the surgical lengthening of the gastrocsoleus complex is the most relevant in the context of this work. Therefore, further explanation of this procedure is presented in the following section.

3.5.1 Gastrocsoleus complex lengthening

Due to equinus deformity being the most common gait deviation in CP children [123], various procedures to correct this anomaly have been reported. Equinus is caused by the isolated contracture of the gastrocnemius or the contracture of the gastrocnemius-soleus complex [13]. Despite both muscles having a common insertion in the Achilles tendon, they have different origins. The gastrocnemius originates from the posterior femoral condyles, meaning it passes through the ankle and knee joints. The origin of the soleus is from the posterior and proximal regions of the tibia, fibula, and interosseus membrane. These two muscles are the main contributors to plantarflexion [80]. In order to differentiate if there is an isolated contracture of the gastrocnemius or the gastrocsoleus complex, the child is subjected to a Silfverskiöld test [133]. This physical exam begins with the dorsiflexion of the ankle with the knee fully extended with the patient laying down. A contracture is present either in the gastrocnemius, the soleus or both if dorsiflexion angle can not surpass 10°. It is necessary to verify that the subtalar joint remains in neutral position. The ankle is once again dorsiflexed with the knee flexed 90 degrees. This should relax the gastrocnemius. If the angle of dorsiflexion improves to more than 10°, the contracture is solely present in the gastrocnemius, if the dorsiflexion angle remains unaltered, both muscles of the triceps surae are contracted [111], [165]. Once the contractures are identified, it is then necessary to decide in which zone and which surgical procedure to apply.

Once the muscle contractures are identified, a lengthening of gastrocsoleus complex is often performed to treat the presence of equinus [46]. The surgical anatomy of the gastrocsoleus complex is divided into three zones [130]. The first zone is between the origin of the gastrocnemius and the end of the belly of the medial gastrocnemius. In this region, the soleus and the gastrocnemius are still separate. For this reason, an isolated

lengthening of the gastrocnemius is possible or even lengthening of both muscles by a different or equal amount. The results of a lengthening procedure in this area are stable and resistant to overlengthening [46]. The surgeries in zone 1 are the proximal gastrocnemius recession reported by Silfverskiöld [133], the intramuscular lengthening of the gastrocnemius and soleus described by Baumann and Koch [14], and Strayer's distal gastrocnemius recession [137]. The termination of the first zone is the beginning of the second, with this one ending in the most distal soleus muscle fibers. In this zone, the gastrocnemius apneurosis and soleus fascia join together, which means the lengthening of both muscles in this area is done by the same amount [146]. Vulpius and Stoffel [151] and Baker [9] describe the recession of the gastrocsoleus complex procedures in this zone. The third zone is comprised of the Achilles tendon. Like the second zone, the lengthening of the Achilles tendon is in equal amounts, but more unstable and more prone to overlengthening [46]. An example of this procedure in zone 3 is the one described by White [154]. Figure 3.5 shows some of the previously mentioned procedures.

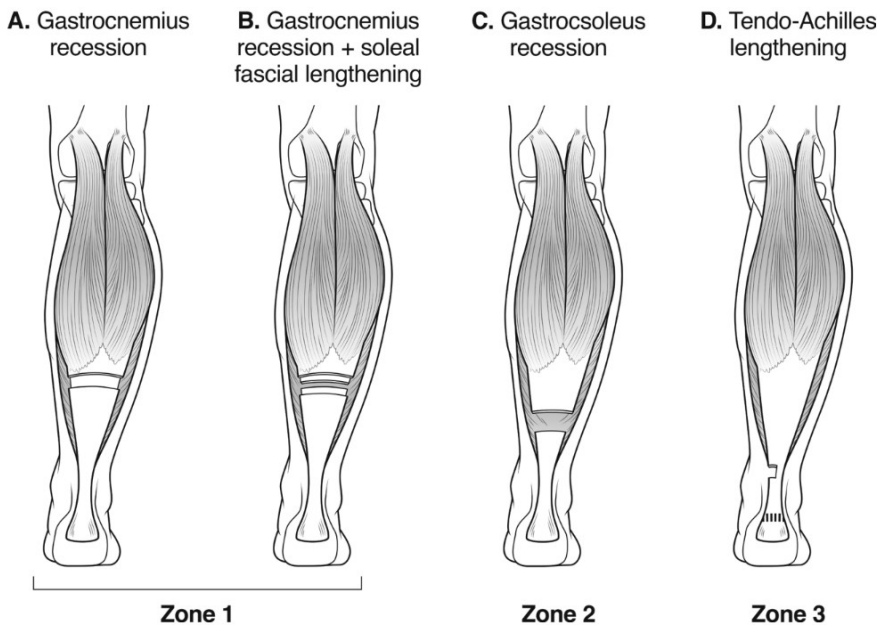

Figure 3.5: Types of lengthening surgery for the gastronemius-soleus muscle-tendon unit. Image (A) shows the Strayer procedure and (B) the Strayer procedure with soleal fascia lengthening in zone 1. Image (C) shows the Vulpius surgery for zone 2 and (D) the tendon-Achilles lengthening described by White. From [123].

When the intervention is in children with diplegia CP, zone 1 surgery is favored over 2 and 3 to treat equinus deformity [123]. In this work, the main interest lies in the Strayer procedure in zone 1. This technique comprises the total release of the gastrocnemius tendon through an incision near the union with the Achilles tendon, which compromises its motor function [42]. Once the separation is achieved, the original Strayer procedure describes the suture of the gastrocnemius to the soleus fascia [137]. However, this step is optional, meaning it is also possible to let the gastrocnemius reattach freely on its

own [42]. An important step is to identify and protect the sural nerve. This is because its location can vary and it might be found in the deep or superficial fascia, or in the posterior region of the gastrocnemius tendon [113]. Once the procedure in the first zone is complete, dorsiflexion is attempted to verify if it reaches over neutral position. If it does not occur, a fascia lengthening (i.e. fasciotomy), which consists of the surgical cut of the fascia to reduce tension [39], of the soleus is required. The surgical intervention of the Strayer procedure together with a soleal fascial lengthening is designated the modified Strayer procedure [47]. There is evidence that places the Strayer surgery as an ideal procedure to treat equinus in children with spastic diplegia [46]. This is supported by literature referencing patients returning to their former level of physical activity, with improvement in ankle dorsiflexion range of motion, and strength over time [47], [165], [125].

3.6 OpenSim

The neuromusculoskeletal system incorporates a variety of elements, such as bones, muscles, and nerves. The full understanding of how these components function and how they interact with one another to produce movement require dynamic simulations since muscle forces and cause-effect relationships are extremely challenging to measure through experimental data alone [37]. Therefore, a framework is necessary to run these simulations with the use of computational models based on the biological elements of movement [34]. OpenSim is an open-source platform created to allow modeling, simulation, and analysis of highly accurate models of the neuromusculoskeletal system. This software was designed to be able to derive equations of motion for dynamic systems, perform numerical integration, and solve constrained non-linear problems [37]. OpenSim incorporates some of the basic functions of SIMM [34], which is a widely used framework that allows users to create, alter and evaluate models of different musculoskeletal structures. For example, one functionality of SIMM present in OpenSim is the capability to edit muscles and plot variables of interest. However, SIMM does not compute muscle excitations and has limited tools to analyse results from dynamic simulations. OpenSim overcomes these limitations, by providing those functions. Simtrack is another important tool in OpenSim and allows the creation of dynamic muscle-driven simulations from motion capture data.

Furthermore, OpenSim's plug-in structure allows users to develop and add new tools, expanding its functionality, while being available to the entire scientific community. Joint reaction forces, muscle induced accelerations, and muscle power calculation are some examples of added functions by users.

The implementation of this software in this work allowed the development of musculoskeletal models and running dynamic simulations to obtain estimations of kinematics, kinetics, muscle forces, and the contribution to the COM acceleration of each muscle during walking.

3.7 Muscle-tendon system

A general understanding of the inner works of the muscle-tendon system is required to ensure a meticulous modelling of this challenging system. There are two systems that should be discussed: the nervous system and the musculoskeletal system. The nervous system allows signal transmission or reception from the brain to the muscle to inhibit or promote its activity. The musculoskeletal system includes lever systems composed of muscles, tendons, bones and the joints and ligaments that link them together. The information sent by the nervous systems dictates how the mentioned lever systems generate force. Both systems work in harmony to provide stable and coherent movement among all their elements and any sort of dysfunction might compromise this balance. It is important to note that CP syndromes can affect muscle-tendon interactions, which perform crucial functions in biomechanical movement.

3.7.1 Structure

Muscles can be classified as skeletal, smooth, and cardiac, depending on structure and function, and generate force through contraction, meaning they can only pull and never push. Muscles have at least two connection points. If the point of connection remains immobile during action, it is called an origin and if it moves when contraction takes place, it is called an insertion. This study will focus on skeletal muscles, which are the only ones capable of voluntary contraction. The skeletal muscle is made of excitable tissue and possesses numerous properties, enabling it to produce movement. The main properties are: contractility, which is the ability to produce muscle tension by shortening of the muscle; irritability, which is the ability to actively respond to a stimulus, whether it has an electrical, chemical, or mechanical origin; elasticity, which is the capacity to return to its original length after extension; and extensibility, being the property to extend. A skeletal muscle is composed of several muscle fibers, which have generally the same length as their respective muscle, and are almost all innervated by one nerve ending. Each bundle of muscle fibers is denominated as a muscle fascicle (Figure 3.6).

The sarcolemma is a thin cellular membrane made of thin collagen fibrils that envelop each fiber and merges with a tendon fiber. These tendon fibers create agglomerates forming tendons composed of fibrous connective tissue, with immense tensile strength, whose function is to connect muscles to bones, allowing muscles to enact body movement. Aponeurosis and fascia are also composed of dense connective tissue. While aponeurosis has a flat, sheetlike format allowing connection between muscles or muscle to bones, the fascia is a fibrous membrane that wraps around nerves, blood arteries, muscles, and muscle groups, holding them together [96]. In addition, joints are connection points that enable bones to move in relation to each other. Muscle fibers have hundreds, if not thousands, of myofibrils. Myofibrils are constituted of polymerized protein molecules designated by actin (thin filaments) and myosin (thick filaments) (Figure 3.7). At the end

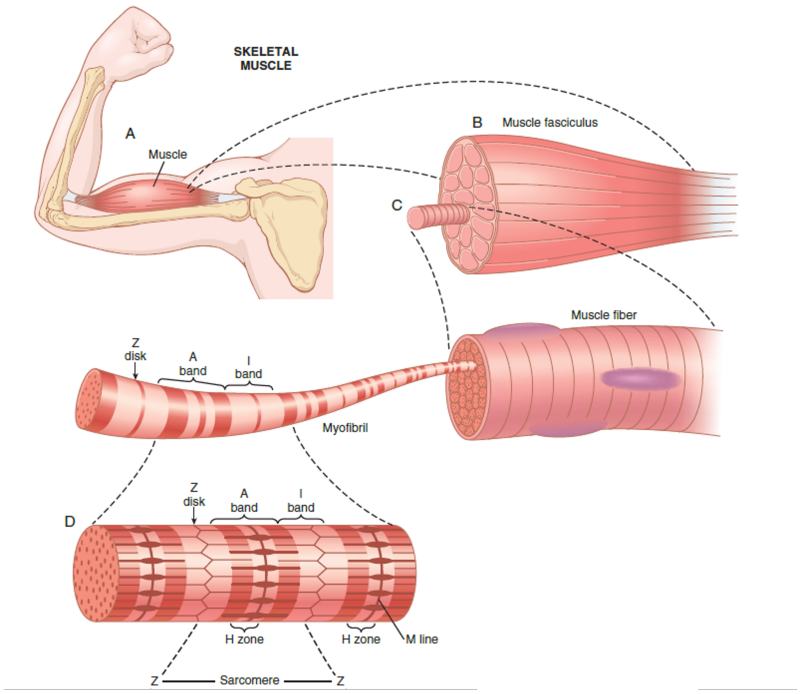

Figure 3.6: Representation of the skeletal muscle structure. Adapted from [61].

of each actin filament, there is a Z disk, which is made of filamentous proteins different from actin and myosin. The actin filaments extend from the Z disks in both directions to run parallel to the myosin filaments. A sarcomere is the section of myofibril between two Z disks. When the sarcomere contracts, and the actin and myosin slide between one another becoming completely interlaced (i.e., the ends of the actin filaments are almost in contact), strength production reaches its peak. The M-band is a perpendicular structure that anchors myosin to the middle of the sarcomere represented as the M line in Figure 3.7. In order for the contractile mechanism of the sarcomere to function correctly, a high number of filamentous molecules of titin, a protein, sustain the side-by-side interaction between the myosin and actin filaments. Titin is a large protein molecule with elastic properties connecting the Z disk to the myosin filament, acting as a spring with the ability to change length as the contraction of the sarcomere occurs.

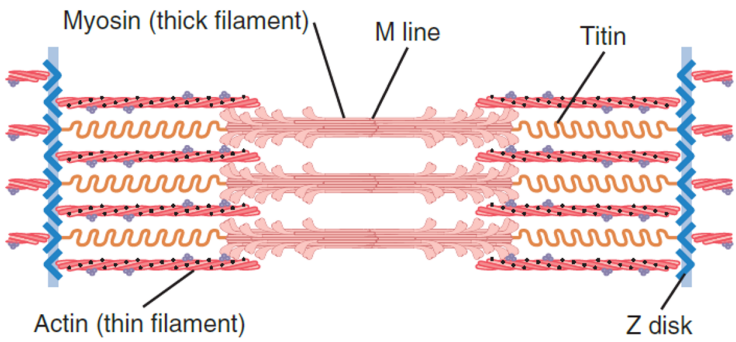

Figure 3.7: Representation of the sarcomere. From [61].

Muscle can have different classifications depending on their architecture, which influences their mechanical roles [159]. A muscle that crosses a single joint (e.g., the soleus participates in ankle plantarflexion) is designated uniarticular, while a muscle that crosses two major joints is biarticular (e.g., the gastrocnemius participates in ankle plantarflexion and knee flexion). Furthermore, muscles can also be classified as pennate or parallel depending on the angle of the muscle fibers' orientation in relation to the direction of the attached tendon axis, designated as the pennation angle. This characteristic in pennate muscles allows them to produce force superior to parallel muscles, which makes them more suited for fast movements (Figure 3.8).

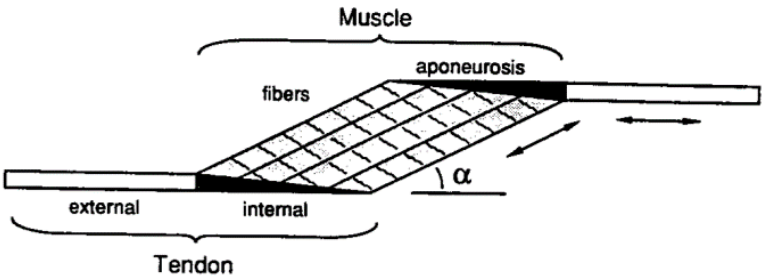

Figure 3.8: Representation of a pennate muscle. The pennation angle is represented by α. From [167].

The nervous system plays a crucial role in muscle contraction, due to having the necessary structure to produce the electrical excitation required for muscle cells to initiate contraction. Motor neurons are the nerve cells responsible for controlling muscle movement. The cell body of these neurons is located in the spinal cord and it extends in order to send the electrical signal to the muscle fibers. As stated before, each muscle fiber is innervated by one nerve cell or motor neuron. However, one motor neuron can connect to multiple muscle fibers through its branches. The complex of a motor neuron connected with its muscle fibers is designated as a motor unit. The electrical activity of a motor neuron regulates the contractile activity of all the muscle fibers in that motor unit (Figure 3.9). Depending on the size and function of the muscle, the number of muscle fibers delegated to a motor neuron varies greatly. The voluntary contraction of a skeletal muscle is the product of numerous motor units working together.

The transmission of the electrical signal from the terminal end of the motor neuron to the muscle fiber occurs in the neuromuscular junction, leading to the contraction of the muscle fiber. Since these cells do not interact physically, a small space exists designated as the synaptic cleft.

There is also a distinction to be made between slow and fast twitch motor units. For slow velocities and extended use, the slow motor units are the most adequate, while fast motor units are employed for quick or explosive movements requiring high velocity, and large power output. Due to their size, small motor neurons have low force production, innervating slow-twitch muscle fibers. In contrast, high force development is produced by large motor neurons while innervating fast-twitch fibers. The capacity to produce

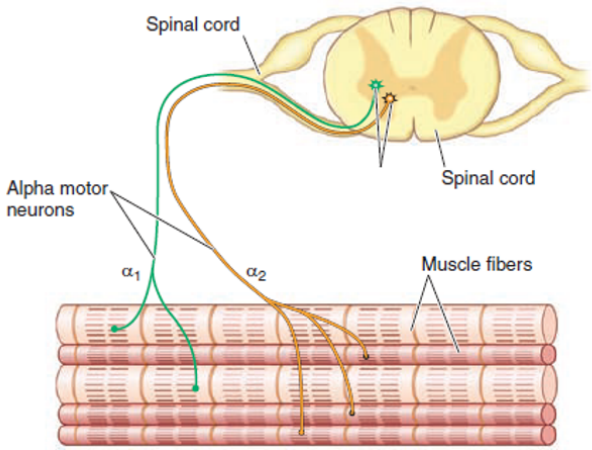

Figure 3.9: Representation of two motor units. From [115].

force can be one hundred times greater in fast muscle fibers, when compared to slow ones, due to having almost four times the shortening velocity. The central nervous system has a sequence of activation where the slow motor units are always summoned prior to the fast motor units [170].

3.7.2 Physiology

As stated in the previous section, a nervous stimulus needs to occur to start the contraction mechanism of muscle fibers. The central nervous system begins this process by creating an electrical impulse that generates an action potential that will travel through the axon of the motor neurons. Once it reaches the nerve endings, the action potential contacts the motor end plate, which is the nearest region of the sarcolemma. This contact happens by secretion of a neurotransmitter, acetylcholine, from the nerve endings to the synaptic cleft. This substance opens acetylcholine-gated cation channels through contact with its protein receptors in the muscle fiber membrane, allowing the diffusion of large quantities of sodium ions to enter and locally depolarize the membrane. This depolarization starts an action potential in the membrane by opening voltage-gated sodium channels. Similarly to how it traveled through the nerve cell, the action potential navigates through the fiber membrane, depolarizing it, and flowing until it reaches its center. Once this event happens, the sarcoplasmic reticulum, which stores large quantities of calcium ions, releases them stimulating the actin and myosin to slide alongside each other. After this process, the calcium ions are once again stored in the reticulum for further use with the arrival of a new action potential [61].

The myosin filament is composed of several molecules of myosin. The tail of this molecule is formed by two heavy polypeptide chains structured in a double helix. Each chain separates and folds forming a globular architecture designated as the myosin heads. The tails group to form the myosin filament, while part of the tail along with the myosin head extend outwards forming an arm-like structure known as a cross-bridge. These

cross-bridges are twisted and pointed out in all directions around the filament.

Proteins of actin, tropomyosin, and troponin are the molecules that compose the actin filaments. The F-actin protein molecule serves as the backbone of the filament having a double-stranded structure like the myosin molecule. The tropomyosin molecule also has a helix shape and is wrapped around the actin strands. The purpose of tropomyosin in its relaxing state is to prevent contraction by lying over active sites blocking the attraction between actin and myosin. The troponin complex is composed of three protein subunits, each with a different role, and is attached to the sides of the tropomyosin. Troponin I is a subunit with a strong affinity for actin, troponin T for tropomyosin, and troponin C for calcium ions. This three unit protein allows the tropomyosin to attach to actin and the affinity for calcium ions is credited as the property that allows the contraction process to begin. This is because, troponin changes its structure when troponin C combines the calcium ions, by moving deeper into the space between the actin strands leading to the uncovering of the myosin binding sites. This happens when the sarcoplasm (i.e., the cytoplasm of the muscle cell) contains calcium ions. The heads of the cross bridges from the myosin filaments become attracted to the now available active site. Once the connection is achieved, a change in the alignment occurs between the head and arm of the cross-bridge with the use of ATP, moving the head toward the arm. This motion of the head is referred to as the power stroke (Figure 3.10). The actin filament, which is attached to the myosin head, is dragged alongside it. The head then disengages the active site, returning to its extended position, ready to combine with the next active site. This process is repeated, allowing the actin filaments to pull the Z discs toward the center of the sarcomere, causing muscle contraction.

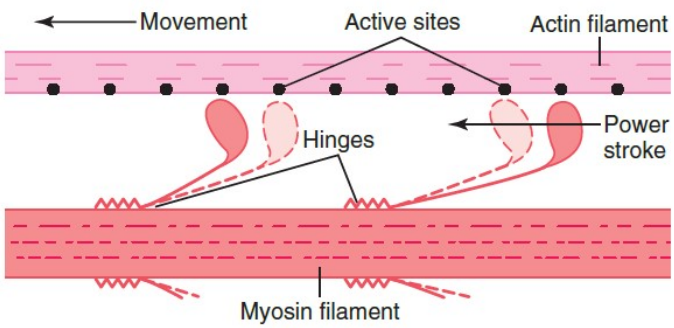

Figure 3.10: Representation of the contraction mechanism. From [61].

3.7.3 Modelling

Computation of the musculoskeletal system needs to take into account several biological and physiological aspects in order to achieve an accurate representation of muscle activity. The ideal scenario would be to have a model that would consider even the smallest detail (e.g., molecular activity). However, this would increase the complexity of the simulation process, leading to a higher computational load. Therefore, the choice of the model needs

to balance its level of complexity with its biological authenticity, while also considering the study at hand.

Since musculoskeletal modeling allows the estimation of physical parameters without invasive methods, it is a promising method to be explored and applied in the clinical sense. Winters and Stark [162], describe three model types based on their structure. These models are the simple second-order order model, the distributed-parameter model based on the Huxley model [74] and the lumped-parameter based on the Hill model [69], [68]. The second-order model is less complex, since it does not include the series elastic element present in the Hill model and operates according to a second-order linear system to characterize the muscle-joint complex. However, this simplicity in mathematical formulation presents severe limitations when it comes to replicating human movement. On the other hand, the distributed-parameter model attempts a more complex and detailed framework, by considering the cross-bridge attachment and detachment dynamics, but it exhibits some drawbacks. For example, it requires high-accuracy modeling of muscle-joint properties (e.g., pennation angle). These complex requirements lead to an impractical implementation in multi-joint simulation. Despite the lumped-parameter model not having the complexity of the Huxley-based model, it is capable of describing muscle function and properties from a purely mechanical perspective. For these reasons, the Hill-based lumped-parameter model is recommended over the other two.

The dynamics of the muscle tissue are divided into activation and contraction dynamics (Figure 3.11) and the Hill model was used to define their behavior.

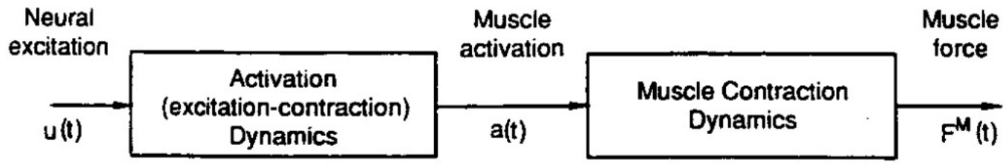

Figure 3.11: Schematic of muscle dynamics. From [167].

3.7.4 Activation dynamics

The process of connecting neural excitation of motor units with muscle activation is denominated activation dynamics. To simulate this mechanism, it is necessary to take into account the delay that it takes for the neural signal to reach the muscle fibers and for these to generate force. Furthermore, muscle relaxation and dispersion of the neural excitation signal are also not instantaneous actions. Moreover, since the process of releasing calcium ions, which enables muscle contraction, is faster than the inflow of calcium ions to the sarcoplasmic reticulum, the time delay of activation is shorter than relaxation. These biological aspects are taken into consideration through the equations 3.1 and 3.2.

The excitation signal for each muscle is implemented as an input of dimensionless quantity (u), between 0 and 1. Through a non-linear first order differential equation (equation 3.1), is possible to correlate this variable to the muscle activation (a), having as

output the activation level, which is also dimensionless and can take values between 0 and 1 [143].

$$\frac{da}{dt} = \frac{u - a}{\tau_a(a, u)} \tag{3.1}$$

The time constant, $\tau_a(a, u)$, alters its value depending on the level of activation and its increasing or decreasing rate (equation 3.2).

$$\tau_a(a, u) = \begin{cases} \tau_{act}(0.5 + 1.5a); & \text{if } u > a \\ \tau_{deact}/(0.5 + 1.5a); & \text{if } u \leq a \end{cases} \tag{3.2}$$

τ_{act} is the activation time constant, while τ_{deact} is deactivation time constant. This equation describes the slower activation rate as the level of activation increases. This occurs because the majority of calcium ions have already been released. On the other hand, the relaxation process happens at a slower rate with the decrease of activation levels, due to shortage of calcium ions to pump back into the sarcoplasmic reticulum [161].

3.7.5 Contraction dynamics

After the activation dynamics phase is completed, the conversion of the muscle activation into muscle force is achieved by a process named contraction dynamics. This stage requires a muscle-tendon unit model to accurately describe the relationship between the force-length and force-velocity properties of the muscle, as well as the elastic properties of the tendon, further explained in this chapter [143], [167]. The previously mentioned Hill model incorporates these characteristics.

The Hill model, represented in Figure 3.12, comprises a contractile element (CE), a series elastic element (SE), and the parallel elastic element (PE). The CE incorporates the muscle's force-length-velocity properties acting as the model's main component since it represents the muscle force originated from the muscle's activation. The SE represents the elasticity of connective tissue, such as the tendon and aponeurosis. Finally, the PE represents the passive resistance imposed by surrounding tissue (e.g., fascia), when the inactive muscle is stretched due to external forces. The last two mentioned elements are modeled as a non-linear spring since the tissue that they are simulating showcases a non-linear elastic behavior. This model also considers the pennation angle (α), since the muscle fibers do not always have the same direction as the SE element. The ability of the muscle to generate force is affected by this angle as well as the muscle's force-length-velocity characteristics since it allows a larger number of muscle fibers per cross-sectional area [66].

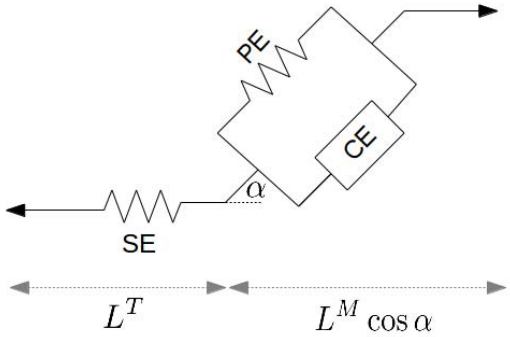

Figure 3.12: Schematic of the Hill muscle model to simulate contraction dynamics. From [41].

From Figure 3.12, it is possible to observe that the length of the musculotendon unit, l^{MT}, is related to the length of the muscle, l^M, the length of the tendon, l^T, and the pennation angle, α. According to Zajac [167], this relationship is explained through following equation:

$$l^{MT} = l^M cos(\alpha) + l^T \tag{3.3}$$

The Hill model provides a mathematical and phenomenological representation of the musculotendon dynamics at the macroscopic level. For these reasons, it is widely used in muscle simulations. However, since it represents a purely mechanical view of the muscle-tendon complex, through the force-length-velocity relationship, it does take into account the muscle's physiological aspects. The simplified muscle architecture is another limitation of the Hill model as it considers unidirectional behavior, uniform fiber length, pennation angle, and line of action when muscles often have highly complex structural variations [85]. Nonetheless, this work is done at the macroscopic level and it does not require a detailed simulation of the physiological perspective. For these reasons, Thelen's model [143], which was based on the generic Hill model and adjusted for each muscle of the musculoskeletal model, was the one used for this work.

Biomechanical models often include two key functional attributes to examine muscle function: the force-velocity and force-length relationship.

3.7.5.1 Force-velocity

The force-velocity property is the relationship between muscle force production relative to the muscle's contraction velocity. From Figure 3.13, it is possible to conclude that the shortening speed and muscle force are inversely related. This translates to an increase in shortening velocity when there is a decrease in muscle force whereas a slower shortening velocity implies a larger force production. Due to the hyperbolic shape of the curve, the variation in force production is narrow for high speeds of shortening, either positive or negative, while for velocities near zero, muscle force can have a wide range of variation

per unit of shortening velocity. Maximum isometric force, F_0^M, is achieved when the shortening velocity is zero. For positive values of shortening speed a concentric contraction occurs, while for negative values an eccentric contraction occurs. The quantification of this property is achieved by a fully activated muscle working against an external load. The maximum velocity of shortening is reached when there is no external load.

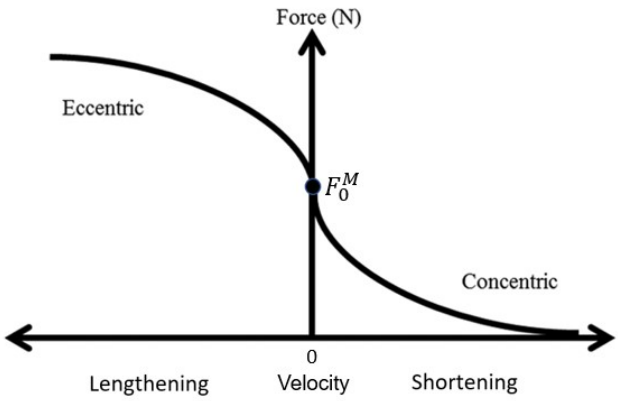

Figure 3.13: Representation of a muscle's force-velocity curve. Adapted from [66].

The mechanism behind this property is due to the time the attachment process of cross-bridges takes to generate force. At slow shortening velocities, there is a higher number of attached cross-bridges, producing more force. On the other hand, with faster shortening velocities, fewer cross-bridges have enough time to attach, generating less force [85].

3.7.5.2 Force-length

The force-length curve allows the understanding of the muscle's ability to produce force throughout a range of lengths (Figure 3.14). Passive force is developed by connective tissues, such as the tendon, to resist increased stretching in the case of no muscle activation. On the other hand, active force is produced when the muscle actively contracts and requires metabolic energy [170]. Through this curve it is possible to obtain the muscle's maximum isometric force, F_0^M, at the point of optimal fiber length, l_o^M, (i.e., active fiber length at which maximum force is produced) represented in Figure 3.14. At this length, the passive force is zero. The total force is the sum of the passive and active forces. At lengths shorter than l_o^M, the total force is purely due to active force, while for longer lengths both passive and active forces contribute to the total force. From Figure 3.14, it is possible to perceive the attainable range of fiber lengths.

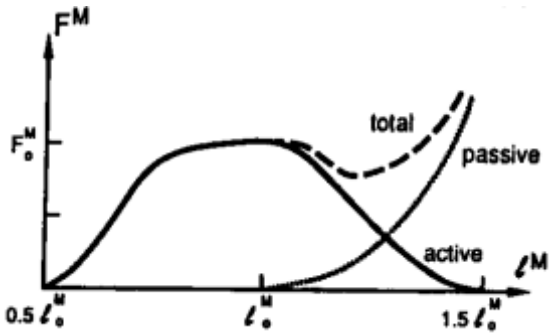

Figure 3.14: Representation of a muscle's force-length curve. From [167].

As it is represented in Figure 3.15, the force-length curve of the sarcomere is defined by four main linear sections. This is because cross-bridge mechanics become the primary factor in the shape of the force-length curve at a single muscle fiber level [19].

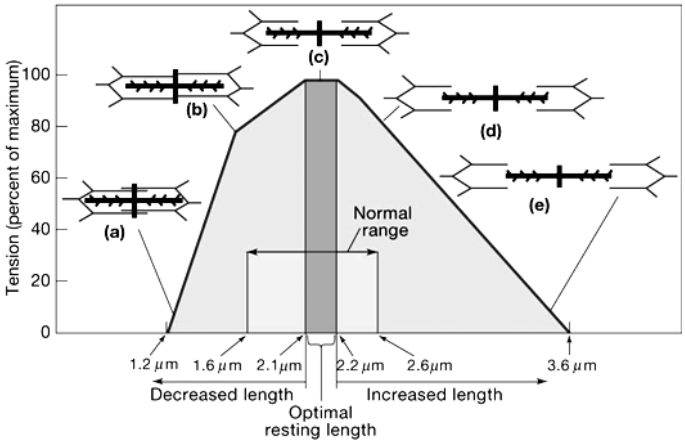

Figure 3.15: Schematic of the sarcomere force-length relationship. From [116].

In the ascending portion, between point (*a*) and (*b*), force production is limited due to excessive overlapping of the myosin and actin filaments, which results in opposing actin filaments to also overlap. This leads to an obstruction of cross-bridge attachments. This limitation diminishes once the sarcomere length gets closer to the optimal fiber length, making force production more efficient. The plateau region, (*c*), represents the sarcomere's optimal length for force production. After this phase, there is a descending region where the actin and myosin filaments pull away from each other, leading to a decrease in cross-bridge formation, resulting in weaker force development [170].

3.7.5.3 Tendon's modeling and force-strain relationship

Most models assume the tendon to incorporate purely elastic properties to reduce complexity. Furthermore, there is a common practice combining the tendon and the muscle's elastic behavior since the tendon is incorporated internally into the muscle structure as well as externally. The properties of both portions are assumed to conduct in the same manner under strain [167]. Zajac [167] describes the tendon model according to two

main parameters: maximum isometric force, F_0^M, and tendon slack length, l_S^T. These two variables express the generic force-strain relationship. Tendon strain refers to the elongation of the tendon relative to its rest length and tendon slack length is the length from which the tendon starts to impose force. The following equation shows how the tendon strain, ε^T, is calculated:

$$\varepsilon^T = \frac{l^T + l_S^T}{l_S^T} \tag{3.4}$$

where l^T is the tendon length, which can be obtained through equation 3.3. Through Figure 3.16, it is possible to observe the three regions of the force-strain relationship: the toe region, the linear region, and the fatigue region.

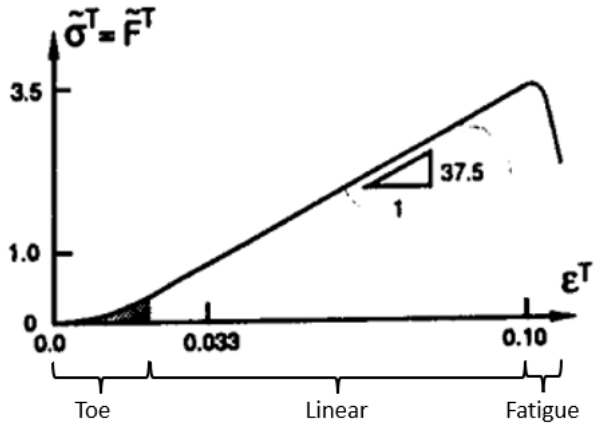

Figure 3.16: Generic tendon force-strain curve. Adapted from [167].

The mechanical loading resulting in the stretch of the tendon alters the conformation of collagen fibrils from their original pattern, leading them to display a behavior represented by the initial nonlinear curve (i.e., the toe region). Next follows the linear section, where an alignment of the fibrils with the direction of the mechanical loading occurs, reflecting the elastic behavior of the tendon. The fatigue stage represents the plastic deformation of the tendon once it exceeds its stretching limit [110].

In order to assure equilibrium between the tendon and the muscle fibers, Thelen's model considers only the toe and linear phases, with the tendon remaining in the linear region instead of displaying fatigue behavior [143].

3.7.5.4 Muscle-tendon actuator

The objective of a muscle-tendon actuator is to incorporate properties capable of modeling activation and contraction dynamics, such as the force-length, force-velocity, and force-strain relationships, in an accurate and realistic setting. To achieve that, the muscle-tendon model encompasses four main parameters: maximum isometric force (F_0^M), optimal muscle fiber length (l_0^M), pennation angle (α_0) at optimal fiber length, and tendon slack length (l_S^T). These parameters allow the computation of the force-length relations

for every actuator in a generic musculoskeletal model [38]. Such parameters vary between actuators and define the muscle and tendon joint function. It is relevant to note that the tendon only takes part in the contractile process, as it is not influenced by muscle activation.

The maximum isometric force is expressed, in equation 3.5, through the multiplication of the muscle's specific tension (σ_0^M) with its physiological cross-sectional area ($PCSA$).

$$F_0^M = \sigma_0^M \times PCSA \tag{3.5}$$

The values of the maximum isometric force were from Anderson and Pandy [4] with the $PCSA$ being provided by Wickiewicz et al. [157] and Friederich and Brand [49]. Since Wickiewicz et al. [157] used elderly cadavers, while Friederich and Brand [49] measure the $PCSA$ on young cadavers, Delp [38] made adjustments and scaled the $PCSA$ values so that the moment curves from both sets of data matched.

The second parameter is the optimal fiber length, which can be expressed through equation 3.6, as being the ratio between the optimal sarcomere length, l_0^S, and the sarcomere length, l^S, multiplied by the muscle fibers length, l^M. This equation assumes that the ratios between the optimal and general length of the sarcomere and the muscle fiber are equivalent [153], [49]. The values for this parameter were the ones reported by Wickiewicz et al. [157]. However, Delp [38] and Wickiewicz et al. [157] used different values for optimal sarcomere length, 2.8 µm and 2.2 µm, respectively, so Delp [38] scaled these values by a factor of 2.8/2.2 to overcome this incongruence.

$$l_0^M = \frac{l_0^S}{l^S} \times l^M \tag{3.6}$$

The pennation angles were also provided by Wickiewicz et al. [157]. This parameter can be obtained from cadaver studies, as well as ultrasound measures [44]. The following equation is used to obtain the pennation angle, α, while assuming that this variable varies according to the muscle's fiber length and that the volume of the muscle remains constant [91].

$$\alpha = \sin^{-1}\left(\frac{l_0^M}{l^M}\sin\alpha_0\right), \quad 0 < \frac{l_0^M}{l^M}\sin\alpha_0 < 1 \tag{3.7}$$

The muscle fiber lengths and pennation angles for muscles not reported by Wickiewicz et al. [157] were included by the ones described by Friederich and Brand [49] in the anatomical position.

Measuring the tendon slack length through experimental procedures is extremely challenging. Therefore, Delp [38] estimated this parameter based on two assumptions. The first is considering that only muscle fibers longer than the optimal fiber length can develop passive force in order to contribute to joint moments. Secondly, the tendon slack length was adjusted in order to equal the joint angles at which the peak total moment of

each joint matched with the *in vivo* joint moments produced during maximum voluntary contractions. It is worth noting that the tendon slack length considers the length of the free tendon, as well as the length of the aponeurosis.

There are other parameters worth mentioning besides the four previously introduced that define the muscle-tendon unit. These parameters characterize the force-length and force-velocity properties of muscles and remain constant for all actuators in the musculoskeletal model. They are included in table A.1.

4

Methodology

This chapter explains the work pipeline implemented to accomplish the objectives set for the present thesis, which is structured into six subsections: **subjects**, where a brief clinical description of the child with CP and the healthy group was made; **data acquisition** and **data processing**, where it was elucidated how the marker coordinates, GRF, and EMG were recorded and processed; **musculoskeletal simulations**, where the theory behind the models and techniques used were clarified; **global gait asymmetry**, where the asymmetry index used for this work is explained; and **statistical validation**, where the statistical tests implemented were described. The acquisition protocol was approved and executed in accordance with the Faculty of Human Kinetics Ethics Committee (CEFMH-2/2019).

4.1 Subjects

For this study, experimental gait data was acquired from one child with spastic diplegia CP and jump gait, classified with level I in GMFCS. Gait data was recorded in three sessions before and after the child underwent a Strayer procedure on the left gastrocnemius, as well as a fasciotomy on the left soleus. Also, botulinum toxin treatment was applied in the left gastrocnemius, and bilaterally in the psoas and hamstrings muscles. The first session of data collection occurred one month before intervention with the intention to be used for gait diagnostic and surgical planning. The second and third session happened 11 months and two years and seven months after the surgical procedure, respectively, to evaluate gait evolution. Subject's physical characteristics are presented in table 4.1. The clinical and biomechanical report stated, before surgery, a constant decrease in pelvis anteversion, and increase in internal rotation on both sides of the hip, and an increase in plantarflexion in both ankles, especially the left one, never reaching dorsiflexion. The left foot motion presented an equinus pattern and increased supination. One year after surgery, the clinical report stated improvements in pelvic tilt, in hip and knee flexion in swing phase, in knee extension during midswing and in ankle dorsiflexion/plantarflexion throughout the gait cycle.

Table 4.1: Subject's age, mass and height at the time of the sessions.

	Age (years)	Weight (kg)	Height (m)
Session 1	8	21	1.23
Session 2	9	20.4	1.28
Session 3	10	27	1.34

The healthy gait data used is from a previous master thesis with a very similar methodology to the one used in this work [22]. It was collected in the same laboratory from 6 typically developed children in the same age (8 ± 1 years), height (127 ± 5 cm), and weight (25 ± 3 kg) category as the child with CP.

4.2 Data acquisition

All data was collected in the Biomechanics and Functional Morphology Laboratory of FMH-UL and the same data collection protocol was used throughout the three sessions. Data acquisition started with a physical examination to assess lower limb range of motion, muscle strength, tone, and spasticity. The acquisition was performed by at least one biomechanist and one clinician (physiotherapist or orthopedic doctor). Following physical examination, overground gait function was assessed using 3D marker-based motion capture, GRF, and muscle EMG measurements, recorded using Qualisys Track Manager software (version 3, Qualisys Inc., Gothenburg, Sweden). The subject was equipped with 27 reflective markers and 4 marker clusters placed in anatomic landmarks (Figure 4.1), according to the calibrated anatomical systems technique (CAST) protocol, used to reconstruct 7 body segments [21]. Marker trajectories were recorded using 14 infrared cameras (Qualisys Oqus 300, Qualysis AB, Gothenburg, Sweden) at 100 Hz. GRF were recorded using three ground embedded force platforms (one Bertec, one AMTI, and one Kistler force plates), at 1000 Hz, represented in Figure 4.2. EMG acquisition was performed through the Trigno Wireless System from Delsys and was submitted to a high-pass filter with a cut-off frequency of 30 Hz and a sampling of 1000 Hz. Prior to gait analysis, a static trial was recorded with the subject in a standing position to allow scaling of a rigid body model according to the subject anthropometry. During the gait trials the child walked at self-selected speed along a 10 m corridor. In the first session, 12 gait trials were successful, whereas, in the second and third sessions, 8 successful trials were recorded.

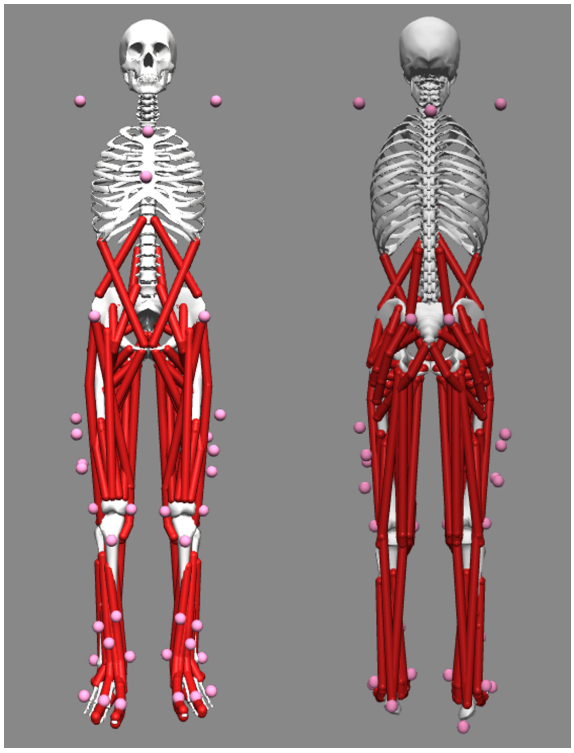

Figure 4.1: Scaled generic musculoskeletal model with the marker set used.

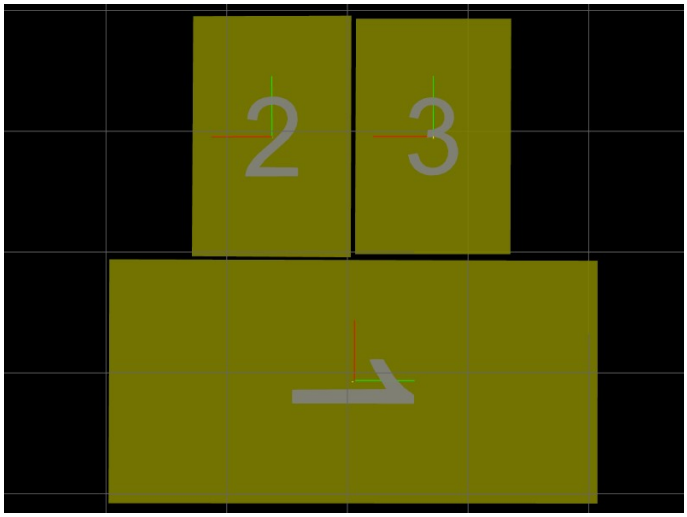

Figure 4.2: Placement of the three force platforms used for this work in Mokka software from the top perspective.

4.3 Data processing

Following data collection, markers were labelled using Qualisys Track Manager software. Marker trajectories, GRF, and EMG signals were then exported to Coordinate 3D (.c3d) files. Using the '.c3d' files, gait events were manually identified for left and right lower limbs using Mokka [101]. Mokka is an open-source and cross-platform software which

allows the analysis of biomechanical data and is part of the Biomechanical ToolKit framework [12]. Among other features, Mokka grants a 3D perspective on marker set data during trials, position of the force platforms, and visualization of GRF. Additionally, it is possible to plot 2D charts with components of 3D data, such as markers, angles, and forces. One the most relevant features is the ability to save important events in the timeline of the trial.

For each gait trial, the single support phase was identified from contra-lateral foot off and contra-lateral foot contact events based on GRF and marker position data. These gait events were selected because the force platforms did not have the dimensions needed to record the GRF of both feet at the beginning and/or end of the stance phase. Therefore, the GRF of the loading response and pre-swing phase (figure 3.2), were not recorded. Thus, for a consistent analysis, the single support period was the section of the gait cycle chosen for further study.

4 out of the 12 trials in the first session were excluded from this work since both feet were in contact with the same force platform during the stance phase. This is because the output from the force platforms is the total resulting GRF vector, which makes it impossible to differentiate the individual GRF vectors of each feet (figure 4.3).

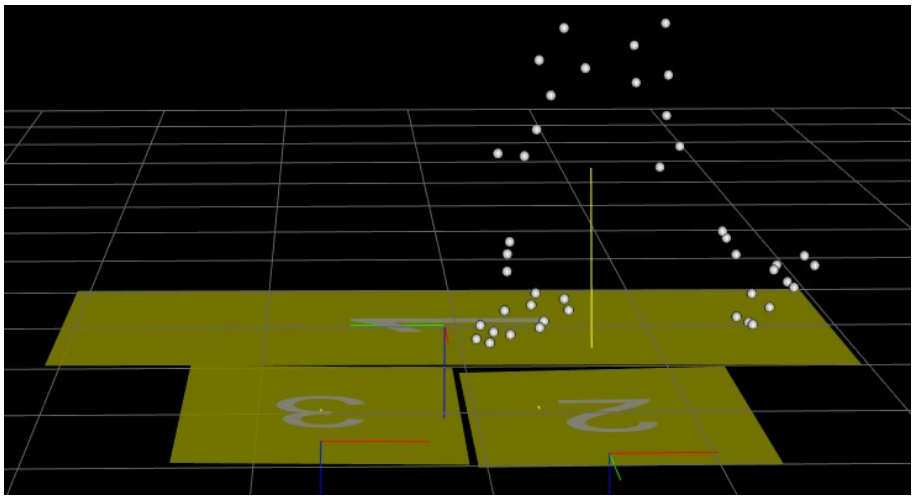

Figure 4.3: Example of a trial removed from further study since both feet were in contact with the same platform.

4.4 Musculoskeletal simulations

As mentioned in 3.6, OpenSim is an open-source software that allows users to perform musculoskeletal simulations [37], [129]. OpenSim combines rigid body models actuated by muscles and reserve torque actuators with signals reflecting GRF (.mot), markers coordinates (.trc), and EMG (.mot) to simulate musculoskeletal interactions. Input files were obtained by converting the information in the '.c3d' files through the use of MOtoNMS (MOtion data elaboration TOolbox for NeuroMusculoSkeletal applications) [94]

and BOPS (Batch OpenSim Processing Scripts) [15] toolboxes. MOToNMS and BOPS are free open-source Matlab toolboxes that allow for faster batch OpenSim implementation and their use is especially convenient when studying data sets with a large number of subjects, trials, or iterative processes. A combination between BOPS and the graphical user interface of OpenSim were used to perform the OpenSim pipeline presented in figure 4.4. OpenSim 4.3 was the version used for this work.

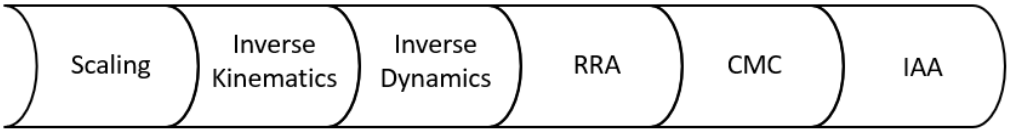

Figure 4.4: All phases of the OpenSim pipeline performed in this work. Residual Reduction Analysis is represented by RRA, Computed Muscle Control by CMC, and Induced Acceleration Analysis by IAA. Available in OpenSim 4.3.

4.4.1 Generic musculoskeletal model

Of the models that are available in the OpenSim platform, the model Gait2392 was the one used during this work. This model was developed by Darryl Thelen (University of Wisconsin-Madison) and Ajay Seth, Frank C. Anderson, and Scott L. Delp (Stanford University). Some features of model Gait2392 include a height of 1.8 m, a mass of 75.16 kg and 92 muscle-tendon actuators to represent 76 muscles in the lower extremities and torso.

4.4.1.1 Bones geometry

When it comes to bone geometry, the surface data relative to the pelvis and thigh was obtained through the marking of the bones surface with a mesh of polygons. With a three-dimensional digitizer, the vertices coordinates were determined. In order to describe the bones of the shank and foot, the data used was from Stredney [138].

4.4.1.2 Joint geometry

The lower body of model Gait2392 is modeled as 11 different segments, one pelvis, two femurs, two tibias, two taluses, two feet and two toe bodies. For each limb, the foot segment incorporates the calcaneus, navicular, cuboid, cuneiforms and metatarsals. Each segment has a fixed reference frame. Figure 4.5 represents the location of each reference frame, with the inclusion of a seventh segment, the patella, which was latter removed by Ajay Seth, who adapted the model in order to avoid kinematic constraints. Table A.2 provides information about the location of the mentioned frames.

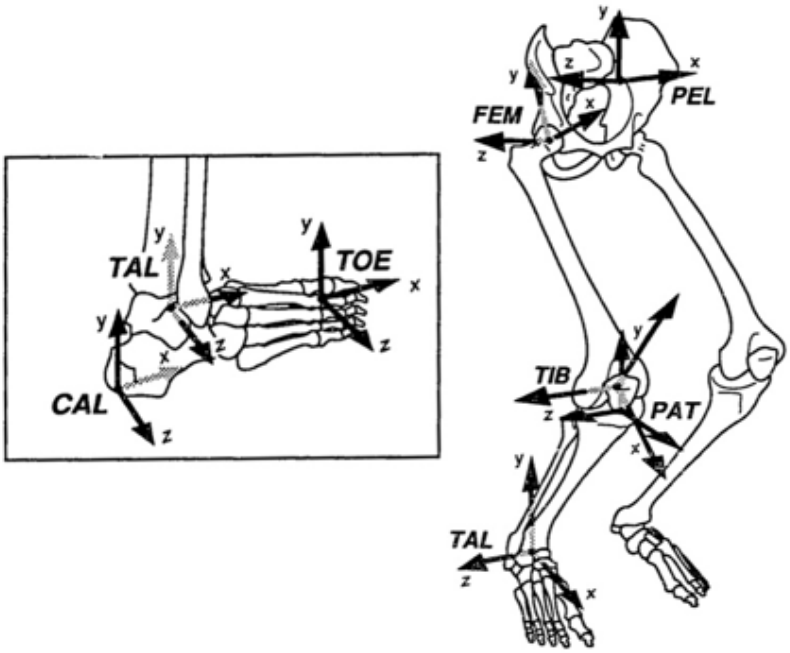

Figure 4.5: Location of the reference frames relative to the body segments. The reference frames are located in the femur (FEM), pelvis (PEL), tibia (TIB), patella (PAT), talus (TAL), toes (TOE), and calcaneus (CAL). From [36].

Before the adaptation by Ajay Seth, there were other contributions, which aimed to overcome the modeling challenges presented by the complex architecture of the knee. Yamaguchi and Zajac [164] developed a simplified version of the knee joint, with only one DOF, in order to reduce the computational cost of calculating the extensor moment arm produced by the quadriceps muscles, accounting for the kinematics of the tibiofemoral and patellofemoral joints in the sagittal plane, along with the patellar levering mechanism. Delp et al. [36] then adapted this model by representing the femoral condyles as ellipses and the tibial plateau as a line segment, making them stay in contact during the knee full range of motion. The point of contact between the tibia and femur were determined according to the knee angle in agreement with the work of Nisell et al. [106].

The hip joint is defined as a ball-and-socket joint. It only allows for rotations of the femoral frame, along the three fixed orthogonal axis in the femoral head, defining the transformation between the reference frames of the pelvis and femur.

Finally, in figure 4.6 is represented the location and orientation of the ankle, subtalar, and metatarsophalangeal joints, which were developed according to the descriptions given by Inman [75]. However, the metatarsophalangeal joint displayed unrealistic motion, since the phalanges separated from the metatarsals. In order to resolve joint disarticulation, an 8-degree rotation around the right-handed vertical axis of the metatarsophalangeal was applied, as stated by Delp [36].

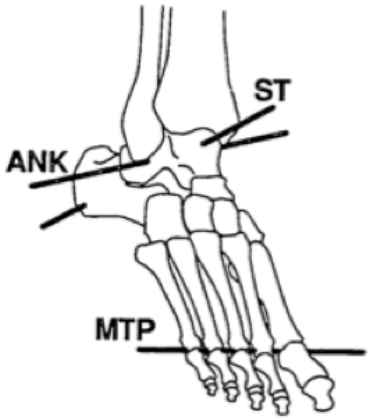

Figure 4.6: Location and orientation of the axes relative to the metatarsophalangeal (MTP), subtalar (ST), and ankle (ANK) joints [36].

4.4.1.3 Muscle geometry

In the model's lower portion, muscle-tendon actuators are defined by a series of line segments, which are based on anatomical landmarks. For most muscles, the origin and insertion points provide enough information to accurately delineate the path of action of the actuator. However, there are muscles that wrap around bone during their range of motion. In these cases, intermediate points, also denominated wrapping points, are introduced in order to achieve a more physiological representation of the muscle path. The number of wrapping points activated varies with body position since each line of action added expands the range of motion of the joint angle [36]. Despite these adjustments, some muscles still pass through bones and might demonstrate unrealistic moment arms during movements at end ranges of motion. However, since walking requires relatively short ranges of motion, the current model was deemed appropriate to implement the musculoskeletal simulations.

4.4.1.4 Inertial properties

Inertial properties of body segments were adapted from a model developed by Anderson and Pandy [4] and segment lengths were based on Delp et al. [36]. With the exception of the hindfeet and toes, mass and inertial properties for all segments were based on average anthropometric data collected from five individuals (age 26 ± 3 years, height 177 ± 3 cm, and weight 70.1 ± 7.8 kg). The parameters of the hindfoot and toes, such as the mass and COM position, were obtained by representing the volume of each segment as a set of connected vertices (table A.3) and scaled by a factor of 1.05626 [4].

4.4.2 Scaling

Scaling is the first stage of musculoskeletal modeling. In this phase, the generic model Gait2392 was scaled to match the anthropometry parameters of the subject. The scale

tool of OpenSim enables adjustments of the body segments and mass properties of the model's scale factors computed by comparing distances between pairs of markers on the generic model and experimental marker positions. The average of multiple scale factors is then used to determine the overall scale factor for each segment. Components connected to body segments, such as muscle actuators and wrapping objects, are also scaled.

Second, the scaling of mass and inertial properties of the body segments was achieved by using the scale factors and input target mass while preserving mass distribution. This allows the mass of the scaled model to correspond to the input target mass.

Finally, components that are length dependent, such as muscle actuators, are also scaled. Parameters that defined these components, such as optimal fibre length and tendon slack length, are scaled by a factor that is determined by the ratio of the length before and after scaling.

When analysing muscle strength of a muscle-tendon unit, a crucial parameter to be considered is the maximum isometric force of each muscle. This is especially relevant when studying children, since the musculoskeletal model used was developed based on data from adult specimens [118]. Maximum isometric force is not scaled during the scaling procedure, and measuring individual muscle forces through a dynamometer is not possible since the device returns the net torque of all the muscles acting on the joint [27]. Maximum isometric force of a muscle could be estimated from MRI driven muscle size [103], [11] by multiplying the physiological cross-sectional area of the muscle by the maximum muscle stress, which is frequently referred to as specific tension [167], [36], [52]. However, the cost associated with MRI scans and variation within the same muscle of some parameters, such as pennation angle and fiber lengths, render this approach difficult to implement.

To overcome these obstacles, the implementation of methods for scaling the peak isometric force became a point of interest. Correa and Pandy [27] tested equation 4.1, on the assumption that muscle volume and body mass are linearly related. This hypothesis was then confirmed by their results. This equation has as input the mass (M) and muscle-tendon lengths (l_{MT}) of the subject and generic model, as well as the maximum isometric force of the generic model $\left(F_{max}^{generic}\right)$. Krogt et al. [84] used equation 4.2 with the same input with the exception of the muscle-tendon lengths.

$$F_{max}^{scaled} = F_{max}^{generic} \times \frac{M^{scaled}}{M^{generic}} \times \frac{l_{MT}^{generic}}{l_{MT}^{scaled}} \tag{4.1}$$

$$F_{max}^{scaled} = F_{max}^{generic} \times \left(\frac{M^{scaled}}{M^{generic}}\right)^{\frac{2}{3}} \tag{4.2}$$

Kainz et al. [78] evaluated both equations and concluded that both approaches had similar results and resulted in successful simulations, meaning either one could be used. For this work, the equation chosen to scale the maximum isometric forces of all muscles was equation 4.2.

Another important aspect of the scaling procedure is marker registration [40]. To allow for an accurate representation of experimental markers in the model frame, the best fit for the marker coordinates is achieved by minimization of a weighted sum of each marker's experimental and model positions. The influence of a marker position on the overall sum of squares algorithm depends on its relative weight. Because placing markers in clearly defined bony landmarks closer to the skin surface is more accurate, higher weights were used in markers placed in these landmarks. Marker clusters and other markers over non-specific body segment areas were weighted zero and allowed to move to their respective parent frame to match their experimental counterpart.

In order to calculate the hip joint centers, the regression equations proposed by Harrington et al. [65] were used, while for the ankle and knee joint centers were calculated as being the average location between the markers placed in the lateral and medial malleoli and femoral condyles, respectively.

4.4.3 Inverse kinematics

Kinematics is defined as the study of motion without regard for the forces or torques acting on a body [152]. The IK tool in OpenSim allows for the study of kinematics by solving a weighted least squares problem to minimize the error between the experimental and modelled marker positions, in each frame of motion. In order to achieve this goal, the following objective function is applied:

$$\min_{q}\left[\sum_{i\in markers} w_i\left\|x_i^{exp}-x_i\left(q\right)\right\|^2+\sum_{j\in unprescribed\,coords} w_j\left(q_j^{exp}-q_j\right)^2\right] \tag{4.3}$$

where q is the output vector of generalized coordinates, x_i^{exp} is the experimental position of marker i, $x_i(q)$ is the position of the corresponding model marker and q_j^{exp} the experimental value for coordinate j. This equation also relies on user defined marker weights (w_i) and coordinate weights (w_j). This tool returns a motion file with the trajectories of generalized coordinates (joint angles and/or translations).

To run the IK tool higher weights were used for markers located and organized in clusters along the body segments instead of bony landmarks, since tracking these clusters increases reliability and reduced kinematic errors [95].

Joint kinematics from healthy children was calculated through another software, Visual 3D. This software includes an offset of 12 degrees in the hip and pelvis in the sagittal plane when compared to OpenSim, which was taken into account when analyzing the results.

4.4.4 Inverse dynamics

Once body kinematics were calculated, the following phase consists in performing an ID analysis. This tool uses body kinematics and measured external loads to compute

generalized forces, such as the net joint moments and forces, in all joints of the model during a provided motion. These values are obtained by solving the following equation of motion:

$$M(q)\ddot{q} + C(q,\dot{q}) + G(q) = \tau \tag{4.4}$$

where q represents the vectors of generalized positions, $\dot{q}$ the velocities, and $\ddot{q}$ the accelerations. The system mass matrix is represented by M, the gravitational forces by G, and the Coriolis and centrifugal forces by C. Since the variables on the left side are known, the ID tool iteratively solves equation 4.4 to determine the unknown generalized forces, represented by τ.

The joint moments obtained through ID tool represent the net internal torques in each joint's axis, which are developed by internal forces. In order to maintain balance during motion, these moments counter the external moments produced by outside forces acting upon the body (e.g., GRF). As an example, in order for the ankle joint to sustain the equinus during jump gait, it needs to produce a plantarflexor moment to contradict the dorsiflexor moment imposed by the GRF, which can be demonstrated in figure 5.3.

4.4.5 Residual reduction algorithm

When modelling body kinematics and kinetics, undesired errors might occur resulting from modeling assumptions or inaccuracies in mass distribution, causing dynamic inconsistencies between the measured kinematics and the GRF. These limitations are reckoned with the introduction of non-physical compensatory forces called residuals. The following equation presents a reformulated Newton's second law in order to include these residual forces:

$$\vec{F}_{exp} + \vec{F}_{Residual} = \sum_{i=1}^{segments} m_i(\vec{a}_i - \vec{g}) \tag{4.5}$$

Where m_i is the mass, $\vec{a}_i$ the acceleration of the body segment i, and $\vec{g}$ the acceleration of gravity. When it comes to the residual moments ($M_{residual}$), a corresponding equation to 4.5 is applied. Residual forces and moments represent the three translational (F_x, F_y, F_z) and the three rotational (M_x, M_y, M_z) DOF between the ground and the pelvis. In OpenSim, the x, y, and z axes indicate the anterior/posterior, axial, medial-lateral directions, respectively. Therefore, the pelvis list, pelvis rotation, and pelvis tilt are DOF represented by M_x, M_y, and M_z, respectively. In order to keep these residual forces and moments at a minimum, the Residual Reduction Algorithm (RRA) tool was used. This tool resorts to the output files of the IK tool to obtain the model's kinematics, while also applying a filter of 6 Hz (figure 4.7).

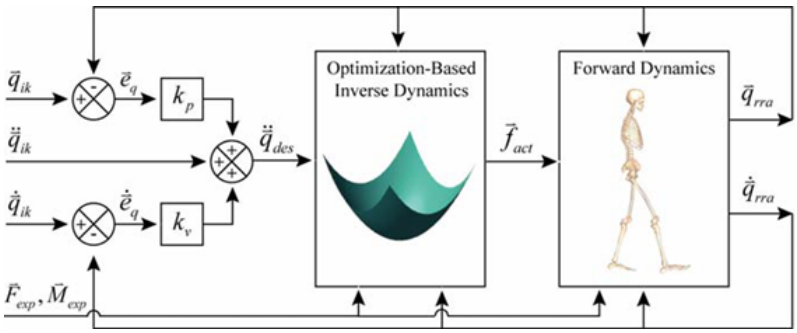

Figure 4.7: Representation of the Residual Reduction Algorithm. From [6].

The RRA algorithm starts with the original body kinematics calculated from the IK tool and advances in time in short intervals until it reaches the final time frame established by the user. Through each time step, the necessary actuator forces, f_{act}, are computed to move the model in order to match the desired configuration at the end of the current time step, determined by the IK tool. This process is done by selecting the forces and moments that minimize the following objective function:

$$J = \sum_{i=1}^{n_x} v_i \left(\frac{f_{act,i}}{f_{act,i}^{opt}} \right)^2 + \sum_{i=1}^{n_q} w_i \left(\ddot{q}_{des,i}(t+T) - \ddot{q}_{rra,i}(t) \right)^2 \tag{4.6}$$

where $f_{act,i}$ and $f_{act,i}^{opt}$ represent the force and the optimal force of the actuator i, while v_i and w_i represent the weight of the actuator stresses and the acceleration errors, respectively. Equation (4.6) is divided in to two parcels. The summation of the left side minimizes the forces of the actuators, while the parcel on the right side minimizes the errors between the accelerations of the model and the desired ones, $\ddot{q}_{des,i}(t+T)$, which are determined by equation 4.7.

$$\ddot{q}_{des,i}(t+T) = \ddot{q}_{ik,i}(t+T) + k_v\left(\dot{q}_{ik,i}(t) - \dot{q}_{rra,i}(t)\right) + k_p\left(q_{ik,i}(t) - q_{rra,i}(t)\right) \tag{4.7}$$

Where k_v and k_p are the gains of velocity and position errors, respectively.

The aim of RRA is to minimize the residuals, while minimally adjusting body accelerations. However, a balance between these two objectives needs to be maintained. This is because a considerable variation of the residuals might cause the kinematic data to deviate from the original data. This was achieved by editing the parameters in the input files of this tool, namely the weights to track coordinates in the tasks' file and optimal forces of residual forces and moments in the actuators' file.

The algorithm then computes the average values for every residual actuator during the task. It follows a mass center adjustment of a selected segment. The torso is, in most cases, the chosen segment due to its large dimensions relative to the other body segments, which leads to a higher probability of mass distribution inaccuracies. Adjustments are calculated using the average of medial-lateral and antero-posterior residual moments. The following equations state the mentioned adjustments:

$$t_x = \frac{dM_z}{mg} \tag{4.8}$$

$$t_z = \frac{dM_x}{mg} \tag{4.9}$$

The recommended mass adjustment for the model mass is determined by the average vertical residual force, F_y, calculated through equation 4.10.

$$dm = \frac{F_y}{g} \tag{4.10}$$

Mass segment adjustments are calculated as a proportion of dm and implemented in a separate step. The mass adjusted model was then used in further RRA iterations, until the residual forces and moments were below threshold values of OpenSim.

The validation of the RRA tool results was done by comparing the maximum, minimum, and root mean square values of the residuals forces and moments with the ones obtained through the ID tool. A noticeable reduction in peak residuals should occur. Furthermore, the position errors are recommended to be below certain thresholds established by OpenSim guidelines for walking tasks.

4.4.6 Computed muscle control

After completing the RRA step, the Computed Muscle Control (CMC) tool was used in order to determine the muscle excitations necessary for the modified models to achieve the desired kinematics. This tool resorts to the CMC algorithm developed by Thelen et al. [145], which consists in implementing both static optimization as well as a proportional-derivative control during a forward dynamic simulation. The following figure presents a schematic representation of the CMC algorithm.

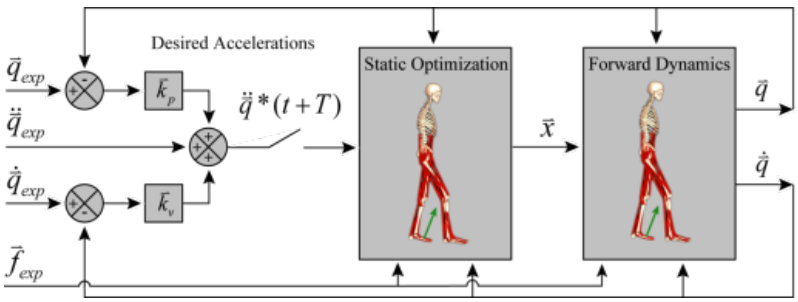

Figure 4.8: Schematic of the Computed Muscle Control pipeline. From [145].

This process occurs at each integrating step with four main phases. In the first phase, the experimental kinematics and current kinematic state of the model are used to compute a set of desired accelerations ($\ddot{\vec{q}}_{des}$). Once this is achieved, the set of accelerations is used to drive the coordinates of the model ($\vec{q}$) to track the experimental-derived coordinates ($\vec{q}_{exp}$). This process is obtained through the proportional-derivative control law (4.11).

$$\ddot{\vec{q}}_{des}(t+T) = \ddot{\vec{q}}_{exp}(t+T) + \vec{k_v}\left[\dot{\vec{q}}_{exp}(t) - \dot{\vec{q}}(t)\right] + \vec{k_p}\left[\vec{q}_{exp}(t) - \vec{q}(t)\right] \tag{4.11}$$

Where $\vec{k_v}$ and $\vec{k_p}$ are the feedback gains on velocity and position errors, respectively. The T in equation 4.11 accounts for the delay, in seconds, that muscle forces take to be applied in the body. Taking that into account, the CMC algorithm is used at each time step T in order to compute the desired accelerations. The errors of velocity and position are driven to zero after the desired accelerations are calculated. For this to happen, the feedback gain, $\vec{k_v}$, is defined through equation 4.12.

$$\vec{k_v} = 2\sqrt{\vec{k_p}} \tag{4.12}$$

In an effort to ensure the reduction of tracking errors to reach zero, in musculoskeletal models, $\vec{k_v} = 20$ and $\vec{k_p} = 100$ are the standard used values [71].

In order to produce the muscle forces necessary to attain the desired accelerations of the first step, a set of actuator controls are computed through a process of static optimization. This process ensures that the load in synergistic actuators is distributed accordingly. In the CMC tool, there are two formulas of static optimization and both were explored in this work. The first one, slow target optimization, is defined as the sum of squared actuator controls plus the sum of the desired acceleration errors, in order to minimize the cost function, J, as follows:

$$J = \sum_{i=1}^{n_x} x_i^2 + \sum_{j=1}^{n_q} w_j(\ddot{q}_{des,j} - \ddot{q}_j)^2 \tag{4.13}$$

The second one, fast target optimization, is characterized by the sum of squared controls (4.14) magnified by a set of equality constraints (4.15), $C_j = 0$, which guarantees the results of the desired accelerations to be within the threshold defined by the optimizer.

$$J = \sum_{i=1}^{n_x} x_i^2 \tag{4.14}$$

$$C_j = \ddot{q}_{des\,j} - \ddot{q}_j \tag{4.15}$$

The standard method of optimization is fast target optimization. However, when used, peaks in residuals far exceeding the acceptable threshold were found in the data that predated the surgical procedure. Despite major efforts, including increasing the value for maximum excitation for reserves and residuals, decreasing weights on coordinates, and lowering optimal forces for reserves, these peaks still remained present. Due to these reasons, slow target optimization was implemented, since OpenSim's documentation suggests that it may be more appropriate for subjects with pathologies [53]. As a result, the above mentioned peaks stopped appearing. The residual forces, moments, errors and reserves were then verified to be within the acceptable range and the kinematics from

RRA were similar to the kinematics from CMC. With these factors in mind, this optimization process was chosen. In order to maintain consistency, slow target optimization was applied in all sessions.

The third step consists in determining muscle excitations by inverting activation and contraction dynamics of the muscle [144]. Finally, the muscle excitations previously calculated serve as input to perform a forward dynamic analysis at each time interval of T, advancing until the simulation reaches its end.

4.4.7 EMG validation

One of the recommendations made by OpenSim and Hicks et al. [67] is to compare the muscular activations from CMC with the available surface EMG signals. In the first and third sessions, the muscles with EMG aquisition were the gluteus medius, rectus femoris, adductor longus, bicep femoris, tibialis anterior, and gastrocnemius medialis. In the second session, instead of the bicep femoris, signal acquisition was obtained for the semitendinosus. These muscles are primary contributors to force development during the gait cycle. The EMG signal was filtered with a moving mean function to remove noise. The normalization of the EMG signals was achieved considering a task where the muscle would exert its maximum activation capability. Since the task at hand is walking, the peak activation required does not translate into the maximum activation that each muscle is capable, leading to an overestimation of EMG activity. Therefore, the comparison was based on the shape rather than intensity between the EMG signals and CMC activation results.

4.4.8 Induced acceleration analysis

Multijoint motion has inherent complexity, due to muscles producing acceleration in all joints and segments, including those to which they do not span or attach (i.e., inertial coupling) [168]. In order to investigate how muscle forces affect joint and mass center accelerations during the single support phase, IAA was performed. This method employs foot-ground contact models to decompose GRF and moments [63]. The IAA tool from OpenSim requires the states and controls originated from CMC as well as the file with experimental GRF. The equation of motion that governs this analysis is represented by equation 4.16.

$$[M]\ddot{q} = G(q) + V(q,\dot{q}) + S(q,\dot{q}) + [R]f \tag{4.16}$$

Where $[M]$ is the mass matrix, q are the generalised coordinates, $G(q)$ accounts for the generalised forces due to gravity, $V(q,\dot{q})$ regards the forces resulting from Coriolis and centrifugal effects, $S(q,\dot{q})$ represents the generalised forces due to contact elements and $[R]$ is the transmission matrix containing the muscle's moment arms which transforms the muscle force, f, into a generalised force.

By manipulating 4.16, it becomes possible to describe the contribution of any force, F_i, to the total acceleration.

$$\ddot{q}_i = [M]^{-1}\left\{F_i\right\} \tag{4.17}$$

However, internal forces, such as muscle forces, do not accelerate the mass center directly. The IAA algorithm analyses the variation of the mass center acceleration due to the influence reaction forces have with the environment, not the internal forces themselves. Therefore, it becomes necessary to decompose the external reaction forces in order to obtain the induced contribution of each internal force relative, not only to the external reaction force, but also to the acceleration of the system. Hence, by manipulating the former equation, it is possible to obtain equation 4.18, which represents the individual contribution of any element to the mass center acceleration.

$$\ddot{q}_i = [M]^{-1}\left\{F_i + S_i\right\} \tag{4.18}$$

Where F_i represents, in this case, the muscle forces, and S_i represents the forces relative to the interaction between the model and the environment, which are the GRF. Both variables are unknown. To overcome this obstacle, the OpenSim software implements kinematic constraints to replace the force contributions accounted by S_i [62]. The equation of motion 4.16 is altered to include these kinematic constraints as follows:

$$[M]\ddot{q} + [C]^T\lambda = G(q) + V(q,\dot{q}) + [R]f \tag{4.19}$$

Where $[C]^T$ represents the constraint matrix and λ the constraint forces. Together with the following equation, the constraint reaction forces are solved.

$$[C]\ddot{q} = B(t,q,\dot{q}) \tag{4.20}$$

Where $B(t,q,\dot{q})$ describes the velocities and positions of the constraint equations as a function of time.

There are several models for constraints that can be used in IAA. Hamner et al. [63], tested if the point, weld, and rolling constraints could accurately simulate a foot-ground contact model in IAA. Simulations were made for walking, running and crouch gait. The study concluded that the point and weld constraint produced inaccurate reaction moments and resulted in conflicting interpretations of muscle functions. However, the rolling constraint was the only one able to reproduce accurate results. Therefore, the rolling constraint, denominated "RollingOnSurface" in OpenSim, was the one used in this work. This constraint imposes restrictions on a rolling body when in contact with a plane defined on another body [62], which, in this case, is the ground. The next four equations define the kinematic characteristics of this constraint.

$$\rho_y(q) = 0 \tag{4.21}$$

$$\dot{\rho_x}(q,\dot{q}) = 0 \tag{4.22}$$

$$\dot{\rho_z}(q,\dot{q}) = 0 \tag{4.23}$$

$$\dot{w_y}(q,\dot{q}) = 0 \tag{4.24}$$

The first equation (4.21), defines a non-penetrating constraint, the second one (4.22) an anterior/posterior no-slip constraint, the third one (4.23) a mediolateral no-slip constraint and the last one (4.24) a no-twist constraint as mentioned in [62].

When implementing the IAA simulation in the present work, 3 out of the 8 trials of the first session did not complete a successful run. This was due to at least one of the feet contacting two platforms at the same time during the stance phase. When an event like this occurs, it is difficult for the contact model to establish the kinematics constraints previously mentioned, compromising the success of the simulation.

4.5 Global gait asymmetry

In order to study the evolution of gait symmetry before and after surgery, the GGA index was used [20]. This index allows for a symmetry analysis of the entire gait cycle or a selected phase of it, being able to differentiate the contribution of each DOF to the gait asymmetry. The output score is a positive number and increases, without any limit, with higher levels of asymmetry. Therefore, zero represents perfect symmetry. The calculation is done through the following equation:

$$GGA = \sum_{v=v_1}^{v_{15}} \sqrt{\sum_{t=t_1}^{t_{101}} [x_l(t) - x_r(t)]^2} \tag{4.25}$$

where v are the angular variables, t represents time instances normalized in 101 time components, x_l and x_r are the values for the left and right side, respectively. The angular variables chosen for further study were the DOF of the ankle, hip, knee, and pelvis. Angular variables were time normalized in both the right and left legs' gait cycles (i.e. during the single support phase). The GGA was computed for each trial and averaged to obtain the final GGA score for each session. The value for each angular variable that contributed to the GGA was also investigated separately to gain insights into the contribution of each DOF.

4.6 Statistical analysis

To assess the existence of significant differences among the CP sessions and between the CP and healthy gait results, two statistical tests were applied. On account of low quantity

of samples, nominal variables, and the uncertainty of normal distribution, the tests chosen were non-parametric tests. Due to performing distinct gait patterns, the samples between healthy and jump gait were considered independent and the Mann-Whitney test was used to compare the means of each group. When making three comparisons in each variable among CP sessions, a Bonferroni correction was implemented with a significance level of $p < 0.017$. When the number of comparisons were two, the p-value was 0.05. The samples between CP sessions were considered paired and the Wilcoxon Signed-Rank test was used to compare the group means.

5

Results

5.1 Joint kinematics and moments

The analysis and comparison of joint angles and moments of the CP child with those of typically developing children will provide helpful insights to understand gait symmetry and muscle function. The results from the IK tool during the gait cycle of the hip, knee, and ankle in the sagittal plane and the pelvis in the frontal, transverse, and sagittal plane are present in Figure 5.1 and 5.2, respectively, of the CP and healthy children. Figure 5.3 presents the results from ID tool of the net moments of the hip, knee, and ankle also in the sagittal plane during the single support phase. These figures show the kinematics and kinetics of the most relevant DOF of jump gait in the sagittal plane, which are hip and knee flexion/extension, ankle plantarflexion/dorsiflexion, and pelvis tilt. Besides, the kinematics of the pelvis list and rotation are also displayed as they are also going to be used to study gait symmetry.

Compared with typically developed children, pre-surgery results show the CP child walked with increased knee flexion and ankle plantarflexion. The hip joint appears to have accentuated extension on the right side, and, on the left side, some trials present an increase in hip flexion during late stance and pre-swing. On the other hand, the pelvis shows increased posterior tilt throughout the gait cycle.

Results after surgery show most joint kinematics to approach those of typically developed children. Out of the two sessions, the session one year post-surgery seems to show kinematic results that are more congruent with healthy gait, with the hip and pelvis tilt overlapping with unimpaired gait. The ankle joint is closest to resembling typical behavior in the one year after surgery out of the three sessions. Two years after surgery, a noticeable decline in kinematic resemblance with the healthy population occurs with the pelvis tilt presenting more posterior movement and the ankle joint with more accentuated plantarflexion during the gait cycle. An increase in extension was also noticeable in the hip. The knee joint showed an increase in flexion throughout the gait cycle, with the exception of the late stance which shows a decrease in knee flexion.

Pre and post-surgery, the child with CP walked with increased hip extensor moment,

especially during mid stance, when compared to healthy children. The knee presented a flexor moment throughout mid stance and an abnormal extensor moment in the final phases of single support period. The ankle shows a plantarflexor moment during single support period while presenting higher torque values at the beginning of this period and lower values going into the push-off phase when compared to those of unimpaired gait. Ankle dorsiflexion moments of the lower limb submitted to gastrocnemius recession were calculated to better understand the restoration of ankle function post-surgery. Mean peak ankle dorsiflexion moment increased 9.9% in the one year post-surgery, and 61.8% two years post-surgery, when compared to the preoperative session.

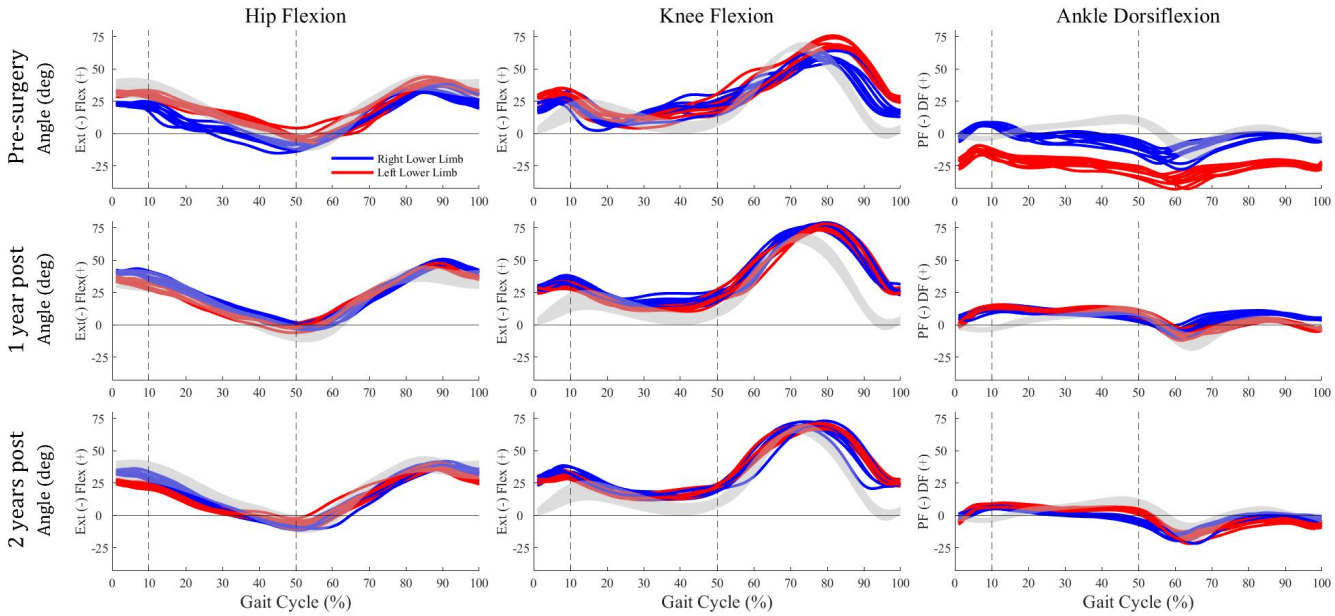

Figure 5.1: Sagittal joint kinematics of the hip, knee, and ankle during the gait cycle of the CP child, pre, 1 year post, and 2 years post-surgical intervention. Grey region indicates the kinematics of typically developed children. The single support period is between the vertical dashed lines.

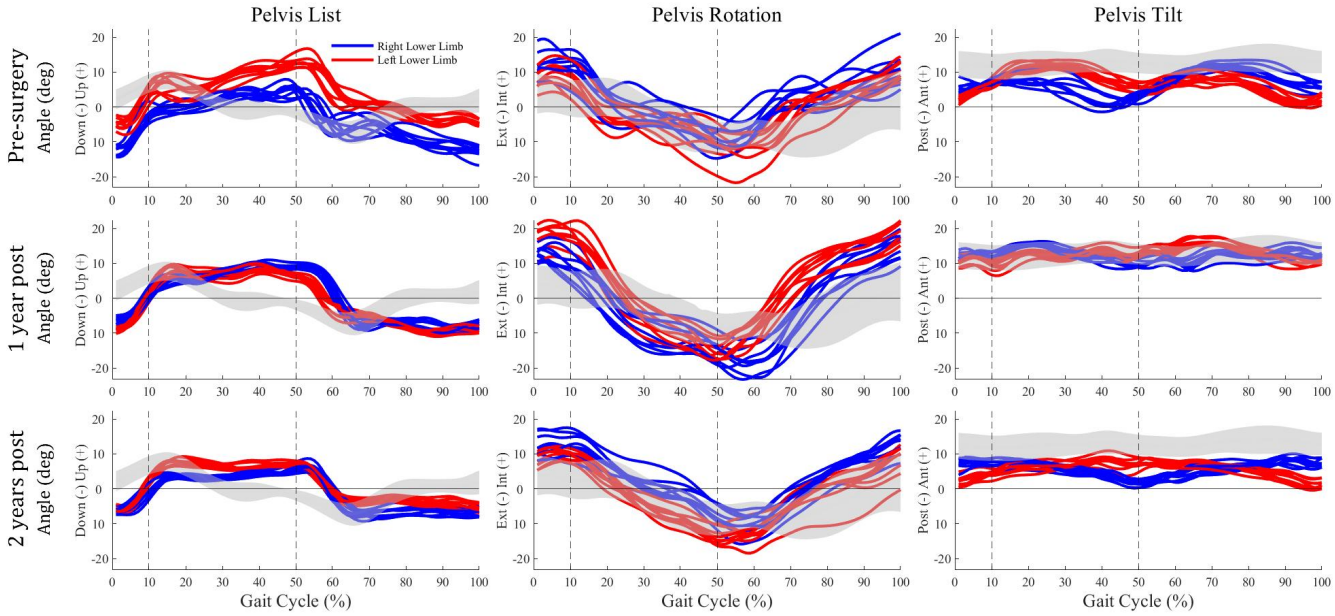

Figure 5.2: Frontal, transverse, and sagittal joint kinematics of the pelvis during the gait cycle of the CP child, pre, 1 year post, and 2 years post-surgical intervention. Grey region indicates the kinematics of typically developed children. The single support period is between the vertical dashed lines.

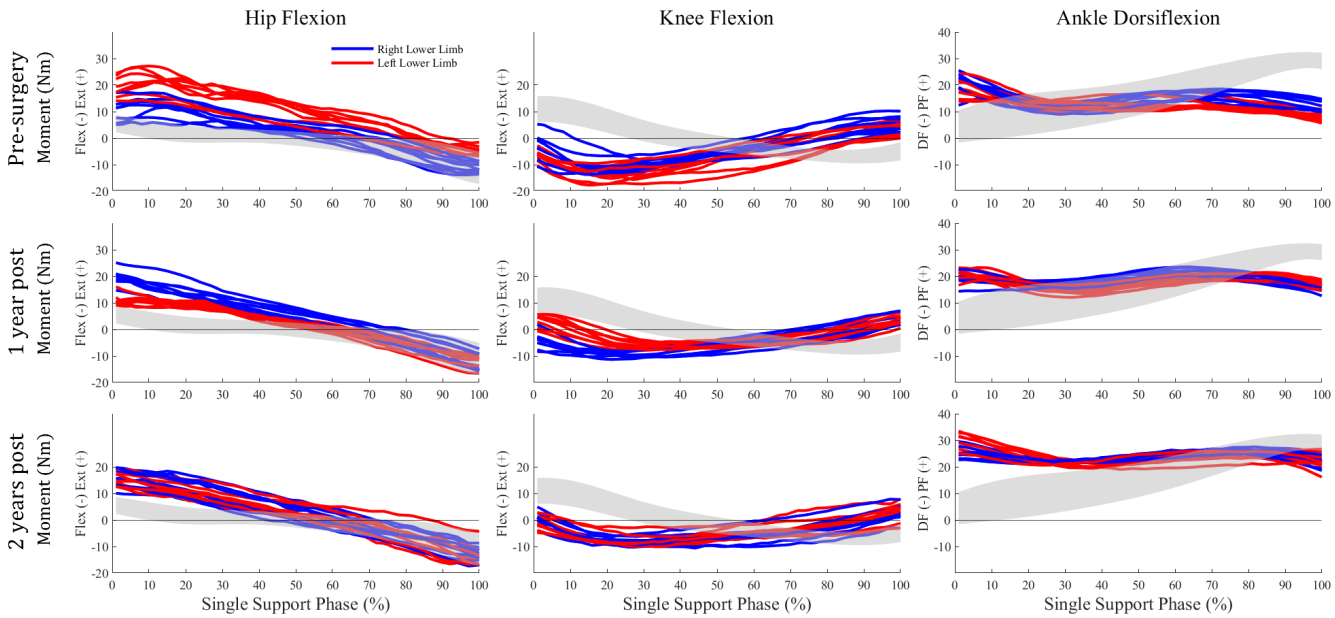

Figure 5.3: Sagittal joint moments of the sessions during the single support period of the CP child, pre, 1 year post, and 2 years post-surgical intervention. Grey region indicates the kinetics of typically developed children.

5.2 Global gait asymmetry index

One of the objectives of this study was to assess the asymmetry between supports. Regarding the time-varying angles curves, it is possible to detect its presence in hip and knee flexion angles, and a more accentuated asymmetry in ankle dorsiflexion of approximately 20 degrees in Figure 5.1, during the preoperative session. All DOF appear to show a decrease in asymmetry in the postoperative sessions, especially the ankle joint, when compared to the preoperative session. Joint moments also show a reduction in asymmetry post-surgery, despite not resembling those seen during healthy gait.

In order to provide a quantitative analysis for the evolution of asymmetry, the GGA index was used. Figure 5.4 reveals a reduction in gait asymmetry of the CP child following surgical procedure. Statistically significant differences were present between the session before the intervention with the two sessions after it. GGA index was significantly lower for the CP child two years after surgery compared with that of healthy population.

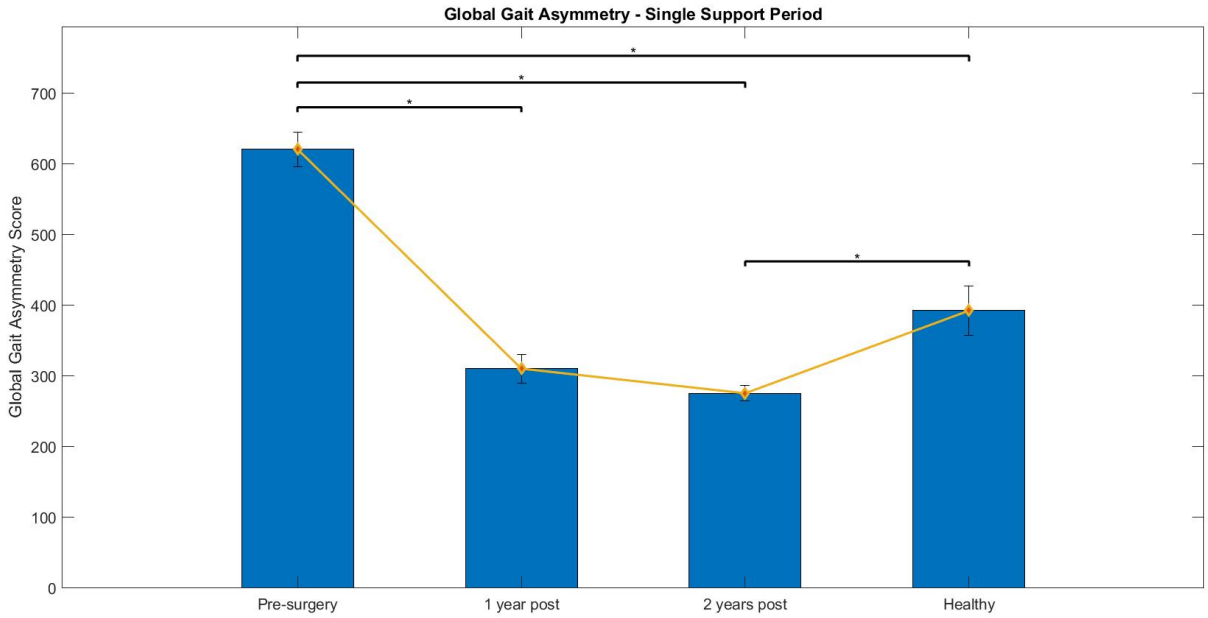

Figure 5.4: Mean GGA index of the sessions pre, 1 year post, and 2 years post-surgical intervention during the single support period. Error bars represent standard error. Asterisks represent significant statistical differences.

By decomposing the GGA index, it becomes possible to evaluate the contribution of each DOF to the overall gait asymmetry. Results are presented in Figure 5.5. The major contributor to gait asymmetry was the ankle dorsiflexion/plantarflexion DOF, which improved to unimpaired levels of asymmetry post-surgery.

The knee angle asymmetry two years after the intervention also improved to levels lower than those with typically developed gait. The sagittal plane hip angles two

years after surgery evolved to having levels of asymmetry comparable to those seen in healthy gait. Hip frontal plane asymmetry score in the child with CP pre-surgery was not significantly different from that of typically developed children. However, two years following surgery, hip frontal plane asymmetry showed significant decreases compared with pre-surgery and values much closer to those seen in typically developed children. Hip rotation showed no statistical differences with healthy gait before and after surgery. After two years of surgery, only the pelvis list showed a statistically significant reduction compared to pre-surgery. Pelvis rotation and list two years after surgery showed lower levels of asymmetry than healthy gait, whereas pelvis tilt still showed greater asymmetry compared with healthy gait.

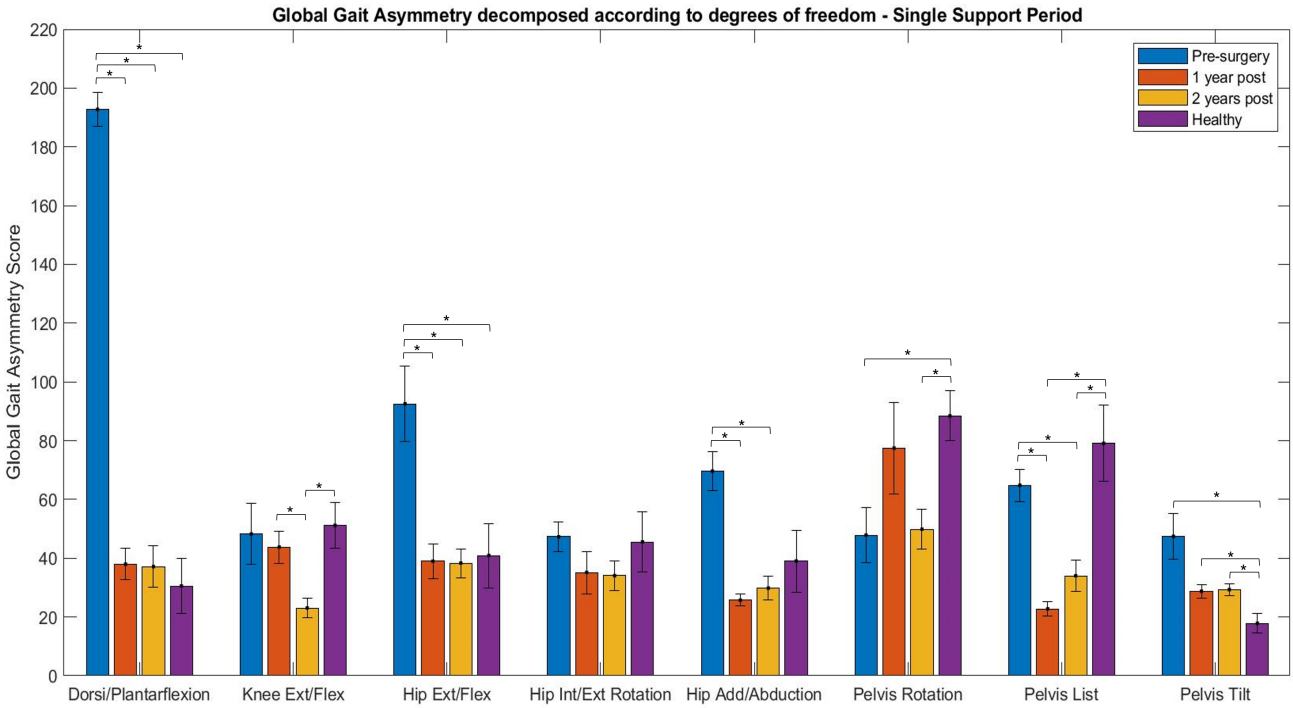

Figure 5.5: Comparing the DOF of the GGA index of the sessions pre, 1 year post, and 2 years post-surgical intervention during the single support period. Error bars represent standard error. Asterisks represent significant statistical differences.

5.3 Residual reduction algorithm

The residual reduction algorithm was performed to diminish the inaccuracies relative to kinematic forces and moments, and model assumptions (e.g., absence of arms in the model). For the majority of trials, at least two iterations of the RRA tool were necessary to achieve significant residual reductions. For all the tables included in the present work, trials identified with the letter "a"and "b"are relative to the right and left lower limbs'

trials, respectively.

Tables A.4, A.5, and A.6 show a reduction in peak residual forces in the trials of all three sessions. The fore-aft direction (FX) exhibited a decrease between 49.2% and 98.9% in the first session, 93.1% and 98.4% in the second session, and 87.7% and 96% in the third session. The vertical direction (FY) displayed a decrease between 69.1% and 99.7%, 97.1% and 99.8%, and 97.8% and 99.8% for the first, second, and third sessions, respectively. In the mediolateral direction (FZ), a reduction within the range of 13.7% and 98.7% in the first session, 88.4% and 97.1% in the second session, and 91.1% and 97.7% in the third session. It is relevant to note that the second lowest decrease after 13.7%, in the first session, was 72.42%. All values of peak residual forces and root mean square are within the optimal limit recommended in the OpenSim documentation (0 to 10 N and 0 to 5 N, respectively).

The decrease of peak residual moments was a more challenging task, becoming unfeasible in some simulations, especially in the vertical direction (MY). The reduction of peak residual moments for the fore-aft direction (MX) presented values in the middle of 18.8% and 94.9% for the first session, with one trial demonstrating an increase of 22.4%. For the second session, the decreased values ranged between 43.2% and 80.5%, and for the third session, reduction ranged between 13% and 72.1%. In the vertical direction, the first and third sessions displayed an increase in residuals in some trials up to 25.1% and 61%, while the highest decrease were 57.5% and 19.4%, respectively. In the second session, the values were reduced between 28.8% and 75.9%. Lastly, in mediolateral direction (MZ), decrease between 30.1% and 88.3% were verified, with one trial presenting an increase of 4.3%, relative to the first session. For the second and third, reduced residuals ranged between 28.8% and 75.9%, and 63.5% and 90%, respectively. Even though peak residual moments increased in a few trials, all peaks were well within the established limits recommended in the OpenSim documentation (0-50 Nm). The same validation was done for the root mean square values, which were all below the suggested threshold of 30 Nm.

The abnormal peaks of the residual moments might have occurred due to discrepancies between GRF and kinematic data. Errors between the force platforms' relative position and the reference frames of the foot might also influence these increases, especially in the vertical axis.

From tables A.7 to A.12, the positional errors of all DOF are displayed. The majority of errors are within the optimal threshold of 2°, with some exceptions (up to 2.6° higher), although these remain under the acceptable limit of 5° recommended in the OpenSim documentation. The translational errors of the pelvis are also below the suggested threshold of 2 cm.

5.4 Computed muscle control

In the last chapter, an explanation of the computed muscle control method was provided, which was based on a forward dynamics approach that allowed the estimation of muscle forces. This procedure implements artificial reserve actuators for each joint DOF present in the model to overcome any shortage of muscle production. These actuators are defined with low optimal force and high threshold levels of excitation. With this parameter setting, the objective function penalizes these actuators if they are required to finish a simulation. All simulations were completed successfully. The optimal forces of the reserve actuators remained unaltered in the RRA and CMC phases.

The values of the reserve actuators for each DOF are stated in the tables A.13, A.14, and A.15. Reserve actuators and root mean squares are all within the recommended limit of 25 Nm and 10 Nm, respectively, in the OpenSim documentation. Positional errors for each joint DOF can be found in the tables A.16, A.17, and A.18. Peak position errors and root mean squares are all below the acceptable threshold of 5°. All of these indicators point to successful CMC results, which made possible the analysis and interpretation of the muscle forces estimated.

The selection of muscles for further analysis consisted in the most active muscles during the stance phase in typically developed gait [131], combined with muscles more commonly affected by neuromuscular deviations in spastic CP [171], and the muscles influenced by the medical interventions. Only single limb support period was analyzed (table 5.1).

Table 5.1: Description of the muscle groups analyzed in this work.

Muscle Groups	Description
Vasti	This muscle group includes the vastus lateralis, intermedius, and medialis. Each is represented by a muscle-tendon actuator.
Hamstrings	The hamstrings include muscle-tendon actuators representing the semitendinosus, semimembranosus, and bicep femoris long and short head.
Iliopsoas	This complex includes two muscle-tendon actuators each representing the psoas and the iliacus.
Soleus	Single actuator referring to the soleus muscle.
Rectus Femoris	Refers to the rectus femoris muscle, represented by a single muscle-tendon actuator.
Gastrocnemius	Refers to the medial and lateral sections of the gastrocnemius, each represented by a musculoskeletal actuator.
Ankle Dorsiflexors	The ankle dorsiflexors are constituted by muscle-tendon actuators representing the anterior tibialis, extensor digitorum, and extensor hallus longus.
Gluteus Maximus	The gluteus maximus is represented by three musculoskeletal actuators in the medial, intermediate, and lateral region.
Gluteus Medius	Refers to the three actuators representing the anterior, posterior, and intermediate components of the gluteus medius.

Figure 5.6 presents the mean muscle force curves for all three sessions together with those of healthy children. Mean muscle forces were used for statistical analysis between sessions (Figure 5.7). The CMC results from Figure 5.7 were organized to allow muscle force comparison between lower limbs and are presented in Figure 5.8.

After two years of surgical intervention, there was a statistically significant increase in muscle force for the left rectus femoris, vasti, soleus and ankle dorsiflexors during walking. In the same time period, a statistically significant decrease in muscle force occurred post-surgery on both hamstrings, on the right iliopsoas, and on the left gluteus maximus and gluteus medius. There was no statistical difference in the left iliopsoas and right rectus femoris and gluteus medius regarding muscle force levels one and two years after surgical intervention. When compared to either pre-surgery, two years post-surgery, or both, the soleus and gastrocnemius on both sides, as well as the right gluteus maximus, and ankle dorsiflexor, showed statistical significant increased muscle force one year after surgery.

When comparing muscle forces two years post-surgery with those of healthy children, the CP child walked with greater hamstring, vasti, soleus, and ankle dorsiflexors muscle force. On the other hand, muscle forces were lower in the right gluteus maximus. The other muscle groups showed no statistical differences from healthy population. Figure 5.6 shows that rectus femoris of unimpaired children produced higher levels of force at the beginning of single support period when compared to the CP child before and after surgery. The gastrocnemius appears to have higher levels of force in the terminal stance in healthy subjects, while in the CP subject the forces produced were more steady during this period.

Pre-surgery, statistical differences between lower limbs were identified between the iliopsoas, rectus femoris, vasti, gluteus maximus, soleus, and ankle dorsiflexors. The left muscles developed more force, with the exception of the gluteus maximus. One year after intervention, only the rectus femoris and gluteus maximus showed statistically significant differences between left and right lower limbs. The left rectus femoris and the right gluteus maximus were the ones providing more force. Two years post-surgery, the same muscle groups show statistical differences together with the ankle dorsiflexors, where the left side generated more force. The healthy population did not present any significant disparities.

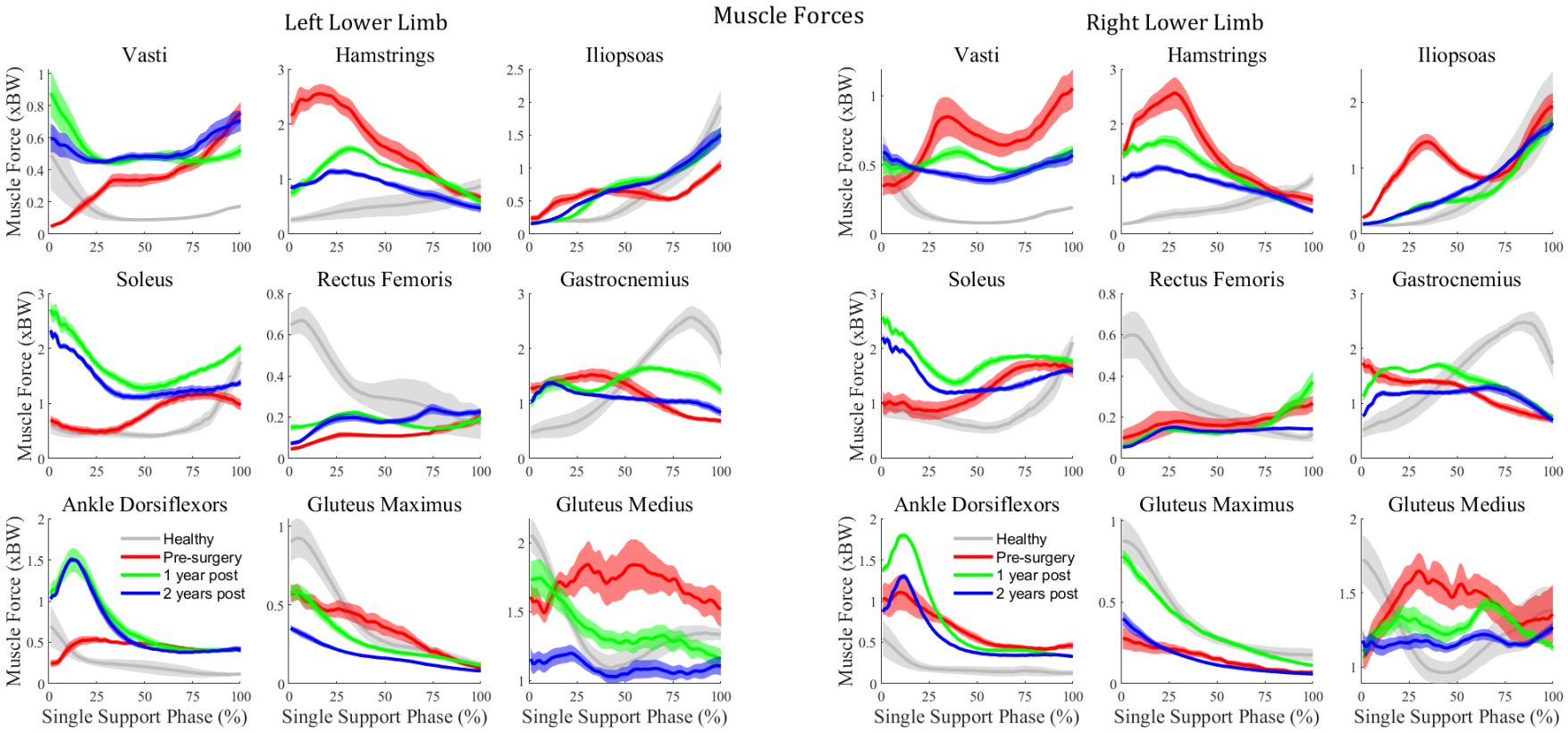

Figure 5.6: Average curves of muscle forces, normalized by body weight (BW), during single support period. The shaded regions represent the standard error. The vertical scale is not uniform to allow for better visualization of the results.

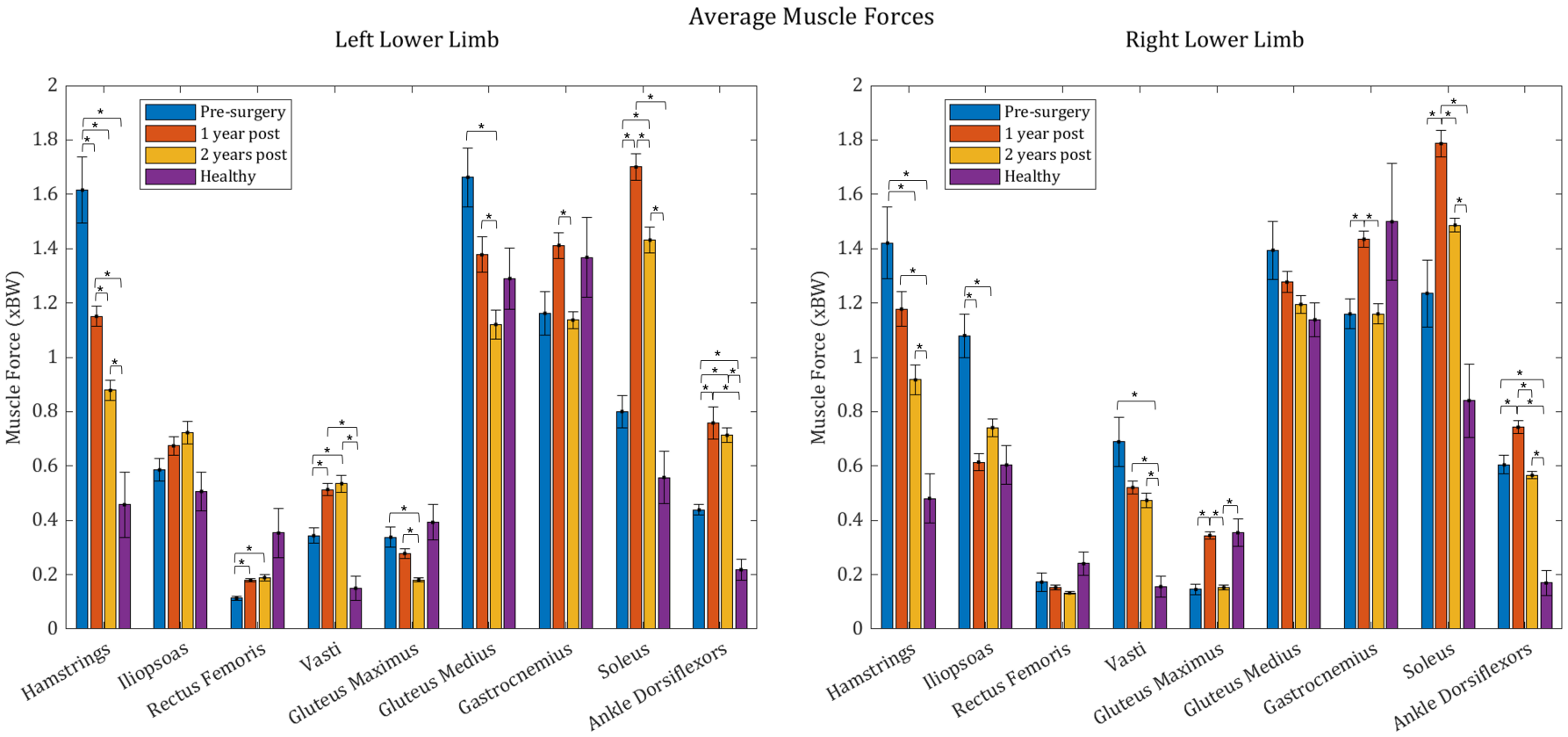

Figure 5.7: Average muscle forces, normalized by body weight (BW), during single support period. Error bars represent the standard error. Asterisks represent significant statistical differences.

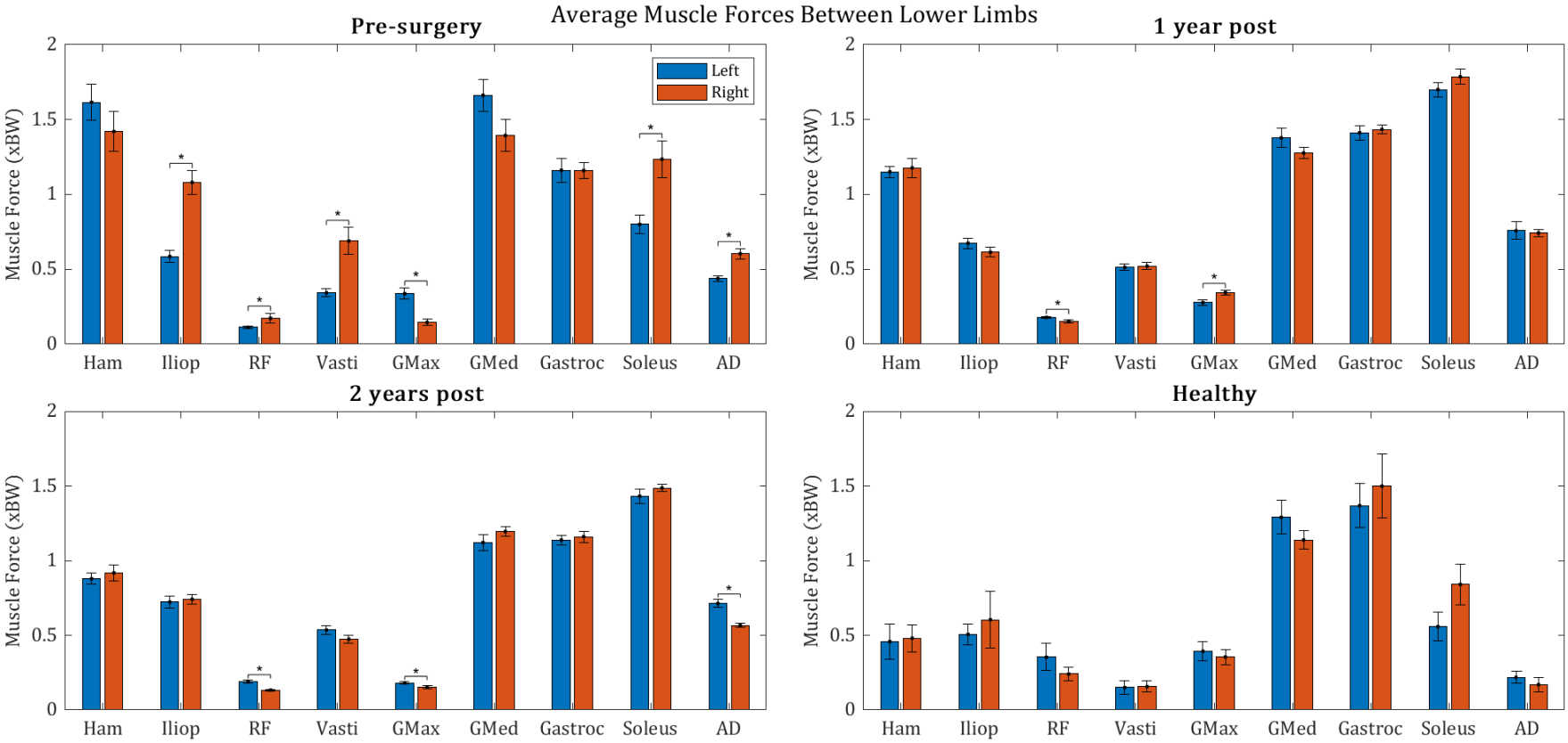

Figure 5.8: Comparison of the average muscle forces between lower limbs, normalized by body weight (BW), of the muscle groups relative to the CP and healthy subjects, during single support period. Error bars represent the standard error. Asterisks represent significant statistical differences.

5.4.1 Muscle activation validation

The EMG results of each session are represented in Figures A.1, A.2, and A.3. Overall, the results match adequately, with some disparities spotted in the rectus femoris, and adductor longus in the first and third sessions, and the left gastrocnemius medialis in the first session. The simulated activations showed especially good outcomes in the second session. For all three sessions, the tibialis anterior and gluteus medius appear to provide the most accurate results.

5.5 Induced acceleration analysis

The last objective of the present work was to analyze each muscle contributions to the COM acceleration along the fore-aft and vertical directions. The results from the IAA tool provided helpful insights regarding the overall capacity of the mass center to support itself and progress during the single support phase. The selection of muscles analyzed remains the same from CMC.

The validation of the IAA results are obtained by demonstrating an overlap between the GRF and the total accelerations along the directions designated for further study. From Figure A.4, it is possible to verify that both match, especially in the vertical direction, while in the fore-aft direction, results show acceptable minor deviations. The GRF from all trials are displayed in Figure A.5.

Figures 5.9 and 5.10 show the average curves representing muscle force contributions in the vertical and fore-aft directions, respectively, during single support period. The potential accelerations were calculated to compare with the results of jump gait from Correa et al. [28] and can be found in A.6 and A.7 for the vertical and fore-aft potentials, respectively.

The bar plots represented in 5.11 and 5.12 display the average of the mean curves of each muscle induced accelerations in the vertical and fore-aft direction, respectively. Besides the selected muscle groups, the acceleration of gravity over the COM is also shown in Figure 5.11, which represents the downward acceleration if no muscles were activated.

In the vertical direction, the main contributors to support the COM against gravity were the soleus and the gastrocnemius in healthy and CP subjects. One year and two years post-surgery, a statistically significant decrease in vertical contribution to the COM was identified in the both iliopsoas and gluteus medius, and left hamstrings. The soleus and ankle dorsiflexors on the left side increased their contribution to vertical acceleration. Both rectus femoris, vasti and gastrocnemius maintained their contribution to vertical acceleration of the COM as well as the hamstrings on the right side.

Two years of post-surgery, the right gastrocnemius and left gluteus medius showed statistically significant lower contribution to vertical accelerations when compared with the healthy population. On the other hand, both soleus and hamstrings showed higher

contribution to vertical accelerations as well as the left ankle dorsiflexors. The remaining muscle groups displayed no statistical differences.

In the fore-aft direction, the hamstrings and gastrocnemius were the largest contributors to anterior acceleration of the COM in CP and unimpaired children. The vasti and rectus femoris were the primary contributors to posterior acceleration of the COM in CP and healthy children, respectively. Following surgery, differences between CP and healthy children were not restored. From before to two years post-surgery, a statistically significant increase in the contribution of the left rectus femoris and vasti to fore-aft COM acceleration was observed. In the same time period, a statistically significant decrease in muscle contribution occurred in the right hamstrings. Both iliopsoas, gastrocnemius, and right rectus femoris did not present statistical differences as well as the left ankle dorsiflexors. The soleus changed its contribution from anterior in pre-surgery, to posterior in post-surgery in the right lower limb, whereas no statistical differences were identified in the left lower limb due to the high variation.

When comparing two years post-surgery and healthy children, the muscle groups that showed statistically significant differences in fore-aft contributions were the vasti, rectus femoris, and hamstrings. In the CP subject, the hamstrings (anterior) and vasti (posterior) showed greater whereas the rectus femoris (posterior) showed lower contributions to fore-aft COM acceleration, when compared to healthy children.

Comparison of mean muscle contributions to vertical and fore-aft COM accelerations between left and right lower limbs are represented in Figure 5.13 and 5.14, respectively. Regarding vertical acceleration, statistical differences were verified in the hamstrings, gluteus maximus, and gluteus medius, pre-surgery. One year after surgery, only the gastrocnemius and iliopsoas showed statistically significant differences between lower limbs. Two years after surgery, differences in muscle contributions to vertical COM acceleration were observed not only for the iliopsoas but also for the rectus femoris, gluteus maximus, and ankle dorsiflexors. The unimpaired group showed no significant distinctions.

Regarding fore-aft direction, the right vasti, rectus femoris and iliopsoas muscles showed significantly greater, while the right gluteus maximus showed significantly lower contributions to COM accelerations, compared with the left lower limb muscles before surgery. One year after surgery, the rectus femoris, gluteus medius, and ankle dorsiflexors displayed statistical differences between lower limbs in muscle contributions to fore-aft COM accelerations. Two years after surgery, statistical differences were verified in the gastrocnemius, gluteus medius, gluteus maximus, rectus femoris, and iliopsoas with higher contributions from the left side with the exception of the gluteus medius.

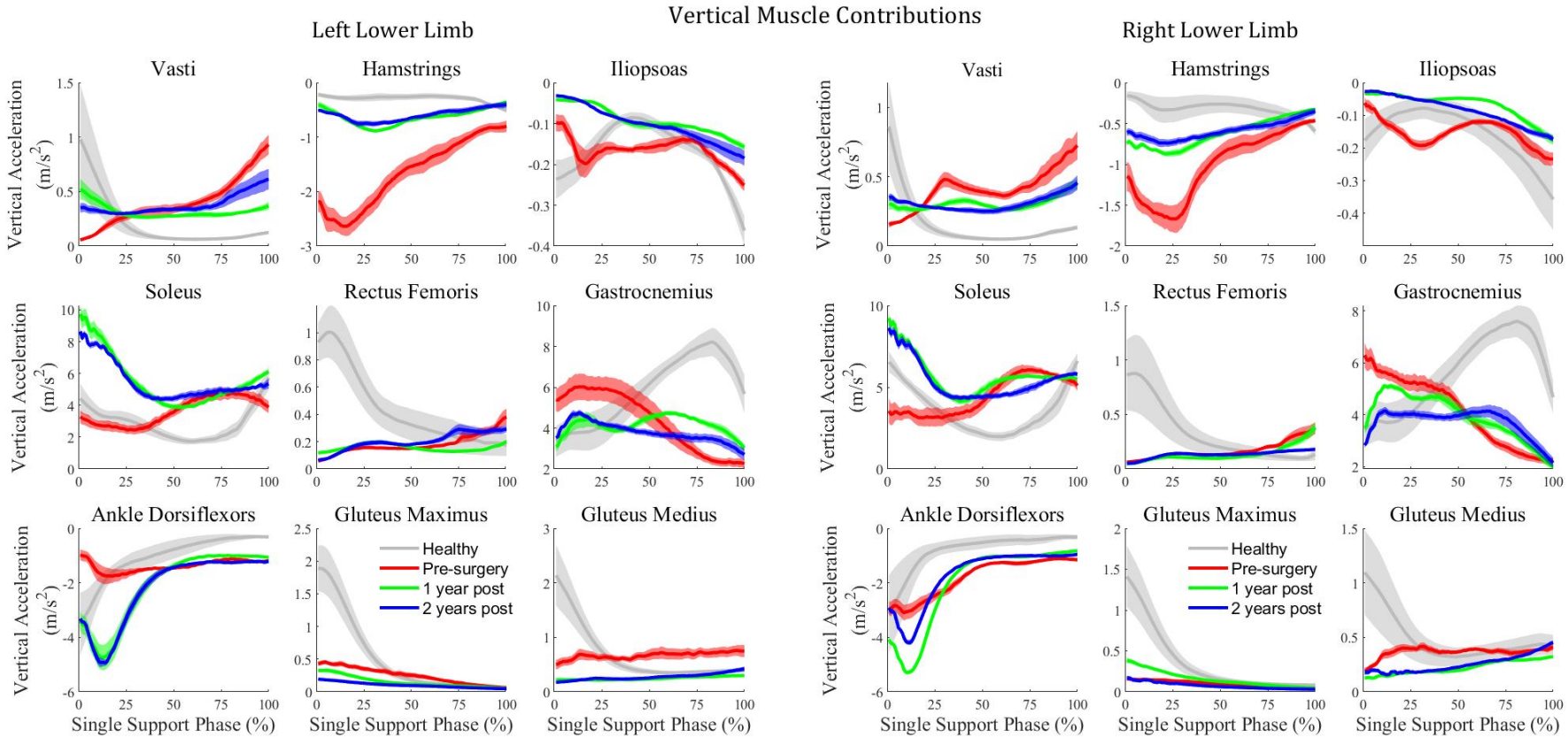

Figure 5.9: Average curves of the muscle contributions to vertical COM acceleration during single support period. The shaded regions represent the standard error. The vertical scale is not uniform to allow for better visualization of the results.

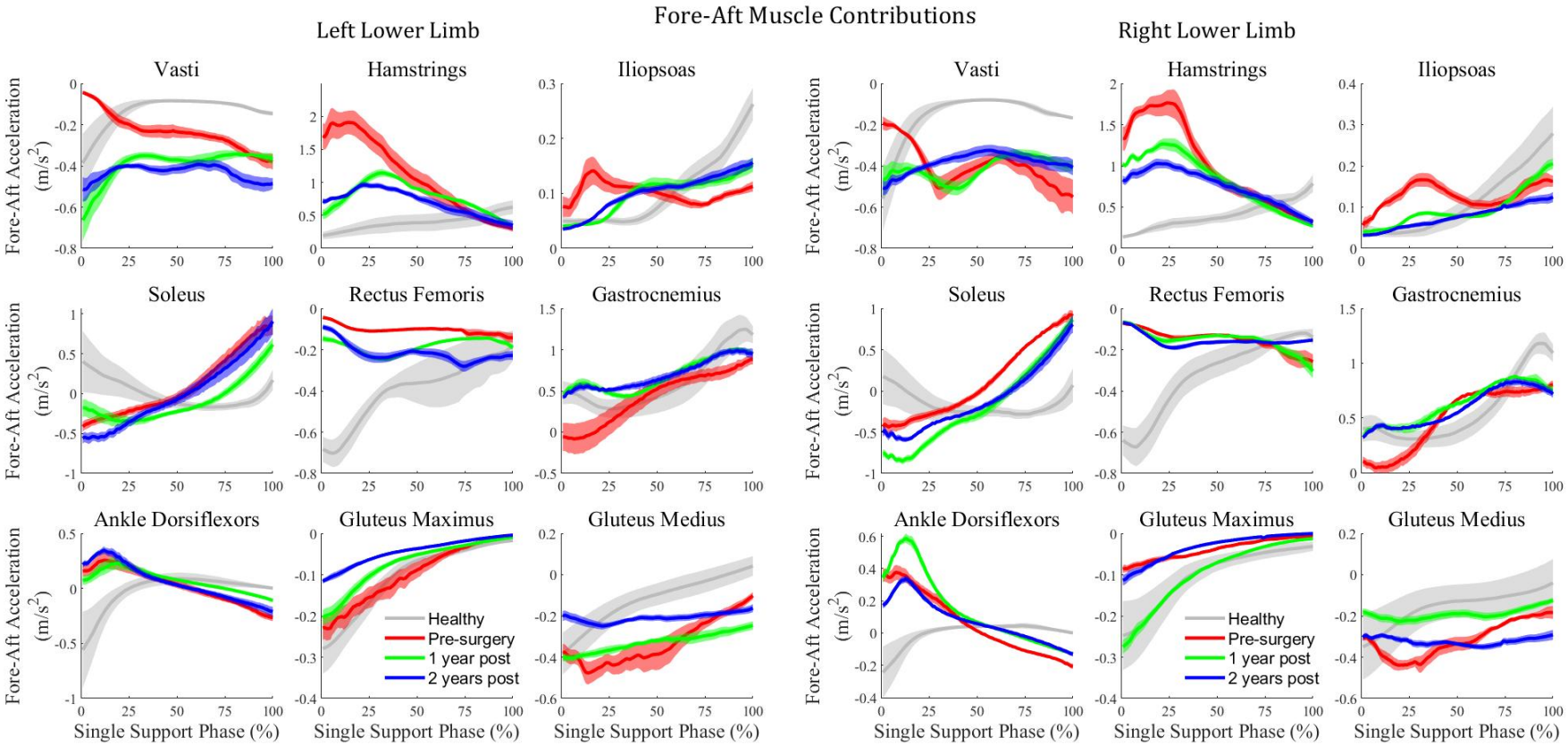

Figure 5.10: Average curves of the muscle contributions to fore-aft COM acceleration during single support period. The shaded regions represent the standard error. The vertical scale is not uniform to allow for a better visualization of the results.

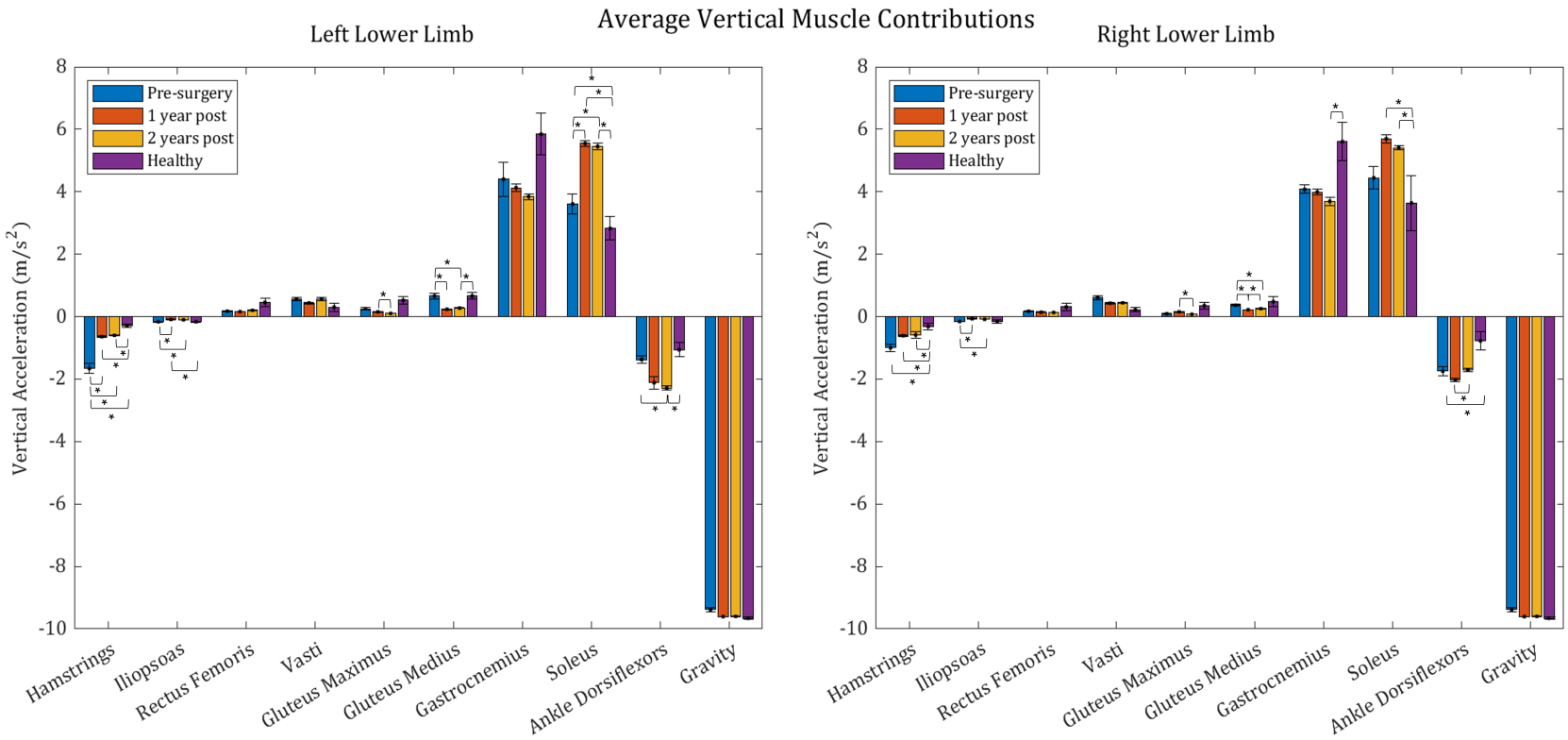

Figure 5.11: Comparison between sessions of the average muscle contributions to vertical COM acceleration during single support period. Error bars represent the standard error. Asterisks represent significant statistical differences.

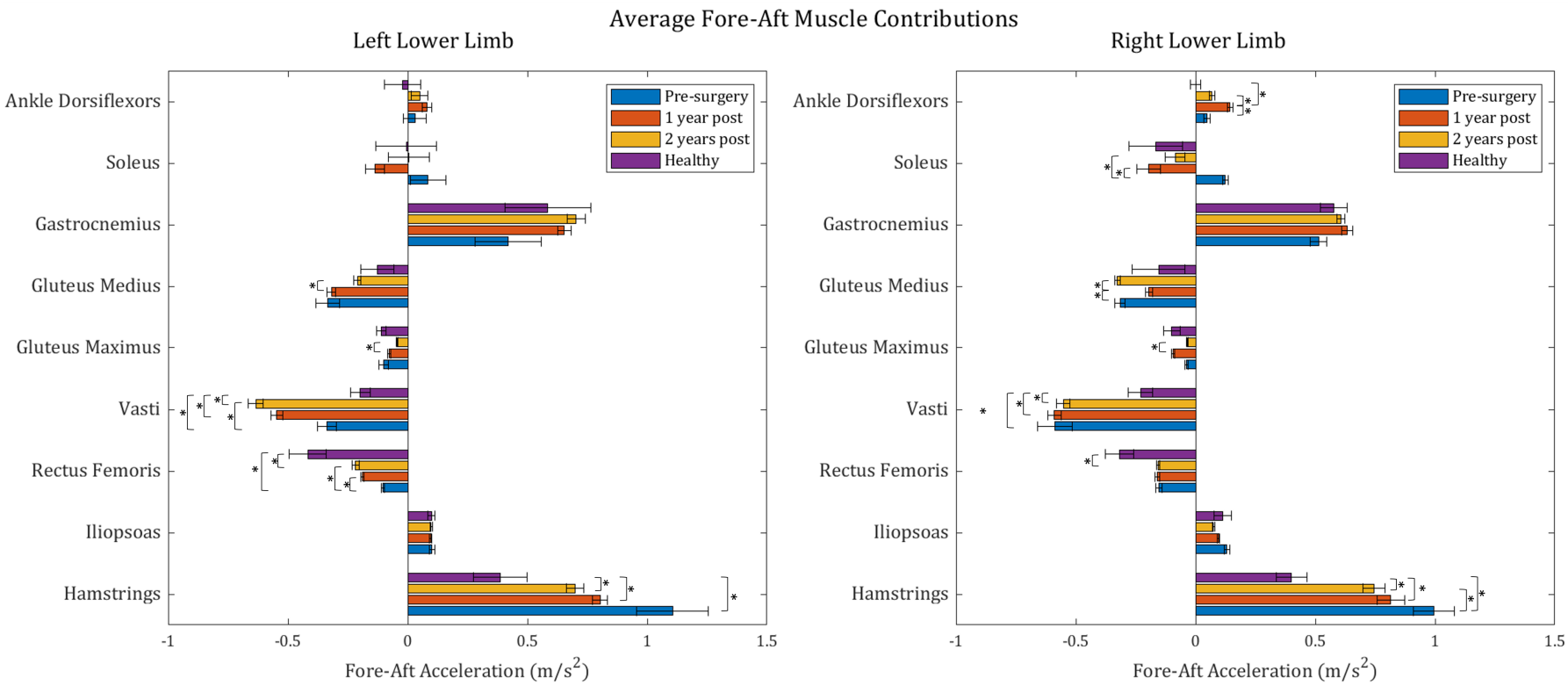

Figure 5.12: Comparison between sessions of the average muscle contributions to fore-aft COM acceleration during single support period. Positive and negative values represent anterior and posterior accelerations, respectively. Error bars represent the standard error. Asterisks represent significant statistical differences.

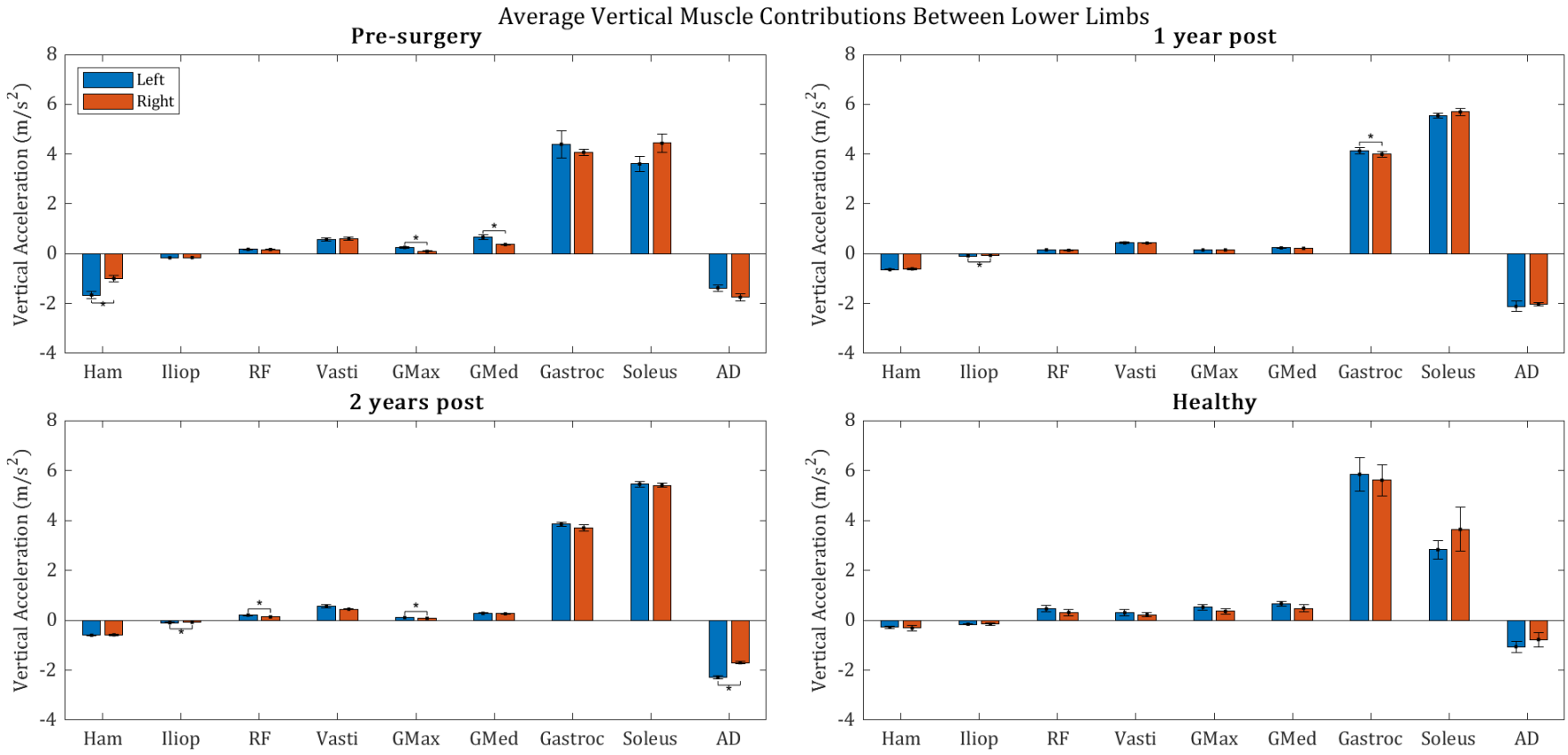

Figure 5.13: Comparison between lower limbs of the average muscle contributions to vertical COM acceleration during single support period. Error bars represent the standard error. Asterisks represent significant statistical differences.

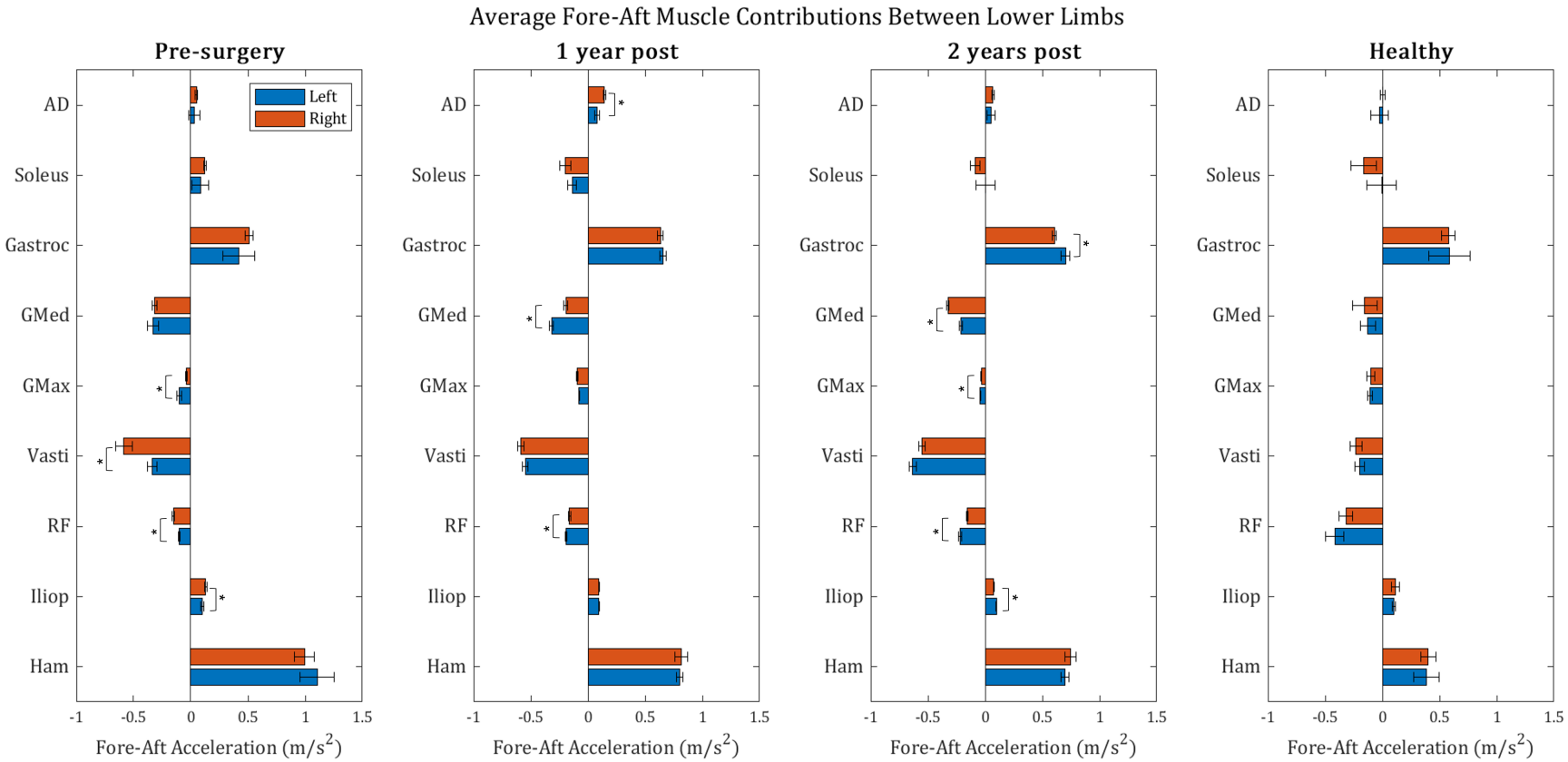

Figure 5.14: Comparison between lower limbs of the average muscle contributions to fore-aft COM acceleration during single support period. Positive and negative values represent anterior and posterior accelerations, respectively. Error bars represent the standard error. Asterisks represent significant statistical differences.

6 Discussion

The purpose of the present work was to compare muscle function during walking in a child with CP (jump gait) before, one and two years after a Strayer procedure. To achieve this goal, gait asymmetry, muscle forces, and muscle induced accelerations of the COM during single support period were compared between time points and with those of typically developed children. The findings and topics further discussed in this section include the improvement of equinus kinematics, reliance on proximal muscles for walking even after surgery, increased soleus muscle function, and suggestions for treatment plans.

6.1 Restoration of ankle function following surgery

In the pre-surgery session, the first rocker (i.e., heel strike) was not present in neither lower limb, with the full stance phase done through toe-walking. This was noticeable, as for this event to happen, the ankle needs to be in only slight plantarflexion and the knee extended. However, due to the accentuated plantarflexion and knee flexion, the foot begins contact in toe-walking which leads to significant dorsiflexion during the loading response in the first double support period. In typically developed children, the single support period is divided almost equally in braking phase and propulsion phase regarding the fore-aft direction [90]. Due to the lack of typical rockers, the deceleration and acceleration processes were altered, as is possible to verify through the GRF, where only the propulsion phase during single support period was present. The braking phase might be present during double support period.

One and two years post-surgery, braking and propulsion motions approached those of healthy gait. From the kinematics analysis, it was observed that one and two years following surgery, the first contact of the left lower limb was still not made with the heel, which was one of the primary goals of equinus treatment [100], but with the toes and metatarsal region, demonstrating that the equinus gait pattern had not been completely resolved. However, one year post-surgery, the left foot reached a flat position, leading to a more regular pattern of ankle motion. Two years post-surgery, the left foot did not reach

flat position showing a regression in the improvement observed one year post-surgery. One and two years post-surgery, the right lower limb presented all three rockers showing a large improvement from pre-surgery. Due to the absence of heel strike after the Strayer procedure and BTX injections on the left lower limb, it might be relevant to consider a revision surgery to increase the dorsiflexion range or an equivalent procedure to restore ankle function. Reducing accentuated knee flexion through surgical intervention could be an option since it persisted post-surgery and could be influencing ankle motion.

The function of the soleus and gastrocnemius consists of ankle plantarflexion, together with knee flexion in the case of the biarticular gastrocnemius. Both have a primary role throughout the entire single support period and the pre-swing [104]. The triceps surae complex muscle force during single support period increased two years post-surgery, which aligns with the improved capacity to generate ankle plantarflexion peak torque. Despite force production of the gastrocnemius being preserved at two years post-surgery, the soleus increased its muscle force when compared to preoperative levels in the left lower limb. This might be due to the increased range for dorsiflexion, on account of the fasciotomy (i.e., lengthening) of the soleus and the gastrocnemius recession, which allows the soleus to reach optimal force production length. The increase in soleus force is in accordance with the assumption that decreasing the sarcomere's lengths in CP's muscle contractures would lead to higher levels of force development [98]. Healthy muscles have shown to have the same fascicle length when compared to contracted muscles in CP, however, the former have longer sarcomeres and less quantity of serial sarcomeres. This leads to a sarcomere length greater than optimal length, which hinders force production, while typically developed muscle can operate at optimal length. After a lengthening procedure, sarcomeres may shorten in length, which, in turn, induces a shift towards optimal force production [98], [120]. The persistence of equinus in post-surgery might explain the increase in muscle force production of the soleus.

It is important to consider the effect of high passive forces inherent to muscle contracture's physiology [48]. In this study, the gastrocnemius EMG showed a decrease in activation during the middle and final portion of single support period, which might be due to the accentuated passive forces (i.e., resistance in stretching) starting to have a leading role in contraction and maintaining equinus posture. On the other hand, the activation estimated by CMC has very high values, with some trials reaching unphysiological activations. The use of a generic model and actuators might be the reason. Altering the tendon slack length would allow the assessment of high passive forces in muscle contractures [48].

The ankle dorsiflexors are primarily active during the double support period in unimpaired gait [5]. In jump gait, dorsiflexors displayed higher levels of force than typically developed gait, which suggests an attempt at countering the accentuated plantarflexion. This also indicates that dorsiflexors weakness is not likely to be present in our CP subject [64], [43]. Post-operation, there was a peak in dorsiflexor force during mid stance, which could be due to the same reason as the increase in soleus strength. A wider range

of dorsiflexion could allow the force-generating capacity of the dorsiflexors to increase.

6.2 Hip and knee function following surgery

The results from the kinematics and kinetics of jump gait were in accordance with the literature [28], with the exception of hip flexion and anterior pelvic tilt kinematics. It was expected an accentuated hip flexion and anterior pelvic tilt, however, increased hip extension and posterior pelvic tilt were present. Despite the joint angles of the hip and pelvis not being what was expected, the diagnostic of pathological gait pattern is attributed to the category which is most suited, which, in this case, was jump gait. One year after surgery, hip kinematics closely resembled healthy hip motion, however, two years after surgery, increased hip extension started to be noted once again.

Increased knee flexion during the stance phase, a common tertiary consequence of equinus in diplegic CP, was present pre-surgery, as expected [100]. Jump gait often incorporates a stiff knee, which consists of excessive knee extension during swing phase due to rectus femoris high activity. Furthermore, this deviation presents a delay in peak knee flexion [33]. Despite a delay being noted, knee flexion is not compromised as the knee joint is capable of flexion comparable to unimpaired gait during the swing phase. The Strayer procedure and BTX injections appear to not have had much effect on knee kinematics, since knee increased flexion persisted post-surgery.

The function of the hamstrings is to promote knee flexion and hip extension during walking. In unimpaired gait, the hamstrings are mainly active during early stance to mid stance [5]. Results pre-surgery show the child with CP walked with greater hamstring muscle forces during mid stance, which might have occurred to counter the increased knee extension in the first half of mid stance. This knee extension appears to be a reaction to the weight acceptance of the lower limb with equinus foot, and it might have been compensated by upward rotation of the pelvis in the frontal plane. The instance where the knee reaches near maximum extension, near the end of mid stance, is denominated as the split second effect, which occurs when dorsiflexion reaches its maximum range and the knee is extended, over stretching the contractured gastrocnemius, leading to incremental damage to the joints [3]. The consequences of such an outcome might have been alleviated or adverted since steep knee extension was reduced post-surgery. After surgery, the hamstrings diminished force production, which might be due to improvement in ankle motion and BTX injections. However, hamstring forces during single support period did not reach unimpaired levels. Increased knee flexion remained throughout the gait cycle, which could explain the higher hamstring force production when compared to the healthy population post-surgery.

The iliopsoas is the strongest hip flexor and produces force in the latter stages of stance [5]. It developed higher levels of force in the preoperative session of the right lower limb, which might have occurred to counter accentuated hip extension present in

this lower limb and prevent over extension. Postoperative muscle forces of the iliopsoas showed no statistical differences with unimpaired gait.

The vasti and rectus femoris have a primary role in knee extension, with the rectus femoris also promoting hip flexion. Therefore, the quadriceps counter knee flexion through eccentric contraction at the beginning of stance and mid stance [169]. Before surgery, the flexion of the knee begins at the end of mid stance and increases in late stance. It coincides with the increase in vasti force production to balance accentuated knee flexion. The higher levels of muscle force from the right vasti, might help to prevent further knee flexion while avoiding the equinus to contact the ground during swing phase. Furthermore, the left knee also has an increased flexion during swing period, which is in line with the objective of preventing toe contact. After surgery, the muscle forces of the vasti were higher than unimpaired gait. Increased vasti muscle forces during walking could be attributed as compensation for the lower rectus femoris contribution, which is also in accordance with toe-walking in able-bodied subjects [126].

The gluteus maximus, which is responsible for hip extension, has major and peak muscle force productions during early and mid stance in order to maintain upright posture during walking [160]. Gluteus maximus muscle forces appear to be closer to unimpaired gait one year post-surgery. Pre-surgery and two years after surgery, the hip was already in increased extension when entering single support period, which might be the reason for lower gluteus maximus force. Since the gluteus maximus was not submitted to any procedure, its decrease in force production from one to two years post-surgery might be related to the CP child stopping physical therapy.

According to Anderson and Pandy [5], the gluteus medius contributes to the support of the COM throughout the single support period. It is responsible for the stabilization of the pelvis and hip and femur movement in the frontal and transverse plane [124]. In the child with CP, results pre-surgery showed a more constant gluteus medius force, possibly to counter the increased upward rotation of the pelvis in the frontal plane. Despite reducing asymmetry post-surgery, the pelvis list accentuated and constant upward rotation was still present, which could be the reason for a differently shaped gluteus medius force curve when compared to unimpaired gait. The wide range of force production of the gluteus medius in unimpaired children, might be the reason significant differences with CP child were not identified. If the statistics were made according to peak muscle force, a significant difference might have been spotted between the groups two years post-surgery with the unimpaired group showing higher levels of force.

6.3 Reduced gait asymmetry following surgery

The asymmetry study based on kinematic data showed that postoperative GGA index was reduced and was lower than that of typically developed children. This supports the claim that asymmetry can be present in unimpaired population [16]. When analyzing each DOF, the results showed either a decrease or conservation of asymmetry in all joints.

The main objective of the modified Strayer procedure was to provide the ankle joint an increase capacity for dorsiflexion, which was verified by the large reduction in ankle asymmetry and equinus improvement. This outcome is in accordance with what was expected [70].

From one year to two years after surgery, there was an increase in the number of muscle groups that significantly differed between lower limbs regarding muscle forces, from two to three muscle groups, and muscle contributions in the vertical and fore-aft directions, from two to four and from three to five muscle groups, respectively. This could indicate a regression in improvement after two years. One possibility might be due to the interruption of physical therapy. Nevertheless, it brings the question about the permanency of improvements of the Strayer procedure and BTX injections.

6.4 Methods to compare muscle forces between groups

Mean plantarflexor muscle forces did not display significant differences between CP and the unimpaired population before surgery. It was expected to find plantarflexor weakness according to Hampton et al. [64], which was attributed due to the ankle being closer to GRF vector. However, the toe-walking studied in [64] was described with a progressive increase of dorsiflexion through stance, while in the present work, the accentuated equinus was present in the entirety of the single support phase. Furthermore, able-bodied subjects could not reach dorsiflexion force levels similar to CP counterparts. Although, if in the present study statistic validation was done by comparing peak force values instead of means, it could result in a significant difference between CP gastrocnemius and its unimpaired counterpart, with the contractured gastrocnemius displaying lower levels of force. This would align with the aim of the Strayer procedure to diminish the primary role of the gastrocnemius in plantarflexion to decrease the negative impacts of severe contracture [165].

6.5 Changes in muscle contributions following surgery

Muscle contributions to the COM acceleration are essential to counter the effect of gravity and allow the progression of the body during gait. In healthy children, the plantarflexors, the gluteus maximus, medius, and the vasti are the primary contributors for upward COM acceleration during mid stance [5], while the plantarflexors become the main contributors in late stance [104]. In the fore-aft direction, the quadriceps provide backward acceleration in the first half of stance and the gastrocnemius and soleus are the primary contributors to forward acceleration in the second half of single support phase [89].

Before surgery, the coordination of the muscle groups contributing to the COM acceleration employ a different strategy with more proximal muscle groups showing larger contribution values. In the vertical direction, the hamstrings show statistically significant higher muscle contributions in both lower limbs when compared to those of unimpaired

gait. In the fore-aft direction, the same occurs in the hamstrings, the vasti and, despite not showing significant differences, the gluteus medius on both sides. Subjects with CP often have accentuated neurological impairments in distal muscles, compromising their control [23], [158]. This might indicate why CP children adopt gait patterns and posture, such as crouch posture [135].

Two years post-surgery, the average vertical contributions of the hamstring and gluteus medius were reduced compared to pre-surgery with the contribution of the hamstrings becoming closer to those observed during unimpaired gait. On the other hand, in both soleus and in the left dorsiflexors, the opposite occurred. In the case of the soleus and dorsiflexors, it might be due to the increased capacity of motion obtained through the Strayer procedure. Regarding the posterior accelerations, the quadriceps increased their contribution to the COM in the left lower limb and maintained them in the right lower limb when compared to those of unimpaired gait. On the other hand, the hamstrings contribution to anterior COM acceleration was statistically lower on the right side two years post-surgery when compared with pre-surgery. However, the hamstrings continued to present a larger contribution to the COM when compared to unimpaired gait. Reliance on proximal muscles might remain, despite surgical interventions, since the neurological impairments (i.e., primary deviations), such as spasticity, are only attenuated by surgical procedure and BTX injections.

The vertical contribution of the left gluteus medius and right gastrocnemius was lower than those of unimpaired children two years after surgery. On the fore-aft direction, the rectus femoris on both sides also showed a lower muscle contribution in the CP child. Since gluteus medius, gastrocnemius, and rectus femoris muscle contributions do not restore to healthy levels two years after surgery, one may suggest including muscle strengthening exercises in the rehabilitation program with the objective to restore muscle contributions to unimpaired levels. Although increasing gluteus medius forces may also contribute to hip movement and stability [124], the effects of strength training on muscle contributions during walking remain to be investigated.

In the preoperative period, the potential accelerations were calculated to compare with the results of jump gait from Correa et al. [28] and can be found in A.6 and A.7 for the vertical and fore-aft potentials, respectively. Since Correa et al. [28] studied the entirety of the stance phase, comparisons with the present work were done not considering significant differences, but considering if results were within the limits obtained in Correa's work. Out of all muscle groups analyzed, only the ankle dorsiflexors were not reported. Regarding vertical direction, results from Correa et al. show lower gastrocnemius and soleus contributions to vertical COM acceleration and higher iliopsoas contributions in both lower limbs together with the right gluteus maximus when compared with the results of this thesis. The other muscle groups appear to be within range of what was expected. In the fore-aft direction, results from Correa et al. regarding muscles involving the hip joint show some differences. The most noticeable are the gluteus maximus and medius, which have forward contributions in the work of Correa et al., and braking

contributions in this work in jump gait. In pathological gait, this alteration could be attributed to the presence of accentuated hip extension and posterior pelvic tilt instead of hip flexion and anterior pelvic tilt. The higher or lower potentials might be attributed to this paper not adjusting peak isometric force for children in CP.

7

Conclusion

The primary objectives of this dissertation were to estimate gait asymmetry, muscle forces and contributions to the COM vertical and fore-aft acceleration in order to obtain a more detailed insight into the effects of the modified Strayer procedure and BTX injections during single support period. Furthermore, gait data from neurologically intact children were also employed to compare the results.

An improvement in capacity for ankle dorsiflexion two years after surgery was identified, by the closer resemblance in gait patterns between the child with CP and health gait. Despite the improvement of ankle motion on both sides, the left lower limb did not present a heel strike. Two years following the Strayer procedure, the child with CP walked with an increase in peak ankle dorsiflexion and decreased gait asymmetry compared to pre-surgery, reaching asymmetry levels below those seen in unimpaired children. It is important to note that, despite the reduction of gait asymmetry being a good indicator of improvement, it does not inherently mean a closer resemblance to a healthy gait.

Results also showed changes in muscle forces following surgery. Before surgery, jump gait appears to rely more on the force-generating capacity of proximal muscles, such as the vasti and hamstrings, to ensure gait support and progression. Two years post-surgery, despite increases in vasti and decreases in hamstring muscle forces during walking, these muscles remained the primary contributors to COM acceleration, especially in the fore-aft direction. Furthermore, the soleus appears to take a central role in ankle plantarflexion two years post-surgery, when compared to the contracted gastrocnemius for vertical support. On the other hand, the gastrocnemius continued to provide essential forward COM acceleration after surgery.

The results from this work may contribute to a more effective treatment plan, by prioritizing the strengthening of weakened muscles (e.g. gluteus medius and rectus femoris) to improve and maintain the positive outcomes of the surgical interventions. Overall, this work showed the positive effects and outcomes of the modified Strayer procedure and BTX injections, while suggesting possible improvements.

7.1 Limitations

The present work and subsequent results should be considered while taking into account its limitations. Despite being broadly used in gait analysis, the generic model utilized in this work is a simplified representation of the musculoskeletal system and is based on the structure of an adult. Adjustments of peak isometric forces were implemented to obtain a closer model structure of a child, however, scaling errors are always a possibility, especially in pathological patients. Furthermore, muscle contractures and weakness are challenging characteristics to scale and model, when taking into account the limited physiological information on the CP subject. For the same reasons, the anatomical outcome of the Strayer procedure and fasciotomy from a subject-specific perspective were also not taken into account. Despite being a common procedure, locking the subtalar and metatarsophalangeal joints is a limitation, as it removes the degrees of freedom regarding the frontal and transverse plane of the foot, by keeping it in a neutral position.

The literature regarding musculoskeletal modeling in jump gait and outcomes of the modified Strayer procured were very limited. Furthermore, the CP did not present the typical kinematic jump gait characteristics in the hip and pelvis list, which made it difficult to compare it with other works.

Lastly, by only analyzing one child CP it remains unclear if the present results are applicable to the larger populations. Finally, the GRF of the first double support period of the CP child and the healthy population were not recorded and, therefore, a thorough examination of the whole stance phase remains to be done.

7.2 Future Work

In the future, a similar study should be done including more participants with CP to allow for a statistical comparison between groups and more robust conclusions. In the present work, only single support was analyzed given the lack of complete foot strikes. Multiple force plates should be used to record GRF allowing for the investigation of the whole gait cycle which would provide a more complete insight into the muscle function of this pathological gait and the outcomes of the procedures.

The elaboration of a subject-specific model would provide helpful insight by comparing its results with the ones obtained through the generic model implemented in this work. The limitation in estimating muscle activation in the contracture gastrocnemius was the main disparity spotted. However, comparing the results with a subject-specific model could unfold other undetected differences. One way to do it would be by using the Calibrated EMG-Informed Neuromusculoskeletal Modeling Toolbox (CEINMS), which uses the EMG signals to adjust the parameters of each actuator, increasing the accuracy of the model [114]. Muscle spasticity could also be simulated through the implementation of a controller plugin which adds the effect of spasticity when performing, for example, CMC simulations [84].

Finally, due to some indications of regression in improvement, it would be relevant to analyze if the positive effects of surgery are long-lasting, by recording new sessions with the CP patient.

Bibliography

[1] A. Agarwal and I. Verma. "Cerebral palsy in children: An overview". In: *Journal of clinical orthopaedics and trauma* 3.2 (2012), pp. 77–81. DOI: https://doi.org/10.1016/j.jcot.2012.09.001 (cit. on p. 9).

[2] A. Alamdari and V. Krovi. "Chapter Two - A Review of Computational Musculoskeletal Analysis of Human Lower Extremities". In: *Human Modelling for Bio-Inspired Robotics*. Ed. by J. Ueda and Y. Kurita. Academic Press, 2017, pp. 37–73. ISBN: 978-0-12-803137-7. DOI: https://doi.org/10.1016/B978-0-12-803137-7.00003-3 (cit. on p. 2).

[3] J. Amis. "The split second effect: the mechanism of how equinus can damage the human foot and ankle". In: *Frontiers in surgery* 3 (2016), p. 38. DOI: https://doi.org/10.3389/fsurg.2016.00038 (cit. on pp. 15, 70).

[4] F. C. Anderson and M. G. Pandy. "A dynamic optimization solution for vertical jumping in three dimensions". In: *Computer methods in biomechanics and biomedical engineering* 2.3 (1999), pp. 201–231. DOI: https://doi.org/10.1080/10255849908907988 (cit. on pp. 30, 38).

[5] F. C. Anderson and M. G. Pandy. "Individual muscle contributions to support in normal walking". In: *Gait & posture* 17.2 (2003), pp. 159–169. DOI: https://doi.org/10.1016/S0966-6362(02)00073-5 (cit. on pp. 69–72).

[6] F. C. Anderson et al. "SimTrack: Software for rapidly generating muscle-actuated simulations of long-duration movement". In: *International Symposium on Biomedical Engineering*. 2006, pp. 3–6. URL: https://simtk.org/docman/view.php/55/1500/Anderson_SimTrack_ISOBME2006.pdf (cit. on p. 42).

[7] H. Anttila et al. "Effectiveness of physical therapy interventions for children with cerebral palsy: a systematic review". In: *BMC pediatrics* 8.1 (2008), pp. 1–10. DOI: 10.1186/1471-2431-8-14 (cit. on p. 11).

[8] S. Armand, G. Decoulon, and A. Bonnefoy-Mazure. "Gait analysis in children with cerebral palsy". In: *EFORT open reviews* 1.12 (2016), pp. 448–460. DOI: 10.1302/2058-5241.1.000052 (cit. on pp. 2, 13).

[9] L. D. Baker. "Triceps surae syndrome in cerebral palsy: an operation to aid in its relief". In: *AMA Archives of Surgery* 68.2 (1954), pp. 216–221. DOI: 10.1001/archsurg.1954.01260050218009 (cit. on p. 17).

[10] R. Baker. "The history of gait analysis before the advent of modern computers". In: *Gait & posture* 26.3 (2007), pp. 331–342. DOI: https://doi.org/10.1016/j.gaitpost.2006.10.014 (cit. on p. 4).

[11] M. M. Bamman et al. "Evaluation of the strength-size relationship in vivo using various muscle size indices." In: *Medicine and science in sports and exercise* 32.7 (2000), pp. 1307–1313. DOI: 10.1097/00005768-200007000-00019 (cit. on p. 39).

[12] A. Barre and S. Armand. "Biomechanical ToolKit: Open-source framework to visualize and process biomechanical data". In: *Computer methods and programs in biomedicine* 114.1 (2014), pp. 80–87. DOI: https://doi.org/10.1016/j.cmpb.2014.01.012 (cit. on p. 35).

[13] H. L. Barske et al. "Current concepts review: isolated gastrocnemius contracture and gastrocnemius recession". In: *Foot & ankle international* 33.10 (2012), pp. 915–921. DOI: 10.3113/FAI.2012.0915 (cit. on p. 16).

[14] J. Baumann and H. Koch. "Lengthening of the anterior aponeurosis of the gastrocnemius muscle". In: *Operat Orthop Traumatol* 1.1 (1989), pp. 254–8 (cit. on p. 17).

[15] B. L. Bedo et al. "BOPS: a Matlab toolbox to batch musculoskeletal data processing for OpenSim". In: *Computer Methods in Biomechanics and Biomedical Engineering* 24.10 (2021), pp. 1104–1114. DOI: https://doi.org/10.1080/10255842.2020.1867978 (cit. on p. 36).

[16] H. Böhm and L. Döderlein. "Gait asymmetries in children with cerebral palsy: do they deteriorate with running?" In: *Gait & posture* 35.2 (2012), pp. 322–327. DOI: https://doi.org/10.1016/j.gaitpost.2011.10.003 (cit. on pp. 7, 71).

[17] A. Brierty et al. "Dynamic muscle-tendon length following zone 2 calf lengthening surgery in two populations with equinus gait: Idiopathic Toe Walkers and Cerebral Palsy". In: *Clinical Biomechanics* 84 (2021), p. 105323. DOI: https://doi.org/10.1016/j.clinbiomech.2021.105323 (cit. on p. 6).

[18] C. L. Brockett and G. J. Chapman. "Biomechanics of the ankle". In: *Orthopaedics and trauma* 30.3 (2016), pp. 232–238. DOI: https://doi.org/10.1016/j.mporth.2016.04.015 (cit. on p. 13).

[19] M. Brughelli and J. Cronin. "Altering the length-tension relationship with eccentric exercise". In: *Sports Medicine* 37.9 (2007), pp. 807–826. DOI: https://doi.org/10.2165/00007256-200737090-00004 (cit. on p. 28).

[20] S. Cabral et al. "A Global Gait Asymmetry Index." In: *Journal of applied biomechanics* 32.2 (2016). DOI: https://doi.org/10.1123/jab.2015-0114 (cit. on pp. 8, 47).

[21] A. Cappozzo et al. "Position and orientation in space of bones during movement: anatomical frame definition and determination". In: *Clinical biomechanics* 10.4 (1995), pp. 171–178. DOI: https://doi.org/10.1016/0268-0033(95)91394-T (cit. on p. 33).

[22] C. G. Cardadeiro. "Model-based comparative biomechanics and muscle function analysis of simulated crouch gait by healthy children and crouch gait in CP children". Master's Thesis. Largo da Torre, 2829-516 Caparica: Nova University of Lisbon, 2020 (cit. on pp. 33, 94).

[23] L. Carr et al. "Patterns of central motor reorganization in hemiplegic cerebral palsy". In: *Brain* 116.5 (1993), pp. 1223–1247. DOI: https://doi.org/10.1093/brain/116.5.1223 (cit. on p. 73).

[24] E. Y. Chang et al. "A review of spasticity treatments: pharmacological and interventional approaches". In: *Critical Reviews™ in Physical and Rehabilitation Medicine* 25.1-2 (2013). DOI: 10.1615/CritRevPhysRehabilMed.2013007945 (cit. on p. 11).

[25] E. M. Chin et al. "Principles of medical and surgical treatment of cerebral palsy". In: *Neurologic clinics* 38.2 (2020), pp. 397–416. DOI: https://doi.org/10.1016/j.ncl.2020.01.009 (cit. on pp. 1, 12).

[26] V. Cimolin and M. Galli. "Summary measures for clinical gait analysis: A literature review". In: *Gait & posture* 39.4 (2014), pp. 1005–1010. DOI: 10.1016/j.gaitpost.2014.02.001 (cit. on p. 1).

[27] T. A. Correa and M. G. Pandy. "A mass-length scaling law for modeling muscle strength in the lower limb". In: *Journal of biomechanics* 44.16 (2011), pp. 2782–2789. DOI: https://doi.org/10.1016/j.jbiomech.2011.08.024 (cit. on p. 39).

[28] T. A. Correa et al. "Potential of lower-limb muscles to accelerate the body during cerebral palsy gait". In: *Gait & posture* 36.2 (2012), pp. 194–200. DOI: https://doi.org/10.1016/j.gaitpost.2012.02.014 (cit. on pp. 5, 60, 70, 73, 114, 115).

[29] R. D. Crowninshield and R. A. Brand. "A physiologically based criterion of muscle force prediction in locomotion". In: *Journal of biomechanics* 14.11 (1981), pp. 793–801. DOI: https://doi.org/10.1016/0021-9290(81)90035-X (cit. on p. 5).

[30] S. P. Das and G. S. Ganesh. "Evidence-based approach to physical therapy in cerebral palsy". In: *Indian journal of orthopaedics* 53.1 (2019), pp. 20–34. DOI: 10.4103/ortho.IJOrtho_241_17 (cit. on p. 11).

[31] G. Davico et al. "Increasing level of neuromusculoskeletal model personalisation to investigate joint contact forces in cerebral palsy: A twin case study". In: *Clinical Biomechanics* 72 (2020), pp. 141–149. DOI: https://doi.org/10.1016/j.clinbiomech.2019.12.011 (cit. on p. 5).

[32] J. R. Davids. "The foot and ankle in cerebral palsy". In: *Orthopedic Clinics* 41.4 (2010), pp. 579–593. DOI: https://doi.org/10.1016/j.ocl.2010.06.002 (cit. on p. 15).

[33] J. R. Davids and A. M. Bagley. "Identification of common gait disruption patterns in children with cerebral palsy". In: *JAAOS-Journal of the American Academy of Orthopaedic Surgeons* 22.12 (2014), pp. 782–790. DOI: 10.5435/JAAOS-22-12-782 (cit. on pp. 14, 15, 70).

[34] S. L. Delp and J. P. Loan. "A computational framework for simulating and analyzing human and animal movement". In: *Computing in Science & Engineering* 2.5 (2000), pp. 46–55. DOI: 10.1109/5992.877394 (cit. on p. 18).

[35] S. L. Delp, K. Statler, and N. C. Carroll. "Preserving plantar flexion strength after surgical treatment for contracture of the triceps surae: a computer simulation study". In: *Journal of Orthopaedic Research* 13.1 (1995), pp. 96–104. DOI: https://doi.org/10.1002/jor.1100130115 (cit. on p. 7).

[36] S. L. Delp et al. "An interactive graphics-based model of the lower extremity to study orthopaedic surgical procedures". In: *IEEE Transactions on Biomedical engineering* 37.8 (1990), pp. 757–767. DOI: 10.1109/10.102791 (cit. on pp. 37–39, 94).

[37] S. L. Delp et al. "OpenSim: Open-Source Software to Create and Analyze Dynamic Simulations of Movement". In: *IEEE Transactions on Biomedical Engineering* 54.11 (2007), pp. 1940–1950. DOI: 10.1109/TBME.2007.901024 (cit. on pp. 18, 35).

[38] S. L. Delp. *Surgery simulation: a computer graphics system to analyze and design musculoskeletal reconstructions of the lower limb*. Stanford University, 1990 (cit. on p. 30).

[39] C. J. Dente, A. D. Wyrzykowski, and D. V. Feliciano. "Fasciotomy". In: *Current problems in surgery* 46.10 (2009), pp. 779–839. DOI: 10.1067/j.cpsurg.2009.04.006 (cit. on p. 18).

[40] J. J. Dunne et al. "A marker registration method to improve joint angles computed by constrained inverse kinematics". In: *Plos one* 16.5 (2021), e0252425. DOI: https://doi.org/10.1371/journal.pone.0252425 (cit. on p. 40).

[41] G. Durandau and W. Suleiman. "Toward a unified framework for EMG signals processing and controlling an exoskeleton". In: *2014 Canadian Conference on Computer and Robot Vision*. IEEE. 2014, pp. 291–298. DOI: 10.1109/CRV.2014.46 (cit. on p. 26).

[42] J. S. Early. "The Evolution of Gastrocnemius-Soleus Lengthening in the Treatment of Acquired Achilles Equinus". In: () (cit. on pp. 17, 18).

[43] J. R. Engsberg et al. "Ankle spasticity and strength in children with spastic diplegic cerebral palsy". In: *Developmental medicine and child neurology* 42.1 (2000), pp. 42–47. DOI: https://doi.org/10.1017/S0012162200000086 (cit. on p. 69).

[44] R. M. Erskine et al. "In vivo specific tension of the human quadriceps femoris muscle". In: *European journal of applied physiology* 106.6 (2009), pp. 827–838. DOI: 10.1007/s00421-009-1085-7 (cit. on p. 30).

[45] A. Fattal-Valevski et al. "Long-term effect of repeated injections of botulinum toxin in children with cerebral palsy: a prospective study". In: *Journal of children's orthopaedics* 2.1 (2008), pp. 29–35. DOI: 10.1007/s11832-007-0075-8 (cit. on p. 11).

[46] G. B. Firth et al. "Lengthening of the gastrocnemius-soleus complex: an anatomical and biomechanical study in human cadavers". In: *JBJS* 95.16 (2013), pp. 1489–1496. DOI: 10.2106/JBJS.K.01638 (cit. on pp. 16–18).

[47] G. B. Firth et al. "Multilevel surgery for equinus gait in children with spastic diplegic cerebral palsy: medium-term follow-up with gait analysis". In: *JBJS* 95.10 (2013), pp. 931–938. DOI: 10.2106/JBJS.K.01542 (cit. on pp. 2, 18).

[48] A. S. Fox et al. "Simulating the effect of muscle weakness and contracture on neuromuscular control of normal gait in children". In: *Gait & posture* 61 (2018), pp. 169–175. DOI: https://doi.org/10.1016/j.gaitpost.2018.01.010 (cit. on p. 69).

[49] J. A. Friederich and R. A. Brand. "Muscle fiber architecture in the human lower limb". In: *Journal of biomechanics* 23.1 (1990), pp. 91–95. DOI: https://doi.org/10.1016/0021-9290(90)90373-B (cit. on p. 30).

[50] J. R. Gage et al. *The identification and treatment of gait problems in cerebral palsy*. Vol. 180. John Wiley & Sons, 2009 (cit. on pp. 2, 14).

[51] D. Ganjwala. "Multilevel orthopedic surgery for crouch gait in cerebral palsy: An evaluation using functional mobility and energy cost". In: *Indian Journal of Orthopaedics* 45.4 (2011), pp. 314–319. DOI: 10.4103/0019-5413.82334 (cit. on p. 12).

[52] B. A. Garner and M. G. Pandy. "Estimation of musculotendon properties in the human upper limb". In: *Annals of biomedical engineering* 31.2 (2003), pp. 207–220. DOI: https://doi.org/10.1114/1.1540105 (cit. on p. 39).

[53] *Getting Started with CMC*. Last accessed November 2022. 2017. URL: https://simtk-confluence.stanford.edu:8443/display/OpenSim/Getting+Started+with+CMC (cit. on p. 44).

[54] J. C. Gonzalez-Islas et al. "Human gait analysis based on automatic recognition: A review". In: *Pädi Boletın Cientıfico de Ciencias Básicas e Ingenierıas del ICBI* 10.Especial3 (2022), pp. 13–21. DOI: https://doi.org/10.29057/icbi.v10iEspecial3.8927 (cit. on p. 4).

[55] M. Gough. "Does botulinum toxin prevent or promote deformity in children with cerebral palsy?" In: *Developmental medicine and child neurology* 51.2 (2009), p. 89. URL: https://onlinelibrary.wiley.com/doi/pdf/10.1111/j.1469-8749.2008.03247.x (cit. on p. 15).

[56] D. Gouwanda. "Further validation of normalized symmetry index and normalized cross-correlation in identifying gait asymmetry on restricted knee and ankle movement". In: *2012 IEEE-EMBS Conference on Biomedical Engineering and Sciences*. IEEE. 2012, pp. 423–427. DOI: 10.1109/IECBES.2012.6498167 (cit. on p. 2).

[57] D. Gouwanda and S. A. Senanayake. "Identifying gait asymmetry using gyroscopes—A cross-correlation and Normalized Symmetry Index approach". In: *Journal of biomechanics* 44.5 (2011), pp. 972–978. DOI: https://doi.org/10.1016/j.jbiomech.2010.12.013 (cit. on p. 8).

[58] H. K. Graham et al. "Erratum: Cerebral palsy". In: *Nature Reviews Disease Primers* 2.1 (2016), pp. 1–1. DOI: https://doi.org/10.1038/nrdp.2016.5 (cit. on pp. 1, 9, 10).

[59] V. Guimarães, I. Sousa, and M. V. Correia. "A Deep Learning Approach for Foot Trajectory Estimation in Gait Analysis Using Inertial Sensors". In: *Sensors* 21.22 (2021), p. 7517. DOI: https://doi.org/10.3390/s21227517 (cit. on p. 5).

[60] S. Gulati and V. Sondhi. "Cerebral palsy: an overview". In: *The Indian Journal of Pediatrics* 85.11 (2018), pp. 1006–1016. DOI: https://doi.org/10.1007/s12098-017-2475-1 (cit. on p. 9).

[61] J. E. Hall. *Guyton and Hall: Textbook of Medical Physiology (13th ed.)* Elsevier Health Sciences, 2016. DOI: 10.4103/sni.sni_327_17 (cit. on pp. 20, 22, 23).

[62] S. R. Hamner, A. Seth, and S. L. Delp. "Muscle contributions to propulsion and support during running". In: *Journal of biomechanics* 43.14 (2010), pp. 2709–2716. DOI: https://doi.org/10.1016/j.jbiomech.2010.06.025 (cit. on pp. 5, 46, 47).

[63] S. R. Hamner et al. "A rolling constraint reproduces ground reaction forces and moments in dynamic simulations of walking, running, and crouch gait". In: *Journal of biomechanics* 46.10 (2013), pp. 1772–1776. DOI: https://doi.org/10.1016/j.jbiomech.2013.03.030 (cit. on pp. 45, 46).

[64] D. A. Hampton, K. W. Hollander, and J. R. Engsberg. "Equinus deformity as a compensatory mechanism for ankle plantarflexor weakness in cerebral palsy". In: *Journal of applied biomechanics* 19.4 (2003), pp. 325–339. DOI: https://doi.org/10.1123/jab.19.4.325 (cit. on pp. 6, 69, 72).

[65] M. Harrington et al. "Prediction of the hip joint centre in adults, children, and patients with cerebral palsy based on magnetic resonance imaging". In: *Journal of biomechanics* 40.3 (2007), pp. 595–602. DOI: https://doi.org/10.1016/j.jbiomech.2006.02.003 (cit. on p. 40).

[66] F. Heinen et al. "Muscle–tendon unit scaling methods of Hill-type musculoskeletal models: An overview". In: *Proceedings of the Institution of Mechanical Engineers, Part H: Journal of Engineering in Medicine* 230.10 (2016), pp. 976–984. DOI: https://doi.org/10.1177/0954411916659894 (cit. on pp. 25, 27).

[67] J. L. Hicks et al. "Is my model good enough? Best practices for verification and validation of musculoskeletal models and simulations of movement". In: *Journal of biomechanical engineering* 137.2 (2015) (cit. on p. 45).

[68] A. V. Hill. "The abrupt transition from rest to activity in muscle". In: *Proceedings of the Royal Society of London. Series B-Biological Sciences* 136.884 (1949), pp. 399–420. DOI: https://doi.org/10.1098/rspb.1949.0033 (cit. on p. 24).

[69] A. V. Hill. "The heat of shortening and the dynamic constants of muscle". In: *Proceedings of the Royal Society of London. Series B-Biological Sciences* 126.843 (1938), pp. 136–195. DOI: https://doi.org/10.1098/rspb.1938.0050 (cit. on p. 24).

[70] J. A. Holtmann et al. "Gastrocnemius recession leads to increased ankle motion and improved patient satisfaction after 2 years of follow-up". In: *The Journal of Foot and Ankle Surgery* 56.3 (2017), pp. 589–593. DOI: https://doi.org/10.1053/j.jfas.2017.01.037 (cit. on p. 72).

[71] *How CMC works*. Last accessed November 2022. 2017. URL: https://simtk-confluence.stanford.edu:8443/display/OpenSim/How+CMC+Works (cit. on p. 44).

[72] J. Howard, J. Sees, and M. W. Shrader. "Management of Spinal Deformity in Cerebral Palsy: Current Concept Review". In: *JPOSNA®* 1.1 (2019). DOI: https://doi.org/10.55275/JPOSNA-2019-8 (cit. on p. 11).

[73] J. L. Hutton. "Cerebral palsy life expectancy". In: *Clinics in perinatology* 33.2 (2006), pp. 545–555. DOI: https://doi.org/10.1016/j.clp.2006.03.016 (cit. on p. 1).

[74] A. F. Huxley and R. M. Simmons. "Proposed mechanism of force generation in striated muscle". In: *Nature* 233.5321 (1971), pp. 533–538. DOI: https://doi.org/10.1038/233533a0 (cit. on p. 24).

[75] V. T. Inman. "The joints of the ankle". In: *Williams & Wilkins, Baltimore* (1976) (cit. on p. 37).

[76] M. M. Jan. "Cerebral palsy: comprehensive review and update". In: *Annals of Saudi medicine* 26.2 (2006), pp. 123–132. DOI: https://doi.org/10.5144/0256-4947.2006.123 (cit. on pp. 1, 9).

[77] H. Kainz et al. "Selective dorsal rhizotomy improves muscle forces during walking in children with spastic cerebral palsy". In: *Clinical Biomechanics* 65 (2019), pp. 26–33. DOI: https://doi.org/10.1016/j.clinbiomech.2019.03.014 (cit. on p. 6).

[78] H. Kainz et al. "The influence of maximum isometric muscle force scaling on estimated muscle forces from musculoskeletal models of children with cerebral palsy". In: *Gait & posture* 65 (2018), pp. 213–220. DOI: https://doi.org/10.1016/j.gaitpost.2018.07.172 (cit. on p. 39).

[79] C. Kamm. "Early onset torsion dystonia (Oppenheim's dystonia)". In: *Orphanet journal of rare diseases* 1.1 (2006), pp. 1–6. DOI: https://doi.org/10.1186/1750-1172-1-48 (cit. on p. 12).

[80] Y. Kawakami, Y. Ichinose, and T. Fukunaga. "Architectural and functional features of human triceps surae muscles during contraction". In: *Journal of applied physiology* 85.2 (1998), pp. 398–404. DOI: https://doi.org/10.1152/jappl.1998.85.2.398 (cit. on p. 16).

[81] A. Kheder and K. P. S. Nair. "Spasticity: pathophysiology, evaluation and management". In: *Practical neurology* 12.5 (2012), pp. 289–298. DOI: http://dx.doi.org/10.1136/practneurol-2011-000155 (cit. on p. 11).

[82] N. Khouri and E. Desailly. "Contribution of clinical gait analysis to single-event multi-level surgery in children with cerebral palsy". In: *Orthopaedics & Traumatology: Surgery & Research* 103.1 (2017), S105–S111. DOI: https://doi.org/10.1016/j.otsr.2016.11.004 (cit. on p. 1).

[83] P. V. Komi. "Relevance of in vivo force measurements to human biomechanics". In: *Journal of biomechanics* 23 (1990), pp. 23–34. DOI: https://doi.org/10.1016/0021-9290(90)90038-5 (cit. on p. 2).

[84] M. M. van der Krogt et al. "Neuro-musculoskeletal simulation of instrumented contracture and spasticity assessment in children with cerebral palsy". In: *Journal of NeuroEngineering and Rehabilitation* 13.1 (2016), pp. 1–11. DOI: https://doi.org/10.1186/s12984-016-0170-5 (cit. on pp. 39, 76).

[85] D. Lee et al. "Modeling and simulation of skeletal muscle for computer graphics: A survey". In: *Foundations and Trends® in Computer Graphics and Vision* 7.4 (2012), pp. 229–276. DOI: http://dx.doi.org/10.1561/0600000036 (cit. on pp. 26, 27).

[86] D. Levine, J. Richards, and M. W. Whittle. *Whittle's gait analysis*. Elsevier health sciences, 2012 (cit. on p. 4).

[87] J. Li et al. "Quantitative analysis of abnormal and normal gait based on inertial sensors". In: *2018 IEEE 22nd International Conference on Computer Supported Cooperative Work in Design ((CSCWD))*. IEEE. 2018, pp. 365–370. DOI: 10.1109/CSCWD.2018.8465248 (cit. on p. 4).

[88] C.-J. Lin et al. "Common abnormal kinetic patterns of the knee in gait in spastic diplegia of cerebral palsy". In: *Gait & posture* 11.3 (2000), pp. 224–232. DOI: https://doi.org/10.1016/S0966-6362(00)00049-7 (cit. on pp. 5, 6).

[89] M. Q. Liu et al. "Muscle contributions to support and progression over a range of walking speeds". In: *Journal of biomechanics* 41.15 (2008), pp. 3243–3252. DOI: https://doi.org/10.1016/j.jbiomech.2008.07.031 (cit. on p. 72).

[90] M. Q. Liu et al. "Muscles that support the body also modulate forward progression during walking". In: *Journal of biomechanics* 39.14 (2006), pp. 2623–2630. DOI: https://doi.org/10.1016/j.jbiomech.2005.08.017 (cit. on p. 68).

[91] D. G. Lloyd and T. F. Besier. "An EMG-driven musculoskeletal model to estimate muscle forces and knee joint moments in vivo". In: *Journal of biomechanics* 36.6 (2003), pp. 765–776. DOI: https://doi.org/10.1016/S0021-9290(03)00010-1 (cit. on pp. 2, 30).

[92] J. M. Lourenço. *The NOVAthesis LaTeX Template User's Manual*. NOVA University Lisbon. 2021. URL: https://github.com/joaomlourenco/novathesis/raw/master/template.pdf (cit. on p. ii).

[93] M. Mansouri et al. "Rectus femoris transfer surgery affects balance recovery in children with cerebral palsy: A computer simulation study". In: *Gait & posture* 43 (2016), pp. 24–30. DOI: https://doi.org/10.1016/j.gaitpost.2015.08.016 (cit. on p. 7).

[94] A. Mantoan et al. "MOtoNMS: A MATLAB toolbox to process motion data for neuromusculoskeletal modeling and simulation". In: *Source code for biology and medicine* 10.1 (2015), pp. 1–14. DOI: https://doi.org/10.1186/s13029-015-0044-4 (cit. on p. 35).

[95] G. Mantovani and M. Lamontagne. "How different marker sets affect joint angles in inverse kinematics framework". In: *Journal of biomechanical engineering* 139.4 (2017). DOI: https://doi.org/10.1115/1.4034708 (cit. on p. 40).

[96] E. N. Marieb and K. Hoehn. *Human anatomy & physiology*. Pearson education, 2007 (cit. on p. 19).

[97] R. B. Mateus et al. "COMPARISON OF INDIVIDUAL MUSCLE CONTRIBUTIONS TO GROUND REACTION FORCES DURING JUMP AND CHANGE OF DIRECTION TESTING AFTER ANTERIOR CRUCIATE LIGAMENT RECONSTRUCTION". In: *ISBS Proceedings Archive* 40.1 (2022), p. 419. URL: https://commons.nmu.edu/isbs/vol40/iss1/100/ (cit. on p. 7).

[98] M. A. Mathewson et al. "High resolution muscle measurements provide insights into equinus contractures in patients with cerebral palsy". In: *Journal of Orthopaedic Research* 33.1 (2015), pp. 33–39. DOI: https://doi.org/10.1002/jor.22728 (cit. on p. 69).

[99] K. Mikkelsen et al. "Exercise and mental health". In: *Maturitas* 106 (2017), pp. 48–56. DOI: https://doi.org/10.1016/j.maturitas.2017.09.003 (cit. on p. 1).

[100] F. Miller. "Ankle equinus in cerebral palsy". In: *Cerebral Palsy* (2020), pp. 2243–2266. DOI: https://doi.org/10.1007/978-3-319-74558-9_199 (cit. on pp. 15, 68, 70).

[101] *Mokka*. (2018) Available from: URL: http://biomechanical-toolkit.github.io/mokka/ (cit. on p. 34).

[102] I. Multani et al. "Botulinum toxin in the management of children with cerebral palsy". In: *Pediatric Drugs* 21.4 (2019), pp. 261–281. DOI: https://doi.org/10.1007/s40272-019-00344-8 (cit. on p. 11).

[103] M. Narici, G. Roi, and L. Landoni. "Force of knee extensor and flexor muscles and cross-sectional area determined by nuclear magnetic resonance imaging." In: *European journal of applied physiology and occupational physiology* 57.1 (1988), pp. 39–44. DOI: 10.1007/bf00691235 (cit. on p. 39).

[104] R. R. Neptune, S. A. Kautz, and F. E. Zajac. "Contributions of the individual ankle plantar flexors to support, forward progression and swing initiation during walking". In: *Journal of biomechanics* 34.11 (2001), pp. 1387–1398. DOI: https://doi.org/10.1016/S0021-9290(01)00105-1 (cit. on pp. 13, 69, 72).

[105] S. Nigg et al. "Development of a symmetry index using discrete variables". In: *Gait & posture* 38.1 (2013), pp. 115–119. DOI: https://doi.org/10.1016/j.gaitpost.2012.10.024 (cit. on p. 8).

[106] R. Nisell, G. Németh, and H. Ohlsén. "Joint forces in extension of the knee: analysis of a mechanical model". In: *Acta Orthopaedica Scandinavica* 57.1 (1986), pp. 41–46. DOI: https://doi.org/10.3109/17453678608993213 (cit. on p. 37).

[107] R. Palisano et al. "Development and reliability of a system to classify gross motor function in children with cerebral palsy". In: *Developmental medicine & child neurology* 39.4 (1997), pp. 214–223. DOI: https://doi.org/10.1111/j.1469-8749.1997.tb07414.x (cit. on pp. 10, 11).

[108] R. J. Palisano et al. "Content validity of the expanded and revised Gross Motor Function Classification System". In: *Developmental Medicine & Child Neurology* 50.10 (2008), pp. 744–750. DOI: https://doi.org/10.1111/j.1469-8749.2008.03089.x (cit. on p. 10).

[109] M. G. Pandy. "Computer modeling and simulation of human movement". In: *Annual review of biomedical engineering* 3.1 (2001), pp. 245–273. DOI: https://doi.org/10.1146/annurev.bioeng.3.1.245 (cit. on p. 5).

[110] M. G. Pandy and R. E. Barr. "Biomechanics of the musculoskeletal system". In: (2004). URL: http://ptik.unhas.ac.id/tahir/BAHAN-KULIAH/BIO-MEDICAL/NEW/HANBOOK/Biomechanics_Of_The_Musculoskeletal_System.pdf (cit. on p. 29).

[111] A. Patel and B. DiGiovanni. "Association between plantar fasciitis and isolated contracture of the gastrocnemius". In: *Foot & ankle international* 32.1 (2011), pp. 5–8. DOI: 10.3113/FAI.2011.0005 (cit. on p. 16).

[112] D. R. Patel et al. "Cerebral palsy in children: a clinical overview". In: *Translational Pediatrics* 9.S1 (2020). ISSN: 2224-4344. URL: https://tp.amegroups.com/article/view/35534 (cit. on p. 9).

[113] S. J. Pinney, B. J. Sangeorzan, and S. T. Hansen Jr. "Surgical anatomy of the gastrocnemius recession (Strayer procedure)". In: *Foot & ankle international* 25.4 (2004), pp. 247–250. URL: https://journals.sagepub.com/doi/pdf/10.1177/107110070402500409?casa_token=pbCDtrzD6eQAAAAA:cnvjEGQwgwkkHUu44khg1M04K8yZzkuyyIt9TIzasPXf_bFu8yp821-FrDQ67NVngJjID5O8EaBj (cit. on p. 18).

[114] C. Pizzolato et al. "CEINMS: A toolbox to investigate the influence of different neural control solutions on the prediction of muscle excitation and joint moments during dynamic motor tasks". In: *Journal of biomechanics* 48.14 (2015), pp. 3929–3936. DOI: https://doi.org/10.1016/j.jbiomech.2015.09.021 (cit. on p. 76).

[115] S. A. Plowman and D. L. Smith. *Exercise physiology for health fitness and performance*. Lippincott Williams & Wilkins, 2013, p. 586 (cit. on p. 22).

[116] G. A. Power. *Neuromuscular Function Following Lengthening Contractions*. The University of Western Ontario (Canada), 2012. URL: https://ir.lib.uwo.ca/cgi/viewcontent.cgi?article=2238&context=etd (cit. on p. 28).

[117] R. Queen et al. "A novel method for measuring asymmetry in kinematic and kinetic variables: the normalized symmetry index". In: *Journal of biomechanics* 99 (2020), p. 109531. DOI: https://doi.org/10.1016/j.jbiomech.2019.109531 (cit. on p. 8).

[118] A. Rajagopal et al. "Full-body musculoskeletal model for muscle-driven simulation of human gait". In: *IEEE transactions on biomedical engineering* 63.10 (2016), pp. 2068–2079. DOI: 10.1109/TBME.2016.2586891 (cit. on p. 39).

[119] T. Rezgui et al. "On the imitation of CP gait patterns by healthy subjects". In: *Gait & Posture* 38.4 (2013), pp. 576–581. DOI: https://doi.org/10.1016/j.gaitpost.2013.01.022 (cit. on p. 6).

[120] C. Rivares et al. "Remodeling of rat m. gastrocnemius medialis during recovery from aponeurotomy". In: *Frontiers in physiology* (2020), p. 1218. DOI: https://doi.org/10.3389/fphys.2020.541302 (cit. on p. 69).

[121] R. Robinson, W. Herzog, and B. M. Nigg. "Use of force platform variables to quantify the effects of chiropractic manipulation on gait symmetry." In: *Journal of manipulative and physiological therapeutics* 10.4 (1987), pp. 172–176. URL: https://europepmc.org/article/med/2958572 (cit. on p. 8).

[122] J. Rodda and H. Graham. "Classification of gait patterns in spastic hemiplegia and spastic diplegia: a basis for a management algorithm". In: *European journal of neurology* 8 (2001), pp. 98–108. DOI: https://doi.org/10.1046/j.1468-1331.2001.00042.x (cit. on pp. 14, 15).

[123] E. Rutz et al. "Indications for gastrocsoleus lengthening in ambulatory children with cerebral palsy: a Delphi consensus study". In: *Journal of children's orthopaedics* 14.5 (2020), pp. 405–414. DOI: 10.1302/1863-2548.14.200145 (cit. on pp. 2, 16, 17).

[124] S. Sadler et al. "Gluteus medius muscle function in people with and without low back pain: a systematic review". In: *BMC musculoskeletal disorders* 20 (2019), pp. 1–17. DOI: https://doi.org/10.1186/s12891-019-2833-4 (cit. on pp. 71, 73).

[125] G. J. Sammarco et al. "The effects of unilateral gastrocsoleus recession". In: *Foot & ankle international* 27.7 (2006), pp. 508–511. URL: https://journals.sagepub.com/doi/pdf/10.1177/107110070602700705?casa_token=xGYeZVMzAaoAAAAA:L2Uy9DlNrfPYY776Cr4qzBJAosk-4Q4nWrpfJfFpNxtA_W5dvxo408nsQVlVL1_VXW3njlqROYIh (cit. on p. 18).

[126] K. Sasaki et al. "Muscle compensatory mechanisms during able-bodied toe walking". In: *Gait & posture* 27.3 (2008), pp. 440–446. DOI: https://doi.org/10.1016/j.gaitpost.2007.05.012 (cit. on pp. 6, 71).

[127] M. H. Schwartz et al. "Comprehensive treatment of ambulatory children with cerebral palsy: an outcome assessment". In: *Journal of Pediatric Orthopaedics* 24.1 (2004), pp. 45–53. URL: https://journals.lww.com/pedorthopaedics/Abstract/2004/01000/Comprehensive_Treatment_of_Ambulatory_Children.9.aspx (cit. on p. 6).

[128] V. B. Semwal et al. "Biped model based on human Gait pattern parameters for sagittal plane movement". In: *2013 International Conference on Control, Automation, Robotics and Embedded Systems (CARE)*. IEEE. 2013, pp. 1–5. DOI: 10.1109/CARE.2013.6733750 (cit. on p. 12).

[129] A. Seth et al. "OpenSim: a musculoskeletal modeling and simulation framework for in silico investigations and exchange". In: *Procedia Iutam* 2 (2011), pp. 212–232. DOI: https://doi.org/10.1016/j.piutam.2011.04.021 (cit. on p. 35).

[130] B. J. Shore, N. White, and H. Kerr Graham. "Surgical correction of equinus deformity in children with cerebral palsy: a systematic review". In: *Journal of children's orthopaedics* 4.4 (2010), pp. 277–290. DOI: 10.1007/s11832-010-0268-4 (cit. on p. 16).

[131] H. F. Al-Shuka et al. "Biomechanics, actuation, and multi-level control strategies of power-augmentation lower extremity exoskeletons: An overview". In: *International Journal of Dynamics and Control* 7.4 (2019), pp. 1462–1488. DOI: https://doi.org/10.1007/s40435-019-00517-w (cit. on p. 55).

[132] H. L. Siebers et al. "Comparison of different symmetry indices for the quantification of dynamic joint angles". In: *BMC Sports Science, Medicine and Rehabilitation* 13.1 (2021), pp. 1–11. DOI: https://doi.org/10.1186/s13102-021-00355-4 (cit. on p. 8).

[133] N. SILFVERSKIÖLD. "Reduction of the uncrossed two-joints muscles of the leg to one-joint muscles in spastic". In: *Acta Chirurgica Scandinavica* 56 (1924), p. 315 (cit. on pp. 16, 17).

[134] P. A. Smith et al. "Brace evaluation in children with diplegic cerebral palsy with a jump gait pattern". In: *JBJS* 91.2 (2009), pp. 356–365. DOI: 10.2106/JBJS.G.01369 (cit. on p. 16).

[135] K. M. Steele et al. "Muscle contributions to support and progression during single-limb stance in crouch gait". In: *Journal of biomechanics* 43.11 (2010), pp. 2099–2105. DOI: https://doi.org/10.1016/j.jbiomech.2010.04.003 (cit. on pp. 5, 73).

[136] N. Stergiou. *Biomechanics and gait analysis*. Academic Press, 2020 (cit. on p. 4).

[137] L. M. Strayer Jr. "Recession of the gastrocnemius: an operation to relieve spastic contracture of the calf muscles". In: *JBJS* 32.3 (1950), pp. 671–676. URL: https://journals.lww.com/jbjsjournal/Citation/1950/32030/RECESSION_OF_THE_GASTROCNEMIUS__An_Operation_to.22.aspx (cit. on p. 17).

[138] D. L. Stredney. "The Representation of Anatomical Structures through Computer Animation for Scientific, Educational and Artistic Applications." MA thesis. 1982 (cit. on p. 36).

[139] E. Surer and A. Kose. "Methods and technologies for gait analysis". In: *Computer analysis of human behavior*. Springer, 2011, pp. 105–123. DOI: 10.1007/978-0-85729-994-9_5 (cit. on p. 4).

[140] G. Surman et al. "Children with cerebral palsy: severity and trends over time". In: *Paediatric and perinatal epidemiology* 23.6 (2009), pp. 513–521. DOI: https://doi.org/10.1111/j.1365-3016.2009.01060.x (cit. on p. 1).

[141] D. H. Sutherland and J. R. Davids. "Common gait abnormalities of the knee in cerebral palsy." In: *Clinical orthopaedics and related research* 288 (1993), pp. 139–147. URL: https://europepmc.org/article/med/8458127 (cit. on pp. 2, 15).

[142] K. Tedroff et al. "Long-term effects of botulinum toxin A in children with cerebral palsy". In: *Developmental Medicine & Child Neurology* 51.2 (2009), pp. 120–127. DOI: https://doi.org/10.1111/j.1469-8749.2008.03189.x (cit. on p. 11).

[143] D. G. Thelen. "Adjustment of muscle mechanics model parameters to simulate dynamic contractions in older adults". In: *J. Biomech. Eng.* 125.1 (2003), pp. 70–77. DOI: https://doi.org/10.1115/1.1531112 (cit. on pp. 25, 26, 29).

[144] D. G. Thelen and F. C. Anderson. "Using computed muscle control to generate forward dynamic simulations of human walking from experimental data". In: *Journal of biomechanics* 39.6 (2006), pp. 1107–1115. DOI: https://doi.org/10.1016/j.jbiomech.2005.02.010 (cit. on p. 45).

[145] D. G. Thelen, F. C. Anderson, and S. L. Delp. "Generating dynamic simulations of movement using computed muscle control". In: *Journal of biomechanics* 36.3 (2003), pp. 321–328. DOI: https://doi.org/10.1016/S0021-9290(02)00432-3 (cit. on p. 43).

[146] A. Tinney et al. "Gastrocsoleus recession techniques: an anatomical and biomechanical study in human cadavers". In: *The Bone & Joint Journal* 96.6 (2014), pp. 778–782. DOI: https://doi.org/10.1302/0301-620X.96B6.33700 (cit. on p. 17).

[147] U. Trinler et al. "A systematic review of approaches to modelling lower limb muscle forces during gait: Applicability to clinical gait analyses". In: *Gait & posture* 61 (2018), pp. 353–361. DOI: https://doi.org/10.1016/j.gaitpost.2018.02.005 (cit. on p. 5).

[148] N. G. A. UK. "Cerebral palsy in under 25s: assessment and management". In: (2017). URL: https://pubmed.ncbi.nlm.nih.gov/28151611/ (cit. on p. 9).

[149] A. Veloso et al. "Subject-specific musculoskeletal model to identify muscle contribution to the acceleration phase in elite sprinting". In: *ISBS-Conference Proceedings Archive*. 2015. URL: https://ojs.ub.uni-konstanz.de/cpa/article/view/6382 (cit. on p. 5).

[150] K. Vitrikas, H. Dalton, and D. Breish. "Cerebral Palsy: An Overview". In: *Am Fam Physician* 101.4 (2020-02), pp. 213–220. DOI: 10.4274/hamidiyemedj.galenos.2021.72792 (cit. on p. 9).

[151] O. Vulpius and A. Stoffel. *Tenotomie der end schnen der mm. gastrocnemius el soleus mittels rutschenlassens nach vulpius*. 1913. DOI: 10.1007/978-3-319-32552-1_2 (cit. on p. 17).

[152] K. J. Waldron and J. Schmiedeler. "Kinematics". In: *Springer handbook of robotics*. Springer, 2016, pp. 11–36 (cit. on p. 40).

[153] S. R. Ward et al. "Are current measurements of lower extremity muscle architecture accurate?" In: *Clinical orthopaedics and related research* 467.4 (2009), pp. 1074–1082. DOI: https://doi.org/10.1007/s11999-008-0594-8 (cit. on p. 30).

[154] J. W. WHITE. "Torsion of the Achilles tendon: its surgical significance". In: *Archives of Surgery* 46.5 (1943), pp. 784–787. DOI: 10.1001/archsurg.1943.01220110200033 (cit. on p. 17).

[155] M. W. Whittle. "Clinical gait analysis: A review". In: *Human movement science* 15.3 (1996), pp. 369–387. DOI: https://doi.org/10.1016/0167-9457(96)00006-1 (cit. on p. 4).

[156] M. W. Whittle. In: *Gait analysis: An introduction*. Butterworth-Heinemann, 2011, pp. 47–100 (cit. on pp. 12, 13).

[157] T. L. Wickiewicz et al. "Muscle architecture of the human lower limb". In: *Clinical Orthopaedics and Related Research®* 179 (1983), pp. 275–283. URL: https://journals.lww.com/clinorthop/Abstract/1983/10000/Muscle_Architecture_of_the_Human_Lower_Limb.42.aspx (cit. on p. 30).

[158] M. E. Wiley and D. L. Damiano. "Lower-extremity strength profiles in spastic cerebral palsy". In: *Developmental Medicine & Child Neurology* 40.2 (1998), pp. 100–107. DOI: https://doi.org/10.1111/j.1469-8749.1998.tb15369.x (cit. on p. 73).

[159] A. Wilson and G. Lichtwark. "The anatomical arrangement of muscle and tendon enhances limb versatility and locomotor performance". In: *Philosophical Transactions of the Royal Society B: Biological Sciences* 366.1570 (2011), pp. 1540–1553. DOI: https://doi.org/10.1098/rstb.2010.0361 (cit. on p. 21).

[160] J. Wilson et al. "A structured review of the role of gluteus maximus in rehabilitation." In: *New Zealand Journal of Physiotherapy* 33.3 (2005). URL: https://www.researchgate.net/profile/Emma-Ferris-6/publication/288948683_A_structured_review_of_the_role_of_gluteus_maximus_in_rehabilitation/links/57cf2c3808ae582e06938d1f/A-structured-review-of-the-role-of-gluteus-maximus-in-rehabilitation.pdf (cit. on p. 71).

[161] J. M. Winters. "An improved muscle-reflex actuator for use in large-scale neuromusculoskeletal models". In: *Annals of biomedical engineering* 23.4 (1995), pp. 359–374. DOI: 10.1007/BF02584437 (cit. on p. 25).

[162] J. M. Winters and L. Stark. "Muscle models: what is gained and what is lost by varying model complexity". In: *Biological cybernetics* 55.6 (1987), pp. 403–420. DOI: https://doi.org/10.1007/BF00318375 (cit. on p. 24).

[163] T. Winters, J. Gage, and R. Hicks. "Gait patterns in spastic hemiplegia in children and young adults". In: *J Bone Joint Surg Am* 69.3 (1987), pp. 437–441. URL: https://www.ifcpf.com/static/upload/raw/f3382393-92a2-1460-7a9f-29dfcdbe75c1/Winters+TF+1987+Gait+patterns+in+spastic+hemiplegia+in+children+and+young+adults.pdf (cit. on p. 14).

[164] G. T. Yamaguchi and F. E. Zajac. "A planar model of the knee joint to characterize the knee extensor mechanism". In: *Journal of biomechanics* 22.1 (1989), pp. 1–10. DOI: https://doi.org/10.1016/0021-9290(89)90179-6 (cit. on p. 37).

[165] C. T. Q. Ying et al. "Return to physical activity after gastrocnemius recession". In: *World Journal of Orthopedics* 7.11 (2016), p. 746. DOI: 10.5312/wjo.v7.i11.746 (cit. on pp. 2, 16, 18, 72).

[166] J. L. Young et al. "Management of the knee in spastic diplegia: what is the dose?" In: *Orthopedic Clinics* 41.4 (2010), pp. 561–577. DOI: https://doi.org/10.1016/j.ocl.2010.06.006 (cit. on p. 15).

[167] F. E. Zajac. "Muscle and tendon: properties, models, scaling, and application to biomechanics and motor control." In: *Critical reviews in biomedical engineering* 17.4 (1989), pp. 359–411. URL: https://europepmc.org/article/med/2676342 (cit. on pp. 21, 24–26, 28, 29, 39).

[168] F. E. Zajac. "Muscle coordination of movement: a perspective". In: *Journal of biomechanics* 26 (1993), pp. 109–124. DOI: https://doi.org/10.1016/0021-9290(93)90083-Q (cit. on pp. 5, 45).

[169] F. E. Zajac, R. R. Neptune, and S. A. Kautz. "Biomechanics and muscle coordination of human walking: part II: lessons from dynamical simulations and clinical implications". In: *Gait & posture* 17.1 (2003), pp. 1–17. DOI: https://doi.org/10.1016/S0966-6362(02)00069-3 (cit. on p. 71).

[170] V. M. Zatsiorsky and B. I. Prilutsky. *Biomechanics of skeletal muscles*. Human Kinetics, 2012 (cit. on pp. 22, 27, 28).

[171] J. Zhou, E. E. Butler, and J. Rose. "Neurologic correlates of gait abnormalities in cerebral palsy: implications for treatment". In: *Frontiers in human neuroscience* 11 (2017), p. 103. DOI: https://doi.org/10.3389/fnhum.2017.00103 (cit. on p. 55).

A

Appendix

Table A.1: Muscle-tendon actuators constant parameters. From [22].

Parameter	Value
ε_0^M : Passive muscle strain during maximum isometric force	0.6
ε_0^T : Tendon strain at maximum isometric force	0.033
ε_{toe}^T : Tendon strain above which tendon force behaves linearly with tendon	$0.608\ \varepsilon_0^T$
k_{toe} : Exponential shape factor for the force–strain relation of the tendon	3
k_{lin} : Linear shape factor for the force–strain property of the tendon	$1.1712/\varepsilon_0^T$
k^{PE} : Exponential shape factor in the passive force-length property of the muscle	4
$\bar{F}_{toe}^T$: Normalized tendon force at tendon strain ε_{toe}^T	0.333
$\bar{F}_{len}^M$: Maximum normalized tendon force	1.8
V_{max}^M : Maximum contraction velocity in the fibers. in optimal fiber lengths/second	10
A_f : Shape factor related to the force-velocity relation of the muscle	0.3
γ : Shape factor for the active force-length Gaussian curve of the muscle	0.5

Table A.2: Description of the location and orientation of the reference frames. From [36].

Pelvis	The pelvic reference frame is fixed at the midpoint of the line connecting the two anterior superior iliac spines
Femur	The femoral frame is fixed at the center of the femoral head
Tibia	The tibial frame is located at the midpoint of the line between the medial and lateral femoral epicondyles
Patella	The patellar frame is located at the most distal point of the patella
Talus	The talar frame is located at the midpoint of the line between the apices of the medial and lateral malleoli
Calcanus	The calcaneal frame is located at the most interior. lateral point on the posterior surface of the calcanus
Toe	The toe frame is located at the base of the second metatarsal

Table A.3: Inertial Properties for the body segments of the model.

		Moments of inertia			Center of mass		
Body Segment	**Mass (kg)**	**xx**	**yy**	**zz**	**x**	**y**	**z**
Torso	34.2366	1.4745	0.7555	1.4314	-0.0300	0.3200	0
Pelvis	11.777	0.1028	0.0871	0.0579	-0.0707	0	0
Right femur	9.3014	0.1339	0.0351	0.1412	0	-0.1700	0
Right tibia	3.7075	0.0504	0.0051	0.0511	0	-0.1867	0
Right talus	0.1000	0.0010	0.0010	0.0010	0	0	0
Right calcaneus	1.2500	0.0014	0.0039	0.0041	0.1000	0.0300	0
Right toe	0.2166	0.0001	0.0002	0.0010	0.0346	0.0060	-0.0175
Left femur	9.3014	0.1339	0.0351	0.1412	0	-0.1700	0
Left tibia	3.7075	0.0504	0.0051	0.0511	0	-0.1867	0
Left talus	0.1000	0.0010	0.0010	0.0010	0	0	0
Left calcaneus	1.2500	0.0014	0.0039	0.0041	0.1000	0.0300	0
Left toe	0.2166	0.0001	0.0002	0.0010	0.0346	0.0060	-0.0175

Table A.4: Ranges of residual forces and moments obtained from RRA and ID, relative to session 1. Root mean Square (RMS) is also presented.

Trial		FX	FY	FZ	MX	MY	MZ
1_a	Range ID	[-19.010;6.726]	[-36.352;38.503]	[-12.113;1.347]	[-4.018;3.271]	[-7.995;1.068]	[-4.018;3.271]
	Range RRA	[-0.157;0.203]	[-0.111;0.046]	[-0.133;0.32]	[-0.619;0.565]	[-3.137;2.052]	[-0.509;0.935]
	RMS	0.108	0.0541	0.155	0.225	1.298	0.506
1_b	Range ID	[-7.074;14.574]	[-17.039;12.078]	[-15.460;8.095]	[-4.898;5.707]	[-1.59;4.682]	[-16.272;2.083]
	Range RRA	[-0.833;7.401]	[-2.444;5.259]	[-2.117;5.889]	[-6.983;5.889]	[-0.341;5.035]	[-9.281;3.262]
	RMS	3.975	6.415	4.657	3.350	1.872	5.334
2_a	Range ID	[-22.775;10.780]	[-22.140;71.299]	[-20.747;16.227]	[-1.615;7.432]	[-2.32;7.378]	[-9.510;4.808]
	Range RRA	[-2.038;8.299]	[-3.080;4.628]	[-5.722;5.265]	[-3.985;4.085]	[-1.404;5.514]	[-9.914;7.392]
	RMS	4.362	2.392	3.207	2.218	3.253	4.398
2_b	Range ID	[-25.721;23.048]	[-34.815;25.585]	[-5.188;13.684]	[-5.300;3.425]	[-19.266;1.061]	[-19.266;1.061]
	Range RRA	[-0.708;1.010]	[-0.941;1.193]	[-1.276;0.675]	[-5.476;2.683]	[-3.516;5.308]	[-8.602;4.579]
	RMS	0.457	0.526	0.586	2.466	1.698	3.107
3_a	Range ID	[-8.775;12.071]	[-26.173;11.353]	[-22.480;17.768]	[-3.349;5.315]	[-3.818;3.303]	[-10.327;2.413]
	Range RRA	[-0.378;0.738]	[-0.546;0.364]	[-0.658;0.833]	[-2.411;1.886]	[-2.304;2.565]	[-4.987;2.888]
	RMS	0.436	0.285	0.371	1.328	1.532	2.113
3_b	Range ID	[-19.540;12.403]	[-25.309;56.501]	[-20.844;11.903]	[-10.950;8.955]	[-1.075;8.768]	[-18.001;4.602]
	Range RRA	[0.143;1.274]	[-0.958;2.034]	[-0.788;1.459]	[-4.859;4.854]	[-0.504;7.716]	[-7.684;2.950]
	RMS	0.745	0.907	0.741	2.389	2.445	2.699
4_a	Range ID	[-4.600;12.121]	[-6.841;77.238]	[-19.140;22.952]	[-10.748;4.691]	[-3.522;4.210]	[-5.341;3.065]
	Range RRA	[-0.061;0.403]	[-0.348;0.332]	[-0.353;0.696]	[-3.552;2.667]	[-2.765;4.377]	[-2.481;3.620]
	RMS	0.209	0.184	0.349	1.436	2.614	1.823
4_b	Range ID	[-8.395;10.253]	[-15.442;32.152]	[-10.890;7.257]	[-3.585;12.614]	[-5.391;1.517]	[-16.547;-2.908]
	Range RRA	[-4.915;2.529]	[-7.888;9.600]	[-9.395;3.563]	[-5.534;5.700]	[-2.291;1.481]	[-11.568;5.637]
	RMS	2.398	5.961	4.504	2.631	1.132	4.680
5_a	Range ID	[-5.308;7.529]	[-24.841;18.927]	[-10.384;27.487]	[-9.346;7.840]	[-2.580;6.313]	[-15.996;8.88]
	Range RRA	[-0.904;0.583]	[-0.494;0.619]	[-0.089;1.688]	[-3.937;4.533]	[-3.006;5.829]	[-5.058;4.319]
	RMS	0.459	0.327	1.000	2.412	3.294	2.499
5_b	Range ID	[-7.892;16.921]	[-28.750;-0.404]	[-15.112;-0.310]	[-3.720;5.940]	[-4.768;0.405]	[-20.173;-0.626]
	Range RRA	[-0.316;1.525]	[-0.526;1.727]	[-3.950;0.377]	[-2.555;2.512]	[-3.333;1.247]	[-5.428;1.269]
	RMS	1.164	0.812	1.674	1.182	1.674	1.879
6_a	Range ID	[-11.098;12.940]	[-29.826;16.822]	[-17.895;26.793]	[-3.802;5.253]	[-3.094;2.501]	[-11.581;7.389]
	Range RRA	[-0.093;0.645]	[-0.469;0.543]	[-0.469;1.330]	[-1.002;1.971]	[-2.472;3.260]	[-3.571;3.360]
	RMS	0.380	0.338	0.665	0.910	1.472	2.065
6_b	Range ID	[-14.677;14.419]	[-41.660;56.536]	[-16.670;21.261]	[-14.762;1.921]	[-3.288;1.443]	[-13.605;3.815]
	Range RRA	[0.060;1.035]	[-1.045;1.355]	[-0.369;0.966]	[-4.980;4.360]	[-2.956;3.836]	[-5.464;6.057]
	RMS	0.683	0.664	0.467	2.149	1.880	2.416
7_a	Range ID	[-8.809;10.326]	[-25.200;0.089]	[-20.867;19.494]	[-4.636;6.443]	[-3.931;2.901]	[-8.276;2.610]
	Range RRA	[-0.635;0.555]	[-0.643;0.855]	[-0.942;1.019]	[-4.909;4.041]	[-3.311;2.419]	[-5.259;5.562]
	RMS	0.326	0.478	0.591	2.620	1.404	2.814
7_b	Range ID	[-10.971;15.837]	[-29.810;59.222]	[-5.420;16.327]	[-11.211;-3.353]	[-3.826;-0.249]	[-8.522;-0.643]
	Range RRA	[-0.103;0.890]	[-0.381;0.860]	[-0.001;0.922]	[-4.679;3.476]	[-3.549;-0.149]	[-4.208;2.048]
	RMS	0.613	0.398	0.604	2.235	1.594	1.987
8_a	Range ID	[-17.153;8.954]	[-32.784;23.028]	[-27.695;11.646]	[0.531;9.654]	[-3.303;1.241]	[-12.387;0.577]
	Range RRA	[-0.085;0.683]	[-0.846;1.332]	[-1.423;-0.467]	[-4.050;2.218]	[-2.893;2.651]	[-5.724;3.337]
	RMS	0.489	0.589	1.018	1.947	1.484	2.406
8_b	Range ID	[-15.486;12.212]	[-22.262;8.930]	[-13.247;8.963]	[-5.888;3.807]	[-3.390;1.111]	[-15.967;0.170]
	Range RRA	[-0.255;0.268]	[-0.774;0.767]	[-1.163;0.774]	[-4.780;2.316]	[-2.291;4.240]	[-5.927;2.830]
	RMS	0.138	0.401	0.614	1.925	1.692	2.249

Table A.5: Ranges of residual forces and moments obtained from RRA and ID, relative to session 2. Root mean Square (RMS) is also presented.

Trial		FX	FY	FZ	MX	MY	MZ
1_a	Range ID	[-36.971;15.736]	[-129.596;252.787]	[-12.395;13.19]	[-3.946;12.943]	[-6.655;6.055]	[-22.305;9.906]
	Range RRA	[-0.220;0.761]	[-1.223;0.600]	[-0.786;0.474]	[-2.655;1.441]	[-2.409;1.238]	[-4.661;4.231]
	RMS	0.425	0.651	0.393	1.184	1.073	2.490
1_b	Range ID	[-25.224;37.747]	[-123.874;66.231]	[-46.095;14.302]	[-12.640;6.595]	[-6.640;7.643]	[-32.046;4.041]
	Range RRA	[-0.396;0.995]	[-1.229;1.055]	[-0.091;1.331]	[-3.975;4.289]	[-2.124;2.777]	[-4.514;2.878]
	RMS	0.462	0.815	0.880	2.662	1.570	2.311
2_a	Range ID	[-35.018;12.911]	[-143.648;269.163]	[-14.904;14.223]	[-1.436;11.397]	[-4.391;5.189]	[-21.346;5.445]
	Range RRA	[-0.139;1.423]	[-1.190;1.349]	[-0.980;0.126]	[-3.309;2.433]	[-1.794;2.479]	[-4.535;4.558]
	RMS	0.865	0.730	0.516	1.542	1.326	2.463
2_b	Range ID	[-26.560;33.128]	[-132.769;196.221]	[-26.029;22.828]	[-9.340;5.999]	[-4.265;5.254]	[-33.430;4.485]
	Range RRA	[-0.097;1.273]	[-2.219;0.331]	[-0.145;1.293]	[-3.375;5.221]	[-2.809;2.661]	[-7.591;6.862]
	RMS	0.779	1.362	0.783	2.998	1.599	3.594
3_a	Range ID	[-31.376;17.407]	[-154.597;254.883]	[-18.896;16.931]	[-3.384;14.020]	[-5.940;6.027]	[-23.103;4.561]
	Range RRA	[-0.219;1.503]	[-1.546;0.722]	[-1.267;0.167]	[-3.725;1.689]	[-2.447;2.557]	[-3.872;3.817]
	RMS	0.954	0.769	0.545	1.542	1.371	1.811
3_b	Range ID	[-22.969;25.168]	[-128.437;169.967]	[-29.033;30.320]	[-13.018;5.538]	[-5.565;6.079]	[-36.015;2.977]
	Range RRA	[-0.103;1.091]	[-3.342;-0.102]	[-0.241;1.756]	[-5.647;6.984]	[-3.344;3.921]	[-6.482;5.983]
	RMS	0.619	1.935	0.924	3.351	2.352	3.838
4_a	Range ID	[-42.763;22.951]	[-55.196;262.643]	[-16.889;18.102]	[-2.094;13.509]	[-5.191;6.840]	[-12.630;3.372]
	Range RRA	[-0.890;0.703]	[-1.723;1.764]	[-2.085;-0.042]	[-5.235;3.167]	[-4.868;3.403]	[-4.486;7.149]
	RMS	0.482	0.890	1.364	2.765	2.461	2.394
4_b	Range ID	[-17.370;31.945]	[-66.000;178.277]	[-28.456;9.154]	[-7.483;7.308]	[-5.343;10.409]	[-49.961;3.509]
	Range RRA	[-0.028;2.208]	[-2.583;0.068]	[-0.245;0.914]	[-2.765;4.158]	[-2.843;1.588]	[-10.064;3.160]
	RMS	1.231	1.506	0.395	2.284	1.511	3.983
5_a	Range ID	[-40.641;25.604]	[-174.164;262.798]	[-13.451;13.639]	[-0.919;17.446]	[-6.099;6.842]	[-30.235;11.771]
	Range RRA	[-0.546;0.692]	[-1.681;0.792]	[-0.772;0.158]	[-3.406;2.079]	[-2.522;1.809]	[-4.793;4.018]
	RMS	0.359	0.751	0.339	1.521	1.570	2.852
5_b	Range ID	[-35.561;29.73]	[-161.016;183.593]	[-33.683;14.659]	[-7.786;14.226]	[-5.325;11.283]	[-32.032;11.775]
	Range RRA	[-0.143;1.668]	[-5.031;0.557]	[-0.298;1.453]	[-1.96;4.524]	[-2.723;1.927]	[-4.238;2.027]
	RMS	0.926	3.870	1.009	2.355	1.416	2.267
6_a	Range ID	[-36.879;16.625]	[-46.585;251.770]	[-21.611;14.686]	[-4.018;12.628]	[-7.217;5.109]	[-13.642;1.389]
	Range RRA	[-0.608;0.420]	[-0.610;0.461]	[-0.645;0.415]	[-2.911;4.066]	[-3.320;2.393]	[-2.696;4.632]
	RMS	0.330	0.277	0.350	1.885	1.788	1.991
6_b	Range ID	[-23.261;33.534]	[-39.141;167.176]	[-21.941;14.690]	[-9.597;3.914]	[-7.215;6.301]	[-32.371;2.903]
	Range RRA	[-0.181;1.107]	[-0.973;0.048]	[-0.105;0.892]	[-4.146;5.448]	[-3.190;3.157]	[-5.616;5.711]
	RMS	0.548	0.595	0.388	2.935	2.004	3.204
7_a	Range ID	[-46.662;14.258]	[-118.967;273.506]	[-14.450;18.534]	[-3.237;15.366]	[-5.272;7.407]	[-26.443;5.712]
	Range RRA	[-0.225;0.941]	[-0.914;0.157]	[-0.816;0.34]	[-4.575;3.614]	[-3.183;2.483]	[-4.342;5.014]
	RMS	0.454	0.419	0.453	1.907	1.755	2.275
7_b	Range ID	[-32.081;23.559]	[-103.936;187.126]	[-31.151;21.659]	[-10.168;7.184]	[-5.385;5.369]	[-28.346;2.026]
	Range RRA	[0.188;1.571]	[-0.235;0.739]	[-0.521;1.061]	[-4.869;5.462]	[-2.666;2.336]	[-9.687;4.763]
	RMS	0.966	0.302	0.504	3.094	1.613	4.323
8_a	Range ID	[-36.072;13.719]	[-155.977;270.205]	[-14.603;17.268]	[-1.096;12.730]	[-4.738;5.462]	[-30.648;1.222]
	Range RRA	[-0.356;0.710]	[-0.600;0.412]	[-1.204;0.269]	[-4.039;3.030]	[-2.872;2.198]	[-2.721;2.349]
	RMS	0.326	0.321	0.666	2.315	1.585	1.021
8_b	Range ID	[-29.338;31.898]	[-129.470;174.015]	[-20.835;24.586]	[-5.835;5.190]	[-4.430;6.847]	[-34.790;4.825]
	Range RRA	[0.012;0.984]	[-0.994;-0.019]	[-0.617;1.609]	[-1.179;2.759]	[-4.024;2.626]	[-6.343;7.437]
	RMS	0.477	0.630	1.186	1.337	1.672	3.718

Table A.6: Ranges of residual forces and moments obtained from RRA and ID, relative to session 3. Root mean Square (RMS) is also presented.

Trial		FX	FY	FZ	MX	MY	MZ
1_a	Range ID	[-13.242;9.219]	[-89.650;-59.586]	[-5.101;13.810]	[-2.320;5.971]	[-0.733;2.442]	[-9.389;2.925]
	Range RRA	[-0.966;0.232]	[-0.237;0.290]	[-0.554;1.226]	[-2.125;3.632]	[-1.139;3.158]	[-0.422;1.079]
	RMS	0.605	0.141	0.521	1.789	1.606	1.606
1_b	Range ID	[-19.410;10.163]	[-99.090;14.616]	[-10.501;8.526]	[-6.099;1.517]	[-1.741;1.688]	[-8.375;15.220]
	Range RRA	[-1.127;0.609]	[-1.174;0.349]	[-0.594;0.494]	[-5.308;0.117]	[-2.061;2.513]	[-0.733;5.560]
	RMS	0.583	0.794	0.358	3.812	1.254	1.486
2_a	Range ID	[-10.344;14.870]	[-104.915;-65.590]	[-7.570;11.496]	[-1.186;4.497]	[-1.235;2.118]	[-7.818;7.580]
	Range RRA	[-0.137;0.635]	[-0.322;0.154]	[-0.602;0.218]	[-2.131;1.820]	[-2.538;3.021]	[-1.220;1.272]
	RMS	0.385	0.128	0.249	1.224	1.601	0.662
2_b	Range ID	[-6.588;13.188]	[-100.833;-63.201]	[-13.510;7.588]	[-5.660;0.545]	[-1.986;1.877]	[-8.290;5.927]
	Range RRA	[0.175;1.081]	[-0.218;0.069]	[-0.724;0.505]	[-3.131;2.298]	[-1.696;2.753]	[-1.512;0.280]
	RMS	0.646	0.0847	0.342	1.671	1.055	0.742
3_a	Range ID	[-12.668;11.252]	[-95.527;-61.899]	[-5.195;12.601]	[-3.822;5.157]	[-0.591;2.455]	[-10.623;-2.860]
	Range RRA	[-1.336;0.332]	[-0.394;0.007]	[-0.708;0.782]	[-3.115;2.422]	[-0.736;2.263]	[-0.439;1.352]
	RMS	0.662	0.245	0.441	1.473	1.472	0.829
3_b	Range ID	[-11.662;12.480]	[-110.579;-51.328]	[-8.498;-1.260]	[-9.196;13.732]	[-1.024;2.831]	[-13.797;0.926]
	Range RRA	[-1.252;0.374]	[-0.180;0.498]	[-0.638;0.584]	[-3.442;1.825]	[-1.321;4.583]	[-1.519;0.847]
	RMS	0.792	0.213	0.403	1.840	1.642	0.737
4_a	Range ID	[-9.471;18.926]	[-96.442;-62.453]	[-12.056;12.840]	[0.224;5.231]	[-0.949;2.296]	[-7.606;9.274]
	Range RRA	[0.388;1.078]	[0.004;0.441]	[-1.008;0.174]	[-2.789;2.309]	[-1.401;2.664]	[-1.500;0.705]
	RMS	0.743	0.225	0.429	1.262	0.964	0.601
4_b	Range ID	[-7.603;17.421]	[-99.661;-62.383]	[-9.361;4.551]	[-1.479;3.064]	[-0.944;1.401]	[-5.963;8.899]
	Range RRA	[0.157;1.196]	[-0.169;0.070]	[-0.708;0.513]	[-1.755;1.596]	[-1.558;2.252]	[-1.894;-0.093]
	RMS	0.871	0.0759	0.340	1.185	0.918	1.107
5_a	Range ID	[-12.282;9.022]	[-7.115;17.834]	[-18.038;14.972]	[-9.073;0.493]	[-2.265;4.760]	[-14.913;-6.177]
	Range RRA	[-0.039;0.687]	[-0.390;0.026]	[-0.543;1.039]	[-2.527;2.403]	[-1.037;4.028]	[-1.451;0.786]
	RMS	0.379	0.217	0.430	1.304	2.374	0.542
5_b	Range ID	[-17.559;7.714]	[-13.094;41.963]	[-19.241;21.462]	[-8.420;4.235]	[-2.635;4.516]	[-12.098;3.136]
	Range RRA	[-2.164;0.095]	[-0.335;0.541]	[-0.686;0.819]	[-3.272;2.835]	[-2.552;3.640]	[-1.139;2.991]
	RMS	1.336	0.161	0.390	2.054	1.426	0.825
6_a	Range ID	[-14.124;10.477]	[-25.068;16.765]	[-19.365;11.310]	[-2.535;4.374]	[-2.345;2.393]	[-8.693;2.925]
	Range RRA	[0.170;0.854]	[-0.095;0.348]	[-0.870;0.016]	[-2.706;1.657]	[-1.878;2.750]	[-1.281;0.615]
	RMS	0.545	0.185	0.433	1.226	1.206	0.623
6_b	Range ID	[-12.167;19.526]	[-14.461;10.552]	[-14.424;22.463]	[-4.876;4.764]	[-2.490;3.141]	[-11.735;0.775]
	Range RRA	[0.105;1.356]	[-0.181;0.245]	[-1.011;0.888]	[-3.706;1.812]	[-2.852;3.406]	[-2.223;0.331]
	RMS	0.656	0.133	0.493	2.403	1.505	1.055
7_a	Range ID	[-16.742;10.484]	[-19.612;4.735]	[-25.989;15.565]	[-5.840;3.574]	[-3.187;4.009]	[-12.386;-2.626]
	Range RRA	[-1.137;0.537]	[-0.228;0.063]	[-1.187;0.285]	[-4.269;3.654]	[-2.097;3.885]	[-0.814;1.256]
	RMS	0.593	0.105	0.521	2.091	2.115	0.506
7_b	Range ID	[-17.018;11.525]	[-9.082;19.632]	[-7.959;22.050]	[-5.422;1.321]	[-1.637;3.464]	[-16.112;1.874]
	Range RRA	[-1.521;-0.019]	[-0.192;0.174]	[-0.504;0.361]	[-2.725;1.476]	[-2.534;3.353]	[-1.362;2.343]
	RMS	0.941	0.099	0.244	1.574	1.729	0.735
8_a	Range ID	[-11.687;13.285]	[-10.764;14.332]	[-15.352;11.175]	[-4.633;3.854]	[-1.669;2.078]	[-11.441;0.000]
	Range RRA	[0.066;0.931]	[-0.272;0.191]	[-0.932;0.267]	[-3.518;2.342]	[-1.251;1.719]	[-1.581;0.760]
	RMS	0.553	0.121	0.421	1.681	1.032	0.677
8_b	Range ID	[-11.599;18.993]	[-16.855;36.157]	[-10.322;23.471]	[-5.134;0.907]	[-2.037;3.658]	[-8.883;7.177]
	Range RRA	[0.111;0.757]	[-0.364;0.351]	[-0.201;1.069]	[-3.212;2.858]	[-3.552;3.501]	[-1.872;0.531]
	RMS	0.479	0.175	0.480	1.653	1.552	1.128

Table A.7: Position errors in the joints degrees of freedom from RRA relative to session 1. The values are in degrees.

Trial		Right Hip Flexion	Right Hip Adduction	Right Hip Rotation	Right Knee Angle	Right Ankle Angle	Left Hip Flexion	Left Hip Adduction	Left Hip Rotation	Left Knee Angle	Left Ankle Angle	Lumbar Extension	Lumbar Bending	Lumbar Rotation
1_a	MAX	0.037	0.049	0.155	0.165	2.592	0.022	0.053	0.030	0.008	0.013	0.031	0.068	0.014
	RMS	0.000	0.000	0.001	0.001	0.021	0.000	0.000	0.000	0.000	0.000	0.000	0.001	0.000
1_b	MAX	0.003	0.009	0.002	0.002	0.001	0.008	0.005	0.037	0.049	0.578	0.012	0.016	0.007
	RMS	0.000	0.000	0.000	0.000	0.000	0.000	0.000	0.000	0.001	0.007	0.000	0.000	0.000
2_a	MAX	0.004	0.006	0.025	0.023	0.460	0.001	0.008	0.004	0.001	0.001	0.009	0.013	0.005
	RMS	0.000	0.000	0.000	0.000	0.004	0.000	0.000	0.000	0.000	0.000	0.000	0.000	0.000
2_b	MAX	0.014	0.022	0.008	0.022	0.006	0.049	0.035	0.066	0.080	0.643	0.043	0.023	0.055
	RMS	0.000	0.000	0.000	0.000	0.000	0.001	0.000	0.001	0.001	0.006	0.001	0.000	0.001
3_a	MAX	0.007	0.013	0.040	0.042	0.878	0.026	0.017	0.007	0.005	0.007	0.024	0.015	0.021
	RMS	0.000	0.000	0.000	0.000	0.006	0.000	0.000	0.000	0.000	0.000	0.000	0.000	0.000
3_b	MAX	0.012	0.026	0.011	0.020	0.007	0.047	0.023	0.085	0.124	1.819	0.049	0.030	0.025
	RMS	0.000	0.000	0.000	0.000	0.000	0.001	0.000	0.001	0.001	0.019	0.001	0.000	0.000
4_a	MAX	0.006	0.037	0.056	0.072	1.446	0.010	0.045	0.016	0.003	0.006	0.015	0.048	0.048
	RMS	0.000	0.000	0.001	0.001	0.013	0.000	0.000	0.000	0.000	0.000	0.000	0.000	0.000
4_b	MAX	0.001	0.005	0.003	0.002	0.001	0.003	0.002	0.019	0.016	0.267	0.004	0.001	0.005
	RMS	0.000	0.000	0.000	0.000	0.000	0.000	0.000	0.000	0.000	0.002	0.000	0.000	0.000
5_a	MAX	0.032	0.072	0.086	0.168	2.090	0.030	0.061	0.045	0.005	0.009	0.028	0.098	0.053
	RMS	0.000	0.001	0.001	0.002	0.020	0.000	0.001	0.000	0.000	0.000	0.000	0.001	0.001
5_b	MAX	0.024	0.027	0.022	0.003	0.005	0.068	0.009	0.199	0.240	2.240	0.084	0.059	0.054
	RMS	0.000	0.000	0.000	0.000	0.000	0.001	0.000	0.002	0.003	0.024	0.001	0.000	0.000
6_a	MAX	0.022	0.044	0.044	0.093	1.400	0.011	0.034	0.026	0.004	0.007	0.025	0.062	0.016
	RMS	0.000	0.001	0.000	0.001	0.013	0.000	0.000	0.000	0.000	0.000	0.000	0.001	0.000
6_b	MAX	0.007	0.035	0.007	0.007	0.002	0.014	0.022	0.052	0.131	2.022	0.032	0.018	0.058
	RMS	0.000	0.000	0.000	0.000	0.000	0.000	0.000	0.000	0.001	0.018	0.000	0.000	0.000
7_a	MAX	0.013	0.025	0.038	0.035	0.480	0.015	0.027	0.009	0.002	0.003	0.013	0.022	0.013
	RMS	0.000	0.000	0.000	0.000	0.005	0.000	0.000	0.000	0.000	0.000	0.000	0.000	0.000
7_b	MAX	0.011	0.042	0.009	0.003	0.003	0.030	0.044	0.111	0.149	2.308	0.057	0.034	0.108
	RMS	0.000	0.000	0.000	0.000	0.000	0.000	0.000	0.001	0.002	0.026	0.001	0.000	0.001
8_a	MAX	0.003	0.021	0.049	0.052	0.832	0.005	0.008	0.012	0.005	0.006	0.030	0.019	0.063
	RMS	0.000	0.000	0.000	0.000	0.006	0.000	0.000	0.000	0.000	0.000	0.000	0.000	0.001
8_b	MAX	0.013	0.027	0.010	0.020	0.005	0.044	0.034	0.069	0.084	0.628	0.037	0.019	0.040
	RMS	0.000	0.000	0.000	0.000	0.000	0.000	0.000	0.001	0.001	0.006	0.000	0.000	0.000

Table A.8: Position errors in the joints degrees of freedom from RRA relative to session 2. The values are in degrees.

Trial		Right Hip Flexion	Right Hip Adduction	Right Hip Rotation	Right Knee Angle	Right Ankle Angle	Left Hip Flexion	Left Hip Adduction	Left Hip Rotation	Left Knee Angle	Left Ankle Angle	Lumbar Extension	Lumbar Bending	Lumbar Rotation
1_a	MAX	0.012	0.016	0.027	0.008	0.619	0.011	0.021	0.006	0.003	0.004	0.004	0.018	0.003
	RMS	0.000	0.000	0.000	0.000	0.006	0.000	0.000	0.000	0.000	0.000	0.000	0.000	0.000
1_b	MAX	0.005	0.019	0.004	0.002	0.001	0.016	0.013	0.023	0.031	0.377	0.004	0.007	0.008
	RMS	0.000	0.000	0.000	0.000	0.000	0.000	0.000	0.000	0.000	0.004	0.000	0.000	0.000
2_a	MAX	0.024	0.030	0.048	0.012	1.044	0.019	0.039	0.006	0.003	0.004	0.006	0.027	0.007
	RMS	0.000	0.000	0.000	0.000	0.011	0.000	0.000	0.000	0.000	0.000	0.000	0.000	0.000
2_b	MAX	0.010	0.031	0.004	0.005	0.003	0.041	0.016	0.066	0.030	0.971	0.002	0.022	0.010
	RMS	0.000	0.000	0.000	0.000	0.000	0.000	0.000	0.001	0.000	0.012	0.000	0.000	0.000
3_a	MAX	0.027	0.021	0.032	0.019	0.944	0.015	0.030	0.003	0.002	0.003	0.007	0.022	0.009
	RMS	0.000	0.000	0.000	0.000	0.010	0.000	0.000	0.000	0.000	0.000	0.000	0.000	0.000
3_b	MAX	0.011	0.034	0.007	0.010	0.004	0.045	0.018	0.069	0.025	0.995	0.003	0.023	0.010
	RMS	0.000	0.000	0.000	0.000	0.000	0.001	0.000	0.001	0.000	0.012	0.000	0.000	0.000
4_a	MAX	0.029	0.013	0.037	0.041	0.378	0.012	0.016	0.005	0.002	0.003	0.007	0.012	0.011
	RMS	0.000	0.000	0.000	0.000	0.004	0.000	0.000	0.000	0.000	0.000	0.000	0.000	0.000
4_b	MAX	0.004	0.036	0.014	0.004	0.005	0.022	0.028	0.086	0.023	1.353	0.017	0.038	0.003
	RMS	0.000	0.000	0.000	0.000	0.000	0.000	0.000	0.001	0.000	0.013	0.000	0.000	0.000
5_a	MAX	0.013	0.012	0.015	0.016	0.270	0.012	0.016	0.004	0.003	0.006	0.003	0.007	0.004
	RMS	0.000	0.000	0.000	0.000	0.003	0.000	0.000	0.000	0.000	0.000	0.000	0.000	0.000
5_b	MAX	0.005	0.047	0.006	0.015	0.004	0.047	0.023	0.117	0.032	1.613	0.010	0.041	0.016
	RMS	0.000	0.000	0.000	0.000	0.000	0.000	0.000	0.001	0.000	0.015	0.000	0.000	0.000
6_a	MAX	0.006	0.012	0.019	0.016	0.272	0.006	0.008	0.004	0.001	0.003	0.005	0.010	0.002
	RMS	0.000	0.000	0.000	0.000	0.001	0.000	0.000	0.000	0.000	0.000	0.000	0.000	0.000
6_b	MAX	0.007	0.019	0.004	0.003	0.003	0.021	0.012	0.032	0.025	0.501	0.002	0.012	0.005
	RMS	0.000	0.000	0.000	0.000	0.000	0.000	0.000	0.000	0.000	0.006	0.000	0.000	0.000
7_a	MAX	0.024	0.016	0.034	0.010	0.739	0.016	0.025	0.002	0.001	0.003	0.002	0.017	0.007
	RMS	0.000	0.000	0.000	0.000	0.008	0.000	0.000	0.000	0.000	0.000	0.000	0.000	0.000
7_b	MAX	0.003	0.020	0.009	0.005	0.004	0.016	0.019	0.031	0.020	0.581	0.008	0.016	0.002
	RMS	0.000	0.000	0.000	0.000	0.000	0.000	0.000	0.000	0.000	0.006	0.000	0.000	0.000
8_a	MAX	0.016	0.016	0.018	0.012	0.357	0.009	0.020	0.003	0.001	0.002	0.002	0.006	0.005
	RMS	0.000	0.000	0.000	0.000	0.004	0.000	0.000	0.000	0.000	0.000	0.000	0.000	0.000
8_b	MAX	0.008	0.032	0.005	0.003	0.001	0.034	0.019	0.074	0.026	0.776	0.003	0.018	0.008
	RMS	0.000	0.000	0.000	0.000	0.000	0.000	0.000	0.001	0.000	0.009	0.000	0.000	0.000

Table A.9: Position errors in the joints degrees of freedom from RRA relative to session 3. The values are in degrees.

Trial		Right Hip Flexion	Right Hip Adduction	Right Hip Rotation	Right Knee Angle	Right Ankle Angle	Left Hip Flexion	Left Hip Adduction	Left Hip Rotation	Left Knee Angle	Left Ankle Angle	Lumbar Extension	Lumbar Bending	Lumbar Rotation
1_a	MAX	0.013	0.087	0.027	0.017	0.166	0.007	0.068	0.019	0.002	0.003	0.033	0.055	0.019
	RMS	0.000	0.001	0.000	0.000	0.001	0.000	0.001	0.000	0.000	0.000	0.000	0.001	0.000
1_b	MAX	0.003	0.219	0.058	0.010	0.007	0.010	0.240	0.014	0.026	0.426	0.014	0.193	0.150
	RMS	0.000	0.002	0.001	0.000	0.000	0.000	0.003	0.000	0.000	0.003	0.000	0.002	0.002
2_a	MAX	0.007	0.054	0.010	0.019	0.178	0.012	0.052	0.017	0.003	0.004	0.018	0.034	0.028
	RMS	0.000	0.001	0.000	0.000	0.001	0.000	0.001	0.000	0.000	0.000	0.000	0.000	0.000
2_b	MAX	0.005	0.051	0.020	0.011	0.004	0.015	0.065	0.024	0.033	0.464	0.038	0.042	0.023
	RMS	0.000	0.001	0.000	0.000	0.000	0.000	0.001	0.000	0.000	0.005	0.000	0.000	0.000
3_a	MAX	0.019	0.039	0.048	0.047	0.787	0.016	0.030	0.007	0.005	0.004	0.044	0.032	0.119
	RMS	0.000	0.000	0.000	0.000	0.008	0.000	0.000	0.000	0.000	0.000	0.000	0.000	0.001
3_b	MAX	0.004	0.044	0.019	0.016	0.003	0.044	0.063	0.056	0.031	1.028	0.013	0.041	0.077
	RMS	0.000	0.001	0.000	0.000	0.000	0.000	0.001	0.000	0.000	0.009	0.000	0.001	0.001
4_a	MAX	0.015	0.043	0.011	0.017	0.488	0.010	0.040	0.009	0.005	0.004	0.039	0.021	0.042
	RMS	0.000	0.001	0.000	0.000	0.005	0.000	0.000	0.000	0.000	0.000	0.000	0.000	0.000
4_b	MAX	0.006	0.041	0.019	0.014	0.005	0.030	0.056	0.024	0.044	0.549	0.058	0.027	0.042
	RMS	0.000	0.000	0.000	0.000	0.000	0.000	0.001	0.000	0.001	0.007	0.001	0.000	0.001
5_a	MAX	0.013	0.045	0.017	0.014	0.287	0.019	0.024	0.009	0.002	0.004	0.017	0.029	0.102
	RMS	0.000	0.000	0.000	0.000	0.003	0.000	0.000	0.000	0.000	0.000	0.000	0.000	0.001
5_b	MAX	0.001	0.065	0.028	0.023	0.004	0.066	0.087	0.126	0.055	2.191	0.041	0.043	0.051
	RMS	0.000	0.001	0.000	0.000	0.000	0.001	0.001	0.001	0.001	0.018	0.000	0.000	0.001
6_a	MAX	0.016	0.048	0.033	0.033	0.611	0.016	0.050	0.011	0.007	0.008	0.022	0.034	0.042
	RMS	0.000	0.000	0.000	0.000	0.006	0.000	0.001	0.000	0.000	0.000	0.000	0.000	0.000
6_b	MAX	0.008	0.100	0.042	0.016	0.007	0.030	0.123	0.034	0.042	0.640	0.045	0.073	0.037
	RMS	0.000	0.001	0.001	0.000	0.000	0.000	0.001	0.000	0.001	0.007	0.001	0.001	0.000
7_a	MAX	0.036	0.067	0.032	0.032	0.853	0.032	0.071	0.020	0.003	0.003	0.034	0.061	0.092
	RMS	0.000	0.001	0.000	0.000	0.009	0.000	0.001	0.000	0.000	0.000	0.000	0.001	0.001
7_b	MAX	0.002	0.053	0.022	0.011	0.005	0.029	0.067	0.058	0.026	1.075	0.032	0.045	0.067
	RMS	0.000	0.001	0.000	0.000	0.000	0.000	0.001	0.000	0.000	0.009	0.000	0.000	0.001
8_a	MAX	0.011	0.067	0.038	0.025	0.842	0.007	0.060	0.021	0.003	0.005	0.020	0.043	0.024
	RMS	0.000	0.001	0.000	0.000	0.006	0.000	0.001	0.000	0.000	0.000	0.000	0.000	0.000
8_b	MAX	0.005	0.059	0.022	0.018	0.003	0.037	0.082	0.085	0.071	1.368	0.035	0.093	0.037
	RMS	0.000	0.000	0.000	0.000	0.000	0.000	0.001	0.001	0.001	0.011	0.000	0.001	0.000

Table A.10: Position errors of the pelvis from RRA relative to session 1. The values are in degrees.

Trial		Pelvis tz	Pelvis tx	Pelvis ty	Pelvis tilt	Pelvis list	Pelvis rotation
1_a	**MAX**	0.128	0.544	0.125	0.538	0.590	0.909
	RMS	0.001	0.002	0.001	0.003	0.004	0.007
1_b	**MAX**	0.527	0.536	1.927	1.363	1.698	1.348
	RMS	0.002	0.002	0.011	0.004	0.011	0.010
2_a	**MAX**	0.170	0.348	0.148	0.550	0.374	0.787
	RMS	0.001	0.002	0.001	0.004	0.002	0.003
2_b	**MAX**	0.091	0.677	0.217	1.004	0.519	0.726
	RMS	0.001	0.004	0.001	0.008	0.004	0.005
3_a	**MAX**	0.656	0.631	0.253	1.483	0.362	1.580
	RMS	0.004	0.002	0.002	0.008	0.001	0.006
3_b	**MAX**	0.244	0.476	0.257	0.737	0.628	1.416
	RMS	0.001	0.002	0.001	0.006	0.004	0.011
4_a	**MAX**	0.348	0.959	0.486	0.901	0.257	1.572
	RMS	0.003	0.005	0.003	0.004	0.002	0.006
4_b	**MAX**	0.093	0.967	0.205	1.839	0.462	0.397
	RMS	0.001	0.006	0.001	0.013	0.003	0.003
5_a	**MAX**	0.338	0.375	0.507	0.377	0.276	0.284
	RMS	0.002	0.003	0.003	0.002	0.001	0.001
5_b	**MAX**	0.131	1.444	0.393	0.694	0.822	1.446
	RMS	0.001	0.006	0.003	0.005	0.005	0.011
6_a	**MAX**	0.493	0.671	0.362	0.890	0.226	1.272
	RMS	0.003	0.003	0.002	0.003	0.001	0.005
6_b	**MAX**	0.125	0.628	0.229	1.387	0.966	0.104
	RMS	0.001	0.004	0.001	0.010	0.007	0.001
7_a	**MAX**	0.619	0.398	0.147	0.424	0.398	0.176
	RMS	0.004	0.002	0.001	0.003	0.003	0.001
7_b	**MAX**	0.170	0.932	0.255	0.404	0.630	1.767
	RMS	0.001	0.004	0.002	0.002	0.004	0.013
8_a	**MAX**	0.273	0.500	0.105	0.425	0.369	0.059
	RMS	0.002	0.003	0.001	0.002	0.003	0.000
8_b	**MAX**	0.487	0.556	0.422	2.204	0.310	0.199
	RMS	0.003	0.004	0.002	0.012	0.002	0.001

Table A.11: Position errors of the pelvis from RRA relative to session 2. The values are in degrees.

Trial		Pelvis tz	Pelvis tx	Pelvis ty	Pelvis tilt	Pelvis list	Pelvis rotation
1_a	**MAX**	0.180	0.365	0.132	0.219	0.152	0.017
	RMS	0.001	0.002	0.001	0.001	0.001	0.000
1_b	**MAX**	0.763	0.300	0.301	0.319	0.248	0.018
	RMS	0.004	0.002	0.002	0.001	0.001	0.000
2_a	**MAX**	0.395	0.726	0.112	0.271	0.194	0.021
	RMS	0.002	0.004	0.001	0.001	0.001	0.000
2_b	**MAX**	0.724	0.563	0.464	0.229	0.383	0.020
	RMS	0.004	0.004	0.002	0.001	0.002	0.000
3_a	**MAX**	0.335	0.802	0.179	0.352	0.238	0.015
	RMS	0.003	0.005	0.001	0.002	0.001	0.000
3_b	**MAX**	0.824	0.437	0.692	0.280	0.339	0.043
	RMS	0.005	0.003	0.004	0.002	0.002	0.000
4_a	**MAX**	1.455	0.312	0.122	0.190	0.717	0.029
	RMS	0.008	0.002	0.001	0.001	0.004	0.000
4_b	**MAX**	0.276	1.082	0.526	0.647	0.269	0.034
	RMS	0.002	0.008	0.003	0.005	0.001	0.000
5_a	**MAX**	0.209	0.219	0.082	0.487	0.191	0.032
	RMS	0.002	0.001	0.000	0.002	0.001	0.000
5_b	**MAX**	0.965	0.832	1.462	0.178	0.404	0.034
	RMS	0.005	0.005	0.008	0.001	0.002	0.000
6_a	**MAX**	0.201	0.122	0.051	0.158	0.269	0.019
	RMS	0.001	0.001	0.000	0.001	0.002	0.000
6_b	**MAX**	0.253	0.357	0.484	0.351	0.162	0.020
	RMS	0.002	0.002	0.002	0.002	0.001	0.000
7_a	**MAX**	0.419	0.380	0.306	0.130	0.214	0.024
	RMS	0.003	0.003	0.002	0.001	0.001	0.000
7_b	**MAX**	0.221	0.689	0.121	0.521	0.242	0.039
	RMS	0.002	0.004	0.001	0.003	0.001	0.000
8_a	**MAX**	0.566	0.154	0.068	0.065	0.337	0.026
	RMS	0.004	0.001	0.000	0.000	0.002	0.000
8_b	**MAX**	1.072	0.375	1.230	0.096	1.539	0.041
	RMS	0.006	0.003	0.006	0.000	0.005	0.000

Table A.12: Position errors of the pelvis from RRA relative to session 3. The values are in degrees.

Trial		Pelvis tz	Pelvis tx	Pelvis ty	Pelvis tilt	Pelvis list	Pelvis rotation
1_a	MAX	1.089	0.093	0.311	2.029	0.392	0.288
	RMS	0.004	0.000	0.002	0.011	0.002	0.002
1_b	MAX	0.356	0.341	0.215	0.088	0.046	0.051
	RMS	0.001	0.002	0.001	0.000	0.000	0.000
2_a	MAX	0.126	0.338	0.240	0.056	0.015	0.024
	RMS	0.001	0.002	0.001	0.000	0.000	0.000
2_b	MAX	1.459	0.474	0.229	0.856	0.612	0.600
	RMS	0.006	0.003	0.001	0.005	0.003	0.003
3_a	MAX	0.322	0.520	0.334	0.546	0.128	0.039
	RMS	0.002	0.003	0.002	0.003	0.001	0.000
3_b	MAX	0.302	1.151	0.732	0.752	0.564	0.047
	RMS	0.002	0.008	0.004	0.006	0.003	0.000
4_a	MAX	0.485	0.602	0.074	0.438	0.251	1.190
	RMS	0.002	0.003	0.000	0.002	0.001	0.005
4_b	MAX	0.226	0.124	0.156	0.034	0.014	0.003
	RMS	0.001	0.001	0.001	0.000	0.000	0.000
5_a	MAX	1.438	0.531	1.042	0.935	0.251	0.116
	RMS	0.006	0.002	0.006	0.006	0.002	0.001
5_b	MAX	1.127	1.157	0.570	1.498	0.617	0.084
	RMS	0.004	0.007	0.003	0.011	0.004	0.001
6_a	MAX	0.874	0.533	0.406	0.629	0.790	0.605
	RMS	0.004	0.003	0.002	0.003	0.006	0.004
6_b	MAX	0.687	1.270	0.765	0.306	0.246	1.200
	RMS	0.004	0.006	0.004	0.002	0.001	0.005
7_a	MAX	0.252	0.117	0.341	0.173	0.156	0.054
	RMS	0.002	0.001	0.002	0.001	0.001	0.000
7_b	MAX	1.469	1.500	0.442	0.475	0.383	0.200
	RMS	0.007	0.009	0.002	0.002	0.002	0.001
8_a	MAX	1.501	0.763	0.115	0.600	0.280	1.079
	RMS	0.008	0.004	0.001	0.004	0.002	0.003
8_b	MAX	0.400	0.362	0.625	0.767	0.658	0.434
	RMS	0.002	0.002	0.004	0.005	0.004	0.002

Table A.13: Ranges of reserve actuators, in Nm, of the joints degrees of freedom from CMC relative to session 1. Root mean Square (RMS) is also presented.

Trial		Right Hip Flexion	Right Hip Adduction	Right Hip Rotation	Right Knee Angle	Right Ankle Angle	Left Hip Flexion	Left Hip Adduction	Left Hip Rotation	Left Knee Angle	Left Ankle Angle	Lumbar Extension	Lumbar Bending	Lumbar Rotation
1_a	Range	[-0.039 ; 0.022]	[-0.43 ; -0.027]	[0.002 ; 0.787]	[-0.105 ; 0.002]	[-0.006 ; 0.034]	[-0.011 ; 0.026]	[-0.043 ; 0.011]	[-0.095 ; 0.019]	[-0.063 ; 0.002]	[0 ; 0.03]	[0.004 ; 0.011]	[-0.005 ; 0.004]	[-0.01 ; 0.017]
	RMS	0.017	0.131	0.299	0.046	0.01	0.015	0.024	0.043	0.027	0.014	0.008	0.003	0.01
1_b	Range	[-0.006 ; 0.025]	[-0.049 ; 0.009]	[-0.038 ; 0.026]	[-0.037 ; 0.002]	[0.004 ; 0.039]	[-0.018 ; 0.018]	[-0.086 ; -0.004]	[-0.042 ; 0.372]	[-0.07 ; 0.002]	[-0.005 ; 0.022]	[0.002 ; 0.014]	[-0.003 ; 0.008]	[-0.029 ; 0.011]
	RMS	0.013	0.022	0.016	0.017	0.025	0.009	0.046	0.108	0.036	0.009	0.01	0.006	0.017
2_a	Range	[-0.043 ; 0.021]	[-0.086 ; 0.002]	[0.014 ; 1.177]	[-0.089 ; 0.008]	[-0.005 ; 0.036]	[0 ; 0.031]	[-0.064 ; 0.009]	[-0.085 ; 0.014]	[-0.046 ; 0]	[0.008 ; 0.028]	[-0.001 ; 0.007]	[-0.006 ; -0.002]	[-0.004 ; 0.011]
	RMS	0.02	0.045	0.46	0.039	0.015	0.019	0.033	0.043	0.026	0.021	0.003	0.005	0.006
2_b	Range	[-0.003 ; 0.029]	[-0.042 ; 0.01]	[-0.04 ; 0.019]	[-0.03 ; 0.001]	[0.001 ; 0.029]	[-0.036 ; 0.016]	[-0.123 ; 0.004]	[-0.024 ; 0.255]	[-0.094 ; 0.002]	[-0.01 ; 0.025]	[0.01 ; 0.018]	[-0.002 ; 0.012]	[-0.045 ; 0.008]
	RMS	0.016	0.023	0.015	0.017	0.018	0.013	0.056	0.093	0.042	0.011	0.014	0.008	0.029
3_a	Range	[-0.039 ; 0.022]	[-0.08 ; 0.002]	[-0.029 ; 0.269]	[-0.077 ; 0.004]	[-0.005 ; 0.023]	[-0.003 ; 0.063]	[-0.083 ; 0.025]	[-0.219 ; 0.046]	[-0.068 ; 0.002]	[0.004 ; 0.032]	[0.002 ; 0.016]	[-0.006 ; 0.001]	[-0.011 ; 0.012]
	RMS	0.015	0.041	0.104	0.041	0.01	0.029	0.037	0.076	0.039	0.024	0.008	0.004	0.008
3_b	Range	[-0.01 ; 0.024]	[-0.042 ; 0.006]	[-0.061 ; 0.028]	[-0.044 ; 0]	[0.004 ; 0.038]	[-0.011 ; 0.019]	[-0.07 ; -0.001]	[-0.044 ; 0.296]	[-0.111 ; 0.003]	[-0.005 ; 0.03]	[0.005 ; 0.018]	[-0.004 ; 0.01]	[-0.03 ; 0.013]
	RMS	0.014	0.022	0.025	0.02	0.025	0.009	0.046	0.08	0.053	0.01	0.014	0.007	0.018
4_a	Range	[-0.016 ; 0.016]	[-0.036 ; -0.004]	[0.041 ; 0.574]	[-0.071 ; 0.005]	[-0.004 ; 0.045]	[-0.002 ; 0.031]	[-0.065 ; 0.003]	[-0.033 ; 0.021]	[-0.047 ; 0.001]	[0.003 ; 0.034]	[0 ; 0.005]	[-0.006 ; -0.003]	[-0.004 ; 0.012]
	RMS	0.009	0.016	0.202	0.033	0.015	0.017	0.023	0.022	0.022	0.025	0.003	0.004	0.006
4_b	Range	[-0.002 ; 0.023]	[-0.037 ; 0.012]	[-0.112 ; 0.09]	[-0.045 ; 0.003]	[0.003 ; 0.038]	[-0.015 ; 0.011]	[-0.083 ; 0.001]	[-0.014 ; 0.239]	[-0.069 ; 0.001]	[-0.005 ; 0.014]	[0.003 ; 0.017]	[-0.004 ; 0.007]	[-0.032 ; 0.008]
	RMS	0.015	0.017	0.043	0.018	0.024	0.008	0.056	0.089	0.051	0.006	0.012	0.005	0.02
5_a	Range	[-0.186 ; 0.006]	[-0.326 ; -0.008]	[0.065 ; 2.961]	[-0.074 ; 0.006]	[-0.005 ; 0.056]	[0 ; 0.034]	[-0.046 ; 0.006]	[-0.135 ; 0.003]	[-0.069 ; 0.002]	[0.001 ; 0.034]	[-0.004 ; 0.012]	[-0.008 ; 0.003]	[-0.018 ; 0.018]
	RMS	0.113	0.196	1.884	0.023	0.013	0.018	0.028	0.07	0.04	0.022	0.006	0.004	0.007
5_b	Range	[-0.006 ; 0.025]	[-0.044 ; 0.008]	[-0.082 ; 0.04]	[-0.056 ; 0.001]	[0.004 ; 0.033]	[-0.015 ; 0.021]	[-0.127 ; -0.02]	[-0.011 ; 0.438]	[-0.109 ; 0]	[-0.031 ; 0.023]	[0.009 ; 0.018]	[-0.006 ; 0.007]	[-0.029 ; 0.011]
	RMS	0.015	0.022	0.036	0.025	0.022	0.013	0.075	0.177	0.081	0.01	0.014	0.004	0.019
6_a	Range	[-0.016 ; 0.027]	[-0.075 ; -0.006]	[0.02 ; 0.363]	[-0.066 ; -0.001]	[-0.005 ; 0.048]	[-0.01 ; 0.034]	[-0.053 ; 0.014]	[-0.199 ; -0.002]	[-0.085 ; 0.004]	[0.006 ; 0.035]	[0.001 ; 0.01]	[-0.006 ; 0.002]	[-0.013 ; 0.012]
	RMS	0.011	0.042	0.133	0.029	0.015	0.019	0.026	0.082	0.035	0.024	0.006	0.004	0.008
6_b	Range	[-0.004 ; 0.038]	[-0.046 ; 0.006]	[-0.061 ; 0.017]	[-0.022 ; 0.002]	[0.002 ; 0.029]	[-0.015 ; 0.009]	[-0.051 ; -0.001]	[0.005 ; 0.098]	[-0.084 ; -0.002]	[-0.005 ; 0.014]	[0.006 ; 0.015]	[-0.003 ; 0.007]	[-0.016 ; 0.022]
	RMS	0.016	0.019	0.018	0.013	0.02	0.008	0.034	0.053	0.039	0.006	0.012	0.005	0.011
7_a	Range	[-0.046 ; 0.029]	[-0.215 ; -0.007]	[0.006 ; 0.969]	[-0.109 ; 0.003]	[-0.005 ; 0.038]	[0.004 ; 0.033]	[-0.064 ; 0.012]	[-0.157 ; 0.011]	[-0.059 ; -0.001]	[0.006 ; 0.028]	[0.002 ; 0.01]	[-0.005 ; 0]	[0.003 ; 0.015]
	RMS	0.019	0.078	0.377	0.047	0.013	0.018	0.025	0.068	0.032	0.022	0.007	0.003	0.01
7_b	Range	[-0.004 ; 0.031]	[-0.051 ; 0.012]	[-0.049 ; 0.016]	[-0.039 ; 0.001]	[0.008 ; 0.033]	[-0.056 ; 0.003]	[-0.082 ; -0.001]	[0.008 ; 0.76]	[-0.033 ; 0.003]	[-0.009 ; 0.001]	[0.003 ; 0.014]	[0 ; 0.009]	[-0.019 ; 0.013]
	RMS	0.018	0.024	0.027	0.021	0.024	0.012	0.034	0.235	0.021	0.004	0.008	0.005	0.009
8_a	Range	[-0.025 ; 0.027]	[-0.048 ; 0.003]	[0.006 ; 0.218]	[-0.076 ; -0.004]	[-0.004 ; 0.026]	[0.001 ; 0.027]	[-0.039 ; 0.013]	[-0.094 ; 0.004]	[-0.039 ; 0.002]	[0.005 ; 0.031]	[0.005 ; 0.017]	[-0.009 ; 0]	[-0.008 ; 0.017]
	RMS	0.011	0.025	0.099	0.042	0.01	0.016	0.018	0.047	0.022	0.022	0.01	0.005	0.009
8_b	Range	[-0.002 ; 0.045]	[-0.056 ; 0.009]	[-0.057 ; 0.009]	[-0.039 ; 0.005]	[0.003 ; 0.03]	[-0.013 ; 0.013]	[-0.07 ; -0.013]	[0.016 ; 0.231]	[-0.04 ; -0.001]	[-0.038 ; 0.001]	[0.011 ; 0.015]	[0.004 ; 0.007]	[-0.027 ; -0.013]
	RMS	0.016	0.019	0.029	0.015	0.017	0.007	0.04	0.1	0.022	0.011	0.012	0.006	0.021

Table A.14: Ranges of reserve actuators, in Nm, of the joints degrees of freedom from CMC relative to session 2. Root mean Square (RMS) is also presented.

Trial		Right Hip Flexion	Right Hip Adduction	Right Hip Rotation	Right Knee Angle	Right Ankle Angle	Left Hip Flexion	Left Hip Adduction	Left Hip Rotation	Left Knee Angle	Left Ankle Angle	Lumbar Extension	Lumbar Bending	Lumbar Rotation
1_a	Range	[-0.008 ; 0.027]	[-0.044 ; -0.002]	[-0.025 ; 0.092]	[-0.029 ; 0.001]	[-0.006 ; 0.096]	[-0.005 ; 0.037]	[-0.048 ; 0.002]	[-0.074 ; -0.011]	[-0.073 ; -0.002]	[0.002 ; 0.036]	[0.004 ; 0.015]	[-0.013 ; -0.005]	[0.013 ; 0.048]
	RMS	0.016	0.029	0.049	0.019	0.026	0.018	0.02	0.04	0.029	0.025	0.01	0.01	0.037
1_b	Range	[0 ; 0.03]	[-0.047 ; 0.01]	[-0.087 ; 0.002]	[-0.045 ; -0.009]	[0.01 ; 0.033]	[-0.015 ; 0.017]	[-0.051 ; -0.004]	[0.004 ; 0.1]	[-0.038 ; 0.006]	[-0.011 ; 0.033]	[-0.006 ; 0.014]	[0.002 ; 0.012]	[-0.037 ; 0.035]
	RMS	0.019	0.027	0.047	0.028	0.024	0.011	0.029	0.044	0.025	0.008	0.009	0.01	0.027
2_a	Range	[-0.018 ; 0.035]	[-0.048 ; -0.023]	[-0.003 ; 0.206]	[-0.036 ; 0.001]	[-0.009 ; 0.066]	[-0.007 ; 0.03]	[-0.03 ; 0.005]	[-0.066 ; -0.001]	[-0.039 ; 0]	[0.001 ; 0.038]	[0.005 ; 0.02]	[-0.013 ; -0.004]	[0.004 ; 0.058]
	RMS	0.013	0.035	0.069	0.024	0.017	0.019	0.016	0.04	0.022	0.025	0.009	0.008	0.034
2_b	Range	[-0.002 ; 0.023]	[-0.041 ; 0.002]	[-0.056 ; 0.001]	[-0.041 ; -0.011]	[0.007 ; 0.024]	[-0.018 ; 0.019]	[-0.058 ; -0.015]	[0.004 ; 0.108]	[-0.048 ; 0.003]	[-0.036 ; 0.082]	[-0.006 ; 0.012]	[0.001 ; 0.01]	[-0.03 ; 0.022]
	RMS	0.017	0.022	0.032	0.024	0.019	0.012	0.039	0.049	0.032	0.021	0.008	0.007	0.019
3_a	Range	[-0.016 ; 0.022]	[-0.044 ; -0.013]	[0 ; 0.207]	[-0.031 ; 0.002]	[-0.014 ; 0.071]	[-0.003 ; 0.024]	[-0.029 ; 0.007]	[-0.094 ; 0.001]	[-0.035 ; 0]	[0.002 ; 0.037]	[0.005 ; 0.015]	[-0.011 ; -0.005]	[0.003 ; 0.043]
	RMS	0.009	0.03	0.061	0.019	0.019	0.017	0.016	0.046	0.022	0.025	0.008	0.007	0.026
3_b	Range	[0.001 ; 0.027]	[-0.036 ; 0.009]	[-0.075 ; 0.009]	[-0.039 ; -0.008]	[0.001 ; 0.038]	[-0.015 ; 0.024]	[-0.069 ; -0.012]	[0.008 ; 0.099]	[-0.045 ; 0.004]	[-0.008 ; 0.015]	[-0.007 ; 0.011]	[0 ; 0.01]	[-0.033 ; 0.029]
	RMS	0.019	0.02	0.048	0.024	0.024	0.014	0.043	0.042	0.029	0.006	0.008	0.007	0.021
4_a	Range	[-0.023 ; 0.016]	[-0.135 ; -0.006]	[-0.01 ; 0.617]	[-0.051 ; 0.002]	[-0.007 ; 0.119]	[-0.006 ; 0.028]	[-0.043 ; 0.004]	[-0.108 ; 0.008]	[-0.047 ; 0]	[0.002 ; 0.041]	[0.006 ; 0.028]	[-0.018 ; 0.003]	[-0.047 ; 0.076]
	RMS	0.008	0.053	0.185	0.026	0.03	0.02	0.026	0.045	0.028	0.026	0.013	0.012	0.037
4_b	Range	[0.002 ; 0.026]	[-0.034 ; -0.004]	[-0.074 ; 0.001]	[-0.042 ; -0.009]	[0.008 ; 0.021]	[-0.013 ; 0.012]	[-0.077 ; -0.01]	[0.003 ; 0.52]	[-0.049 ; 0.002]	[-0.009 ; 0.058]	[-0.002 ; 0.01]	[0 ; 0.008]	[-0.03 ; 0.001]
	RMS	0.016	0.022	0.045	0.025	0.018	0.008	0.047	0.209	0.028	0.019	0.005	0.005	0.018
5_a	Range	[-0.017 ; 0.019]	[-0.041 ; -0.005]	[0.003 ; 0.166]	[-0.029 ; 0.002]	[-0.008 ; 0.144]	[-0.005 ; 0.03]	[-0.038 ; 0.002]	[-0.081 ; 0.007]	[-0.043 ; -0.003]	[0.001 ; 0.041]	[-0.001 ; 0.013]	[-0.011 ; 0.002]	[-0.028 ; 0.028]
	RMS	0.008	0.032	0.064	0.017	0.032	0.022	0.022	0.044	0.028	0.026	0.006	0.007	0.016
5_b	Range	[-0.006 ; 0.025]	[-0.024 ; 0.007]	[-0.055 ; 0.005]	[-0.029 ; -0.008]	[0.009 ; 0.041]	[-0.016 ; 0.028]	[-0.044 ; -0.021]	[0.009 ; 0.058]	[-0.038 ; 0.007]	[-0.01 ; 0.039]	[0.001 ; 0.011]	[0.004 ; 0.008]	[-0.026 ; 0.001]
	RMS	0.018	0.013	0.039	0.019	0.026	0.014	0.037	0.03	0.026	0.011	0.005	0.006	0.013
6_a	Range	[-0.018 ; 0.029]	[-0.037 ; -0.008]	[-0.001 ; 0.229]	[-0.038 ; 0.005]	[-0.507 ; 0.077]	[-0.004 ; 0.027]	[-0.034 ; 0.004]	[-0.081 ; 0.013]	[-0.037 ; -0.001]	[0.002 ; 0.048]	[0.006 ; 0.014]	[-0.011 ; 0]	[-0.028 ; 0.033]
	RMS	0.014	0.027	0.074	0.02	0.099	0.017	0.017	0.044	0.021	0.027	0.009	0.009	0.026
6_b	Range	[-0.001 ; 0.029]	[-0.042 ; 0]	[-0.082 ; 0.007]	[-0.038 ; -0.008]	[0.004 ; 0.026]	[-0.016 ; 0.015]	[-0.041 ; -0.011]	[0.009 ; 0.216]	[-0.038 ; 0.005]	[-0.015 ; 0.071]	[-0.007 ; 0.011]	[0.003 ; 0.01]	[-0.027 ; 0.034]
	RMS	0.02	0.023	0.036	0.026	0.021	0.009	0.027	0.085	0.021	0.019	0.006	0.007	0.017
7_a	Range	[-0.019 ; 0.014]	[-0.046 ; -0.018]	[-0.002 ; 0.16]	[-0.048 ; 0.002]	[-0.012 ; 0.072]	[-0.002 ; 0.029]	[-0.042 ; 0.004]	[-0.087 ; 0.001]	[-0.04 ; -0.002]	[0.002 ; 0.04]	[0.008 ; 0.017]	[-0.012 ; 0]	[-0.023 ; 0.049]
	RMS	0.008	0.033	0.053	0.028	0.019	0.019	0.023	0.043	0.024	0.026	0.011	0.01	0.036
7_b	Range	[-0.001 ; 0.023]	[-0.038 ; 0.006]	[-0.054 ; 0.006]	[-0.033 ; -0.011]	[0.007 ; 0.023]	[-0.01 ; 0.013]	[-0.034 ; -0.01]	[0.01 ; 0.186]	[-0.043 ; 0.002]	[-0.005 ; 0.051]	[-0.006 ; 0.009]	[-0.001 ; 0.009]	[-0.027 ; 0.02]
	RMS	0.016	0.021	0.03	0.023	0.018	0.008	0.024	0.074	0.027	0.023	0.006	0.006	0.018
8_a	Range	[-0.015 ; 0.018]	[-0.049 ; -0.016]	[-0.008 ; 0.127]	[-0.049 ; 0.001]	[-0.006 ; 0.069]	[-0.002 ; 0.029]	[-0.037 ; 0.004]	[-0.096 ; 0.009]	[-0.045 ; 0]	[0.001 ; 0.052]	[0.006 ; 0.012]	[-0.011 ; 0.002]	[-0.025 ; 0.038]
	RMS	0.009	0.039	0.037	0.031	0.017	0.019	0.019	0.045	0.025	0.028	0.009	0.007	0.027
8_b	Range	[0.001 ; 0.026]	[-0.029 ; 0.009]	[-0.107 ; 0.007]	[-0.039 ; -0.009]	[0.005 ; 0.032]	[-0.016 ; 0.022]	[-0.075 ; -0.027]	[0.007 ; 0.16]	[-0.04 ; 0.003]	[-0.022 ; 0.162]	[-0.004 ; 0.012]	[-0.003 ; 0.011]	[-0.039 ; 0.036]
	RMS	0.018	0.016	0.058	0.024	0.023	0.013	0.052	0.058	0.029	0.032	0.005	0.005	0.019

Table A.15: Ranges of reserve actuators, in Nm, of the joints degrees of freedom from CMC relative to session 3. Root mean Square (RMS) is also presented.

Trial		Right Hip Flexion	Right Hip Adduction	Right Hip Rotation	Right Knee Angle	Right Ankle Angle	Left Hip Flexion	Left Hip Adduction	Left Hip Rotation	Left Knee Angle	Left Ankle Angle	Lumbar Extension	Lumbar Bending	Lumbar Rotation
1_a	Range	[-0.015 ; 0.01]	[-0.042;-0.003]	[0.017;0.43]	[-0.019;0.001]	[-0.005;0.033]	[-0.003;0.016]	[-0.018;0.004]	[-0.017;0.011]	[-0.018;-0.001]	[0.001;0.023]	[0.002;0.007]	[-0.004;-0.003]	[0.005;0.013]
	RMS	0.007	0.025	0.188	0.012	0.007	0.011	0.009	0.01	0.011	0.018	0.005	0.003	0.009
1_b	Range	[-0.004 ; 0.025]	[-0.018;0.005]	[-0.036;0.026]	[-0.056;-0.004]	[0.004;0.032]	[-0.022;0.01]	[-0.096;-0.011]	[0.016;0.769]	[-0.026;0.002]	[-0.009;0.052]	[-0.003;0.007]	[-0.001;0.004]	[-0.018;0.01]
	RMS	0.012	0.008	0.014	0.02	0.017	0.008	0.04	0.302	0.012	0.013	0.004	0.003	0.009
2_a	Range	[-0.012 ; 0.017]	[-0.067;-0.009]	[0.019;0.596]	[-0.021;0.002]	[-0.034;0.044]	[-0.003;0.015]	[-0.021;0.006]	[-0.022;0.011]	[-0.03;-0.002]	[0.004;0.022]	[0;0.006]	[-0.005;-0.001]	[-0.007;0.012]
	RMS	0.009	0.028	0.195	0.014	0.013	0.009	0.009	0.014	0.013	0.016	0.003	0.003	0.008
2_b	Range	[-0.003 ; 0.016]	[-0.013;0.003]	[-0.026;0.009]	[-0.017;-0.001]	[0.003;0.017]	[-0.009;0.013]	[-0.035;-0.009]	[0.016;0.218]	[-0.023;0.001]	[-0.01;0.083]	[0;0.007]	[0.002;0.005]	[-0.013;0.002]
	RMS	0.01	0.007	0.014	0.01	0.013	0.007	0.024	0.089	0.017	0.022	0.004	0.003	0.008
3_a	Range	[-0.036 ; 0.013]	[-0.098;-0.019]	[0.022;0.861]	[-0.032;0.002]	[-0.005;0.034]	[-0.001;0.018]	[-0.023;0.007]	[-0.046;0.009]	[-0.019;0.001]	[0;0.038]	[-0.001;0.006]	[-0.004;0]	[0;0.012]
	RMS	0.013	0.044	0.282	0.02	0.008	0.012	0.009	0.022	0.011	0.022	0.004	0.003	0.008
3_b	Range	[-0.001 ; 0.013]	[-0.012;0.001]	[-0.016;0.001]	[-0.017;-0.002]	[0.008;0.015]	[-0.011;0.016]	[-0.024;-0.002]	[-0.003;0.085]	[-0.023;0.001]	[-0.01;0.048]	[0.003;0.009]	[0.001;0.007]	[-0.017;0.01]
	RMS	0.009	0.008	0.009	0.01	0.013	0.005	0.017	0.036	0.014	0.017	0.006	0.005	0.011
4_a	Range	[-0.023 ; 0.007]	[-0.075;-0.001]	[0.019;0.806]	[-0.014;0.002]	[-0.005;0.035]	[-0.004;0.017]	[-0.022;0.004]	[-0.039;0.013]	[-0.028;-0.001]	[0.001;0.024]	[0;0.006]	[-0.005;0]	[-0.01;0.007]
	RMS	0.008	0.032	0.306	0.008	0.009	0.01	0.012	0.017	0.014	0.018	0.003	0.003	0.004
4_b	Range	[-0.003 ; 0.012]	[-0.01;0.007]	[-0.011;0.004]	[-0.016;-0.003]	[0.003;0.018]	[-0.008;0.015]	[-0.047;-0.004]	[0.012;0.182]	[-0.017;0.001]	[-0.008;0.044]	[0.001;0.007]	[0.002;0.005]	[-0.018;0.004]
	RMS	0.008	0.006	0.006	0.01	0.014	0.008	0.027	0.067	0.012	0.012	0.004	0.003	0.011
5_a	Range	[-0.041 ; 0.009]	[-0.092;-0.015]	[0.025;0.93]	[-0.029;0.003]	[-0.009;0.036]	[-0.003;0.017]	[-0.023;0.005]	[-0.031;0.012]	[-0.027;-0.002]	[0;0.026]	[0.001;0.007]	[-0.004;0.001]	[-0.008;0.014]
	RMS	0.017	0.054	0.398	0.016	0.007	0.01	0.01	0.016	0.013	0.019	0.004	0.002	0.008
5_b	Range	[-0.005 ; 0.018]	[-0.02;0.004]	[-0.03;0.02]	[-0.044;0]	[0.005;0.029]	[-0.012;0.011]	[-0.03;-0.003]	[0.012;0.273]	[-0.02;0.004]	[-0.035;0.057]	[0.003;0.008]	[0.002;0.006]	[-0.015;0.008]
	RMS	0.011	0.009	0.017	0.014	0.018	0.006	0.017	0.117	0.012	0.014	0.005	0.004	0.01
6_a	Range	[-0.012 ; 0.011]	[-0.044;-0.006]	[0.016;0.479]	[-0.024;0.002]	[-0.004;0.035]	[-0.004;0.015]	[-0.019;0.005]	[-0.026;0.009]	[-0.031;-0.002]	[0.001;0.023]	[-0.001;0.008]	[-0.004;0]	[-0.012;0.01]
	RMS	0.006	0.023	0.159	0.015	0.01	0.01	0.01	0.013	0.012	0.017	0.004	0.003	0.006
6_b	Range	[-0.003 ; 0.016]	[-0.014;0.001]	[-0.019;0.009]	[-0.024;-0.003]	[0.004;0.017]	[-0.007;0.017]	[-0.044;-0.011]	[0.01;0.212]	[-0.029;0.002]	[-0.013;0.046]	[0;0.007]	[0;0.005]	[-0.013;0.01]
	RMS	0.01	0.009	0.011	0.011	0.014	0.008	0.026	0.085	0.016	0.016	0.004	0.003	0.009
7_a	Range	[-0.034 ; 0.006]	[-0.107;-0.009]	[0.024;0.894]	[-0.021;0.004]	[-0.01;0.037]	[-0.002;0.019]	[-0.026;0.005]	[-0.055;0.012]	[-0.026;-0.001]	[0.002;0.027]	[0.001;0.009]	[-0.004;0.001]	[-0.016;0.013]
	RMS	0.011	0.049	0.305	0.011	0.01	0.011	0.012	0.025	0.014	0.017	0.005	0.003	0.009
7_b	Range	[-0.001 ; 0.016]	[-0.014;0.009]	[-0.036;0.02]	[-0.032;-0.002]	[0.005;0.017]	[-0.014;0.018]	[-0.04;-0.002]	[0.008;0.196]	[-0.019;0.004]	[-0.73;0.047]	[0.001;0.007]	[0.002;0.007]	[-0.022;0.011]
	RMS	0.011	0.008	0.021	0.013	0.014	0.008	0.023	0.083	0.011	0.135	0.005	0.005	0.013
8_a	Range	[-0.008 ; 0.013]	[-0.046;-0.005]	[0.019;0.282]	[-0.023;0.001]	[-0.008;0.041]	[-0.003;0.015]	[-0.013;0.009]	[-0.048;0.012]	[-0.021;-0.001]	[0.003;0.021]	[0;0.004]	[-0.003;-0.001]	[-0.003;0.009]
	RMS	0.007	0.026	0.119	0.015	0.011	0.01	0.008	0.023	0.012	0.016	0.002	0.002	0.006
8_b	Range	[-0.004 ; 0.017]	[-0.016;-0.001]	[-0.02;0.012]	[-0.038;-0.002]	[0.003;0.02]	[-0.009;0.015]	[-0.049;-0.012]	[0.016;0.308]	[-0.028;0.001]	[-0.005;0.049]	[0.001;0.005]	[0;0.005]	[-0.011;0.011]
	RMS	0.011	0.009	0.009	0.015	0.015	0.009	0.031	0.115	0.015	0.014	0.003	0.004	0.007

Table A.16: Position errors in the joints degrees of freedom from CMC relative to session 1. The values are in degrees.

Trial		Right Hip Flexion	Right Hip Adduction	Right Hip Rotation	Right Knee Angle	Right Ankle Angle	Left Hip Flexion	Left Hip Adduction	Left Hip Rotation	Left Knee Angle	Left Ankle Angle	Lumbar Extension	Lumbar Bending	Lumbar Rotation
1_a	MAX	0.973	0.982	0.387	0.582	0.154	0.502	1.011	0.456	1.789	0.196	2.051	1.628	1.365
	RMS	0.010	0.011	0.003	0.007	0.001	0.005	0.012	0.005	0.024	0.003	0.021	0.017	0.012
1_b	MAX	0.707	1.354	1.573	1.361	0.211	0.459	0.598	0.825	0.335	0.267	1.426	0.750	1.711
	RMS	0.005	0.012	0.018	0.011	0.002	0.004	0.007	0.007	0.003	0.003	0.015	0.010	0.021
2_a	MAX	0.646	0.336	0.421	0.256	0.325	1.800	0.755	0.856	1.851	0.148	0.406	0.411	0.160
	RMS	0.008	0.004	0.003	0.003	0.004	0.021	0.009	0.008	0.021	0.002	0.005	0.004	0.001
2_b	MAX	1.084	0.937	0.767	0.997	0.320	0.334	0.449	1.840	1.421	0.299	0.282	0.377	0.548
	RMS	0.012	0.009	0.008	0.011	0.004	0.003	0.004	0.017	0.017	0.003	0.003	0.004	0.006
3_a	MAX	0.462	1.001	0.161	0.378	0.173	0.715	1.538	0.961	2.107	0.199	1.358	1.312	1.234
	RMS	0.004	0.010	0.001	0.003	0.001	0.009	0.016	0.011	0.024	0.002	0.010	0.012	0.010
3_b	MAX	1.256	0.707	1.122	1.527	0.205	0.498	0.521	0.793	0.403	0.190	0.556	0.408	0.535
	RMS	0.013	0.007	0.010	0.012	0.002	0.006	0.005	0.008	0.003	0.001	0.007	0.005	0.005
4_a	MAX	0.181	0.546	0.833	0.285	0.151	0.956	1.251	0.685	1.837	0.310	0.528	0.577	0.509
	RMS	0.001	0.005	0.009	0.003	0.001	0.011	0.013	0.007	0.023	0.004	0.004	0.005	0.004
4_b	MAX	1.467	1.314	1.374	2.668	0.410	0.242	0.670	0.404	0.247	0.156	0.126	0.458	0.225
	RMS	0.017	0.015	0.014	0.031	0.005	0.002	0.008	0.004	0.002	0.001	0.001	0.004	0.003
5_a	MAX	0.243	0.613	0.831	0.309	0.262	1.518	1.067	0.150	2.908	0.348	0.172	0.332	0.142
	RMS	0.003	0.006	0.007	0.003	0.003	0.018	0.012	0.001	0.036	0.004	0.002	0.003	0.001
5_b	MAX	2.363	1.745	1.053	4.022	1.043	0.674	0.770	0.590	0.339	0.302	0.514	0.520	0.635
	RMS	0.028	0.020	0.011	0.046	0.014	0.007	0.009	0.006	0.003	0.003	0.005	0.005	0.005
6_a	MAX	0.338	0.841	0.952	0.218	0.298	1.279	1.493	0.203	1.994	0.221	0.336	0.330	0.304
	RMS	0.003	0.009	0.011	0.002	0.003	0.014	0.017	0.001	0.022	0.002	0.003	0.004	0.003
6_b	MAX	1.637	2.118	1.408	2.235	0.285	0.516	0.853	0.806	0.177	0.076	0.442	0.343	0.641
	RMS	0.018	0.018	0.013	0.024	0.003	0.006	0.008	0.008	0.001	0.001	0.005	0.003	0.008
7_a	MAX	0.359	0.714	0.481	0.334	0.218	1.536	1.447	0.395	2.452	0.243	0.167	0.471	0.274
	RMS	0.003	0.008	0.004	0.003	0.002	0.019	0.017	0.003	0.029	0.003	0.002	0.005	0.002
7_b	MAX	2.334	2.124	1.020	3.147	0.550	0.758	0.775	0.284	0.191	0.088	0.579	0.583	0.434
	RMS	0.027	0.025	0.012	0.035	0.007	0.008	0.009	0.002	0.002	0.001	0.007	0.007	0.005
8_a	MAX	0.174	0.645	0.300	0.538	0.254	1.786	1.525	0.676	3.146	0.553	0.243	0.552	0.209
	RMS	0.001	0.007	0.003	0.006	0.002	0.021	0.017	0.006	0.038	0.004	0.002	0.005	0.002
8_b	MAX	1.463	1.936	1.007	1.891	0.626	0.451	0.600	0.381	0.227	0.150	0.211	0.212	0.152
	RMS	0.016	0.021	0.011	0.021	0.008	0.004	0.006	0.003	0.002	0.001	0.002	0.002	0.001

Table A.17: Position errors in the joints degrees of freedom from CMC relative to session 2. The values are in degrees.

Trial		Right Hip Flexion	Right Hip Adduction	Right Hip Rotation	Right Knee Angle	Right Ankle Angle	Left Hip Flexion	Left Hip Adduction	Left Hip Rotation	Left Knee Angle	Left Ankle Angle	Lumbar Extension	Lumbar Bending	Lumbar Rotation
1_a	MAX	0.387	0.726	0.534	0.110	0.132	0.239	1.601	0.623	0.872	0.104	1.325	1.102	1.490
	RMS	0.003	0.008	0.006	0.001	0.002	0.002	0.019	0.007	0.008	0.001	0.016	0.013	0.017
1_b	MAX	1.131	0.477	1.444	1.479	0.260	0.598	0.292	0.380	0.333	0.263	0.571	0.930	1.689
	RMS	0.013	0.004	0.015	0.020	0.003	0.007	0.002	0.004	0.004	0.004	0.006	0.010	0.018
2_a	MAX	0.159	0.206	0.367	0.090	0.068	0.174	0.439	0.198	0.244	0.171	0.033	0.082	0.169
	RMS	0.002	0.002	0.004	0.001	0.001	0.002	0.005	0.001	0.002	0.001	0.000	0.001	0.002
2_b	MAX	0.052	0.212	0.606	0.127	0.167	0.065	0.182	0.566	0.061	0.209	0.068	0.138	0.225
	RMS	0.001	0.002	0.008	0.001	0.002	0.001	0.002	0.007	0.001	0.003	0.001	0.002	0.003
3_a	MAX	0.056	0.204	0.312	0.132	0.149	0.209	0.433	0.564	0.236	0.162	0.060	0.121	0.124
	RMS	0.000	0.002	0.003	0.001	0.002	0.002	0.005	0.006	0.002	0.002	0.001	0.001	0.001
3_b	MAX	0.085	0.263	0.872	0.288	0.133	0.088	0.251	1.054	0.079	0.069	0.115	0.164	0.408
	RMS	0.001	0.003	0.011	0.003	0.001	0.001	0.003	0.014	0.001	0.000	0.001	0.002	0.005
4_a	MAX	0.204	0.131	0.248	0.113	0.468	0.181	0.188	0.568	0.144	0.176	0.094	0.099	0.280
	RMS	0.002	0.001	0.003	0.001	0.007	0.002	0.002	0.006	0.002	0.001	0.001	0.001	0.003
4_b	MAX	0.121	0.128	0.327	0.225	0.217	0.110	0.059	0.511	0.097	0.252	0.048	0.087	0.215
	RMS	0.001	0.002	0.004	0.003	0.003	0.001	0.001	0.006	0.001	0.003	0.000	0.001	0.002
5_a	MAX	0.109	0.214	0.141	0.122	0.146	0.217	0.345	0.225	0.222	0.188	0.035	0.092	0.088
	RMS	0.001	0.003	0.002	0.001	0.002	0.002	0.004	0.003	0.002	0.002	0.000	0.001	0.001
5_b	MAX	0.041	0.091	0.492	0.260	0.103	0.094	0.079	0.194	0.039	0.185	0.110	0.071	0.126
	RMS	0.000	0.001	0.006	0.003	0.001	0.001	0.001	0.001	0.000	0.002	0.001	0.001	0.002
6_a	MAX	0.111	0.083	0.187	0.214	0.206	0.108	0.118	0.315	0.213	0.126	0.030	0.055	0.117
	RMS	0.001	0.001	0.002	0.002	0.003	0.001	0.001	0.003	0.002	0.001	0.000	0.000	0.001
6_b	MAX	0.230	0.318	0.916	0.131	0.152	0.163	0.231	0.378	0.052	0.168	0.073	0.133	0.291
	RMS	0.002	0.003	0.010	0.001	0.001	0.001	0.003	0.004	0.001	0.002	0.001	0.001	0.004
7_a	MAX	0.173	0.069	0.383	0.079	0.070	0.170	0.125	0.537	0.098	0.107	0.054	0.095	0.124
	RMS	0.002	0.001	0.004	0.001	0.001	0.002	0.001	0.005	0.001	0.001	0.001	0.001	0.001
7_b	MAX	0.119	0.144	0.339	0.133	0.146	0.138	0.101	0.816	0.176	0.132	0.107	0.111	0.189
	RMS	0.001	0.002	0.004	0.001	0.002	0.002	0.001	0.011	0.002	0.001	0.001	0.001	0.002
8_a	MAX	0.172	0.237	0.465	0.285	0.039	0.261	0.328	0.451	0.323	0.187	0.073	0.101	0.172
	RMS	0.002	0.003	0.005	0.002	0.000	0.002	0.003	0.004	0.003	0.002	0.001	0.001	0.002
8_b	MAX	0.246	0.242	0.586	0.182	0.133	0.084	0.099	0.829	0.170	0.175	0.048	0.063	0.139
	RMS	0.002	0.002	0.007	0.002	0.001	0.001	0.001	0.010	0.002	0.002	0.000	0.001	0.002

Table A.18: Position errors in the joints degrees of freedom from CMC relative to session 3. The values are in degrees.

Trial		Right Hip Flexion	Right Hip Adduction	Right Hip Rotation	Right Knee Angle	Right Ankle Angle	Left Hip Flexion	Left Hip Adduction	Left Hip Rotation	Left Knee Angle	Left Ankle Angle	Lumbar Extension	Lumbar Bending	Lumbar Rotation
1_a	MAX	0.122	0.066	0.138	0.128	0.169	0.068	0.048	0.064	0.170	0.223	0.039	0.030	0.051
	RMS	0.001	0.001	0.001	0.001	0.002	0.001	0.000	0.001	0.001	0.002	0.000	0.000	0.001
1_b	MAX	0.102	0.065	0.151	0.357	0.240	0.066	0.114	0.222	0.045	0.191	0.015	0.092	0.125
	RMS	0.001	0.001	0.002	0.003	0.002	0.001	0.001	0.002	0.000	0.003	0.000	0.001	0.001
2_a	MAX	0.109	0.051	0.439	0.127	0.247	0.094	0.061	0.028	0.184	0.174	0.072	0.057	0.036
	RMS	0.001	0.000	0.005	0.001	0.003	0.001	0.001	0.000	0.002	0.002	0.001	0.001	0.000
2_b	MAX	0.133	0.219	0.136	0.191	0.226	0.134	0.146	0.827	0.103	0.191	0.063	0.134	0.120
	RMS	0.002	0.003	0.002	0.002	0.003	0.002	0.002	0.011	0.001	0.002	0.001	0.002	0.001
3_a	MAX	0.082	0.041	0.261	0.188	0.082	0.064	0.078	0.062	0.134	0.101	0.028	0.012	0.049
	RMS	0.001	0.000	0.002	0.002	0.001	0.001	0.001	0.001	0.001	0.001	0.000	0.000	0.000
3_b	MAX	0.062	0.171	0.024	0.061	0.192	0.113	0.126	0.408	0.130	0.077	0.083	0.106	0.061
	RMS	0.001	0.002	0.000	0.000	0.002	0.001	0.002	0.005	0.001	0.001	0.001	0.001	0.001
4_a	MAX	0.170	0.059	0.634	0.058	0.195	0.054	0.099	0.151	0.189	0.182	0.033	0.079	0.072
	RMS	0.001	0.001	0.005	0.000	0.002	0.001	0.001	0.002	0.001	0.002	0.000	0.001	0.001
4_b	MAX	0.053	0.150	0.187	0.067	0.201	0.061	0.114	0.246	0.053	0.144	0.048	0.112	0.080
	RMS	0.001	0.002	0.002	0.000	0.002	0.001	0.001	0.002	0.001	0.002	0.000	0.001	0.001
5_a	MAX	0.133	0.025	0.269	0.125	0.140	0.081	0.043	0.026	0.163	0.106	0.028	0.019	0.057
	RMS	0.001	0.000	0.003	0.001	0.002	0.001	0.000	0.000	0.001	0.001	0.000	0.000	0.001
5_b	MAX	0.058	0.075	0.053	0.163	0.115	0.084	0.052	0.435	0.089	0.247	0.018	0.052	0.040
	RMS	0.001	0.001	0.000	0.001	0.001	0.001	0.000	0.005	0.001	0.003	0.000	0.001	0.000
6_a	MAX	0.139	0.082	0.406	0.168	0.099	0.084	0.105	0.072	0.214	0.208	0.081	0.034	0.095
	RMS	0.002	0.001	0.005	0.002	0.001	0.001	0.001	0.001	0.002	0.002	0.001	0.000	0.001
6_b	MAX	0.093	0.199	0.291	0.291	0.250	0.175	0.126	0.698	0.047	0.163	0.045	0.165	0.109
	RMS	0.001	0.003	0.004	0.002	0.003	0.002	0.002	0.008	0.000	0.002	0.000	0.002	0.001
7_a	MAX	0.065	0.077	0.307	0.068	0.137	0.093	0.143	0.219	0.115	0.088	0.022	0.051	0.107
	RMS	0.001	0.001	0.003	0.001	0.002	0.001	0.002	0.002	0.001	0.001	0.000	0.000	0.001
7_b	MAX	0.117	0.171	0.260	0.313	0.286	0.098	0.226	1.161	0.096	0.291	0.064	0.153	0.228
	RMS	0.001	0.002	0.003	0.002	0.003	0.001	0.003	0.014	0.001	0.004	0.001	0.002	0.003
8_a	MAX	0.074	0.066	0.352	0.084	0.296	0.053	0.076	0.067	0.097	0.186	0.021	0.051	0.094
	RMS	0.001	0.001	0.004	0.001	0.004	0.001	0.001	0.001	0.001	0.002	0.000	0.001	0.001
8_b	MAX	0.072	0.258	0.149	0.212	0.230	0.020	0.135	0.171	0.111	0.170	0.032	0.120	0.131
	RMS	0.001	0.004	0.002	0.002	0.003	0.000	0.002	0.002	0.001	0.002	0.000	0.002	0.002

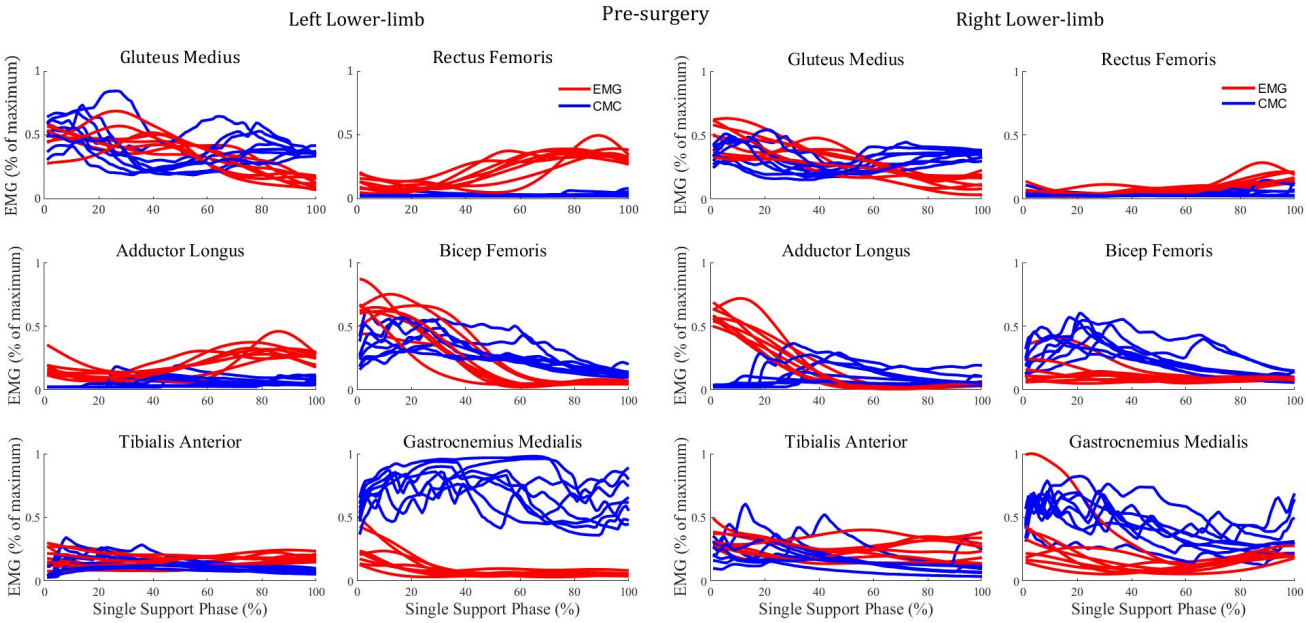

Figure A.1: Comparison between CMC results with the EMG aquisitions of the session before surgery.

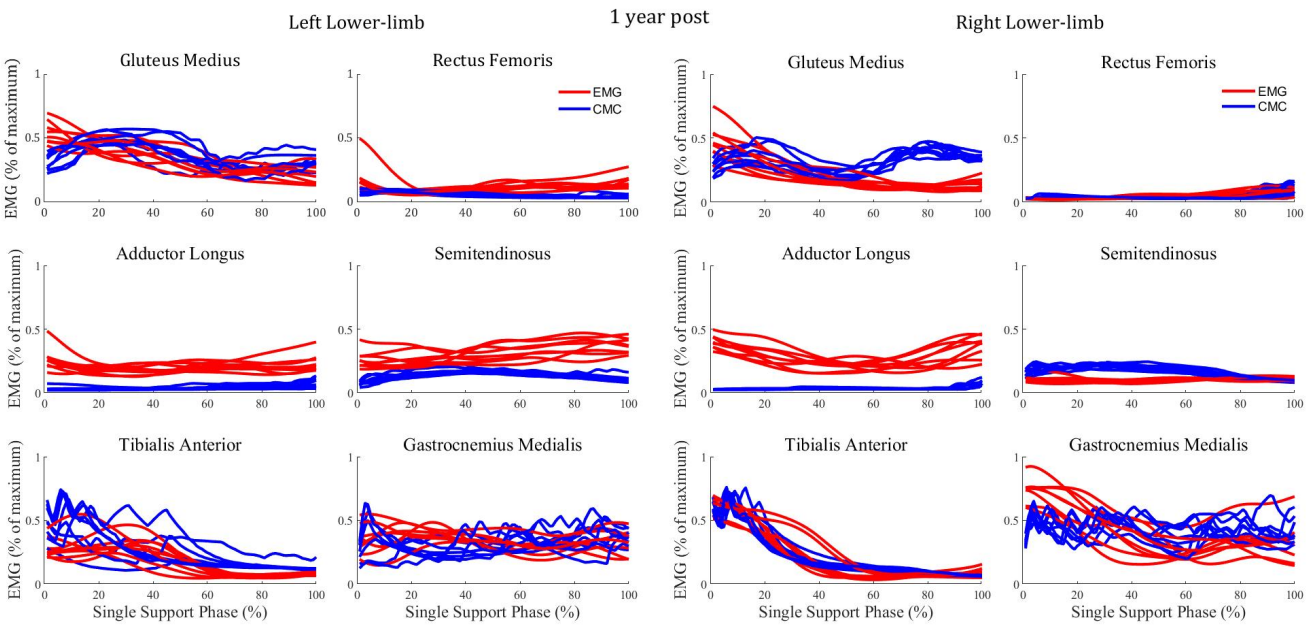

Figure A.2: Comparison between CMC results with the EMG acquisitions of the session one year after surgery.

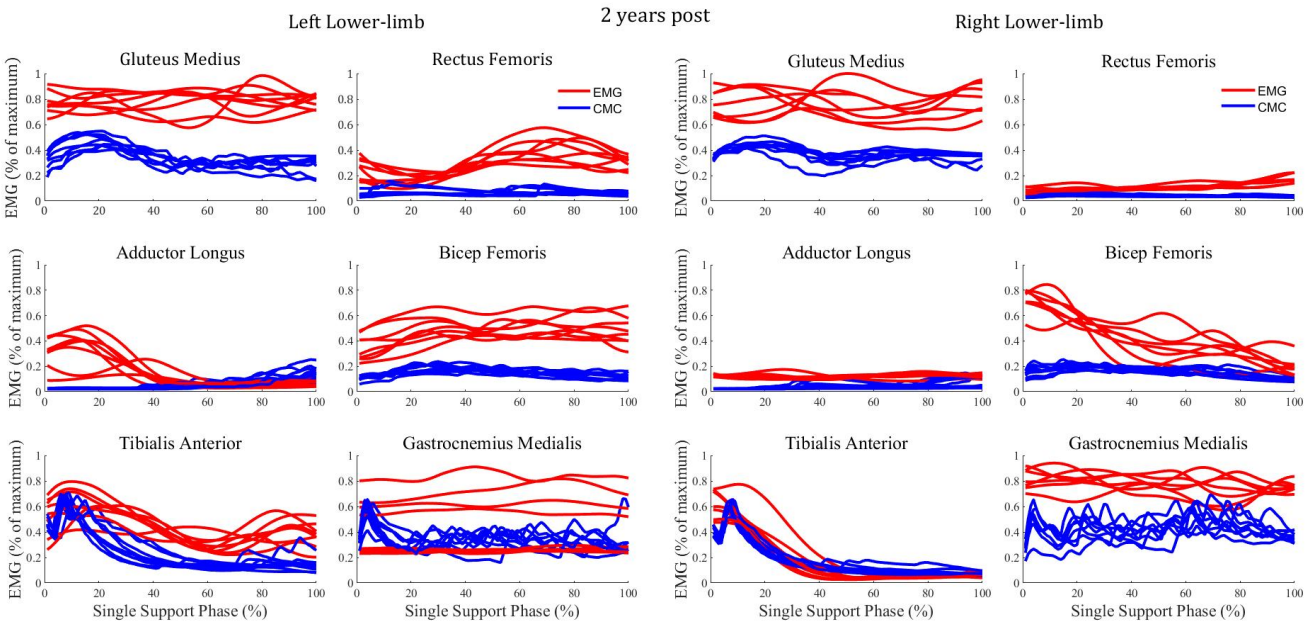

Figure A.3: Comparison between CMC results with the EMG acquisitions of the session two years after surgery.

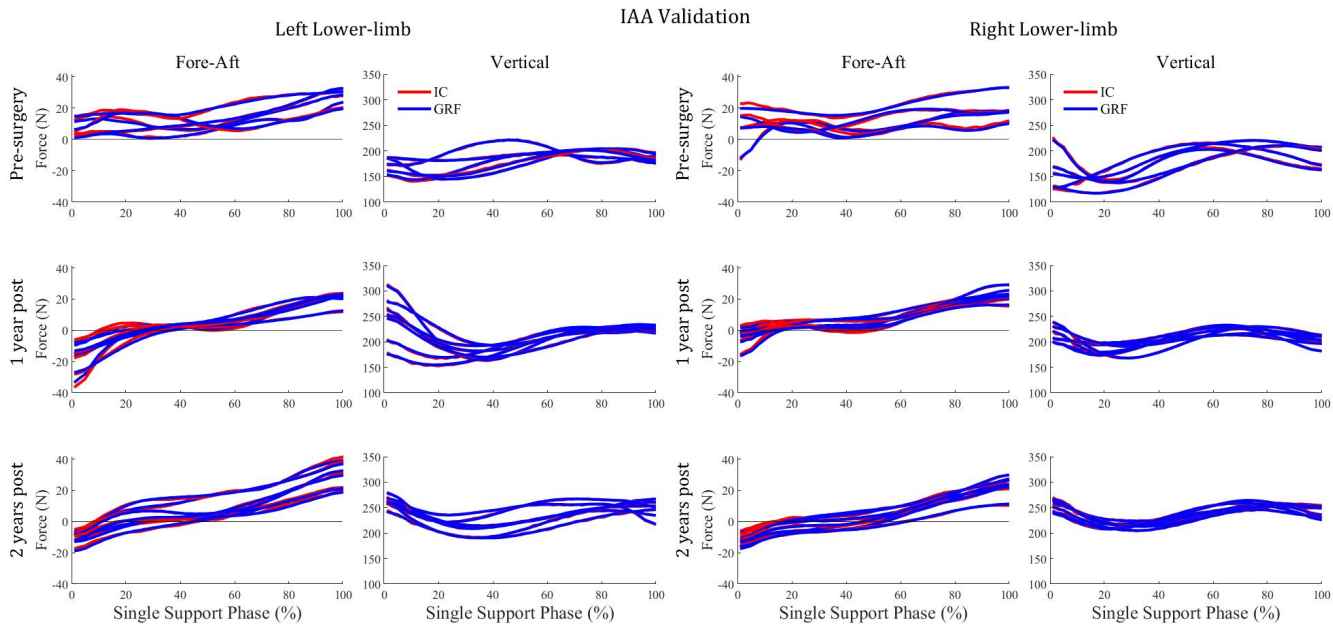

Figure A.4: Validation of the IAA results from the total accelerations of the induced constraints (IC) file with the GRF.

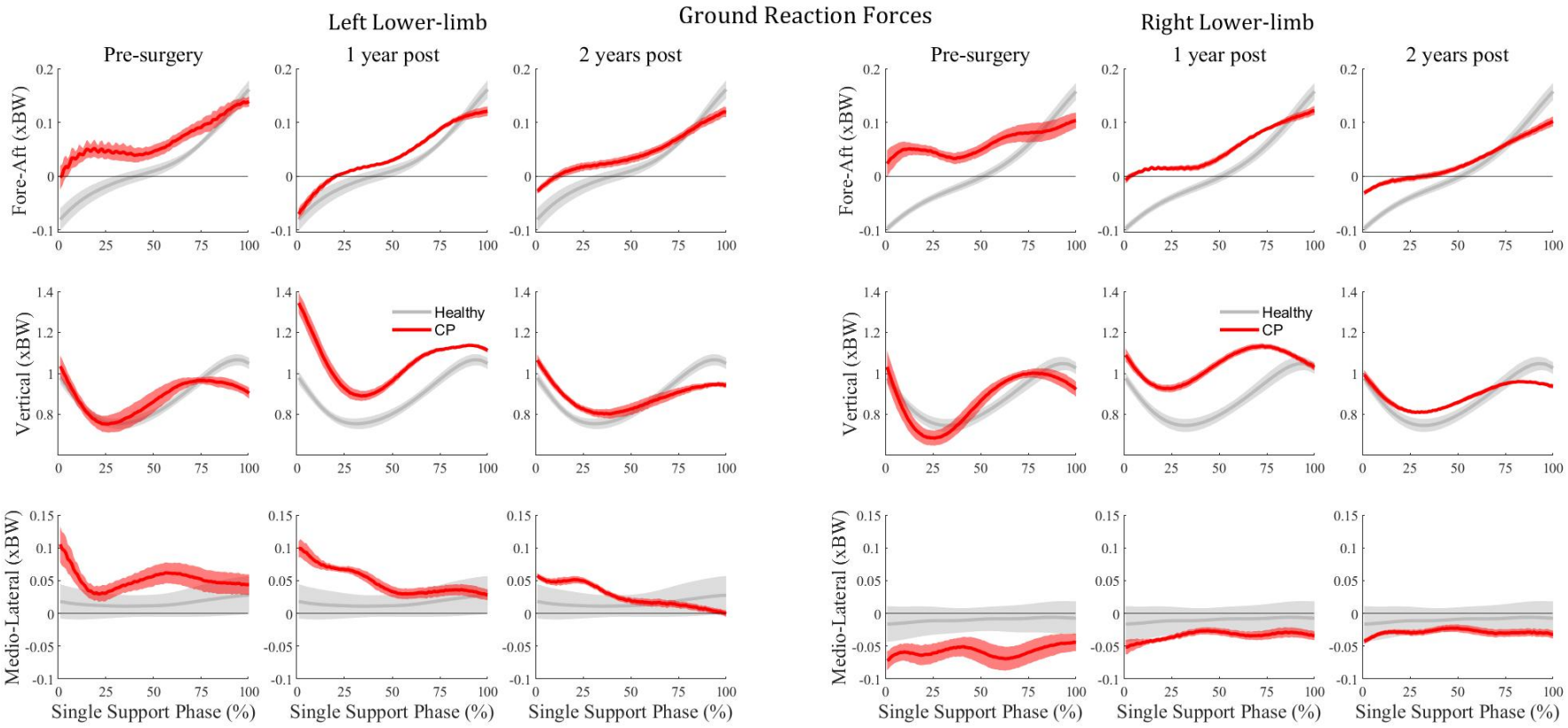

Figure A.5: Ground reaction forces in all three directions of healthy population and the CP subject, normalized by body weight. The shaded regions represent the standard error. The vertical scale is uniform for each direction.

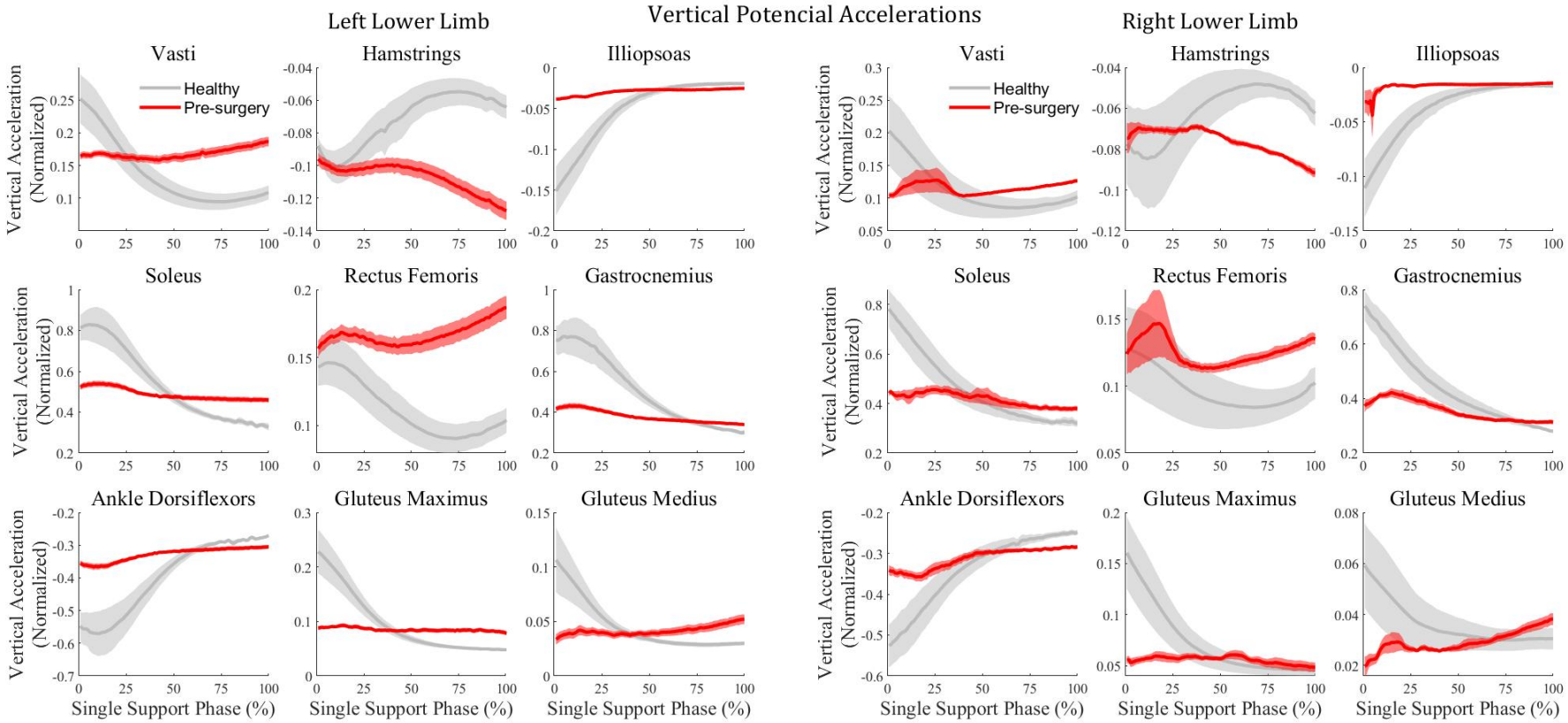

Figure A.6: Potentials of left and right lower-limb muscles to produce vertical COM accelerations. Normalized values calculated by dividing muscle induced accelerations (m/s^2) by the division between total muscle force (N) and subjects mass (kg) [28]. The shaded regions represent the standard error. The vertical scale is not uniform to allow for better visualization of the results.

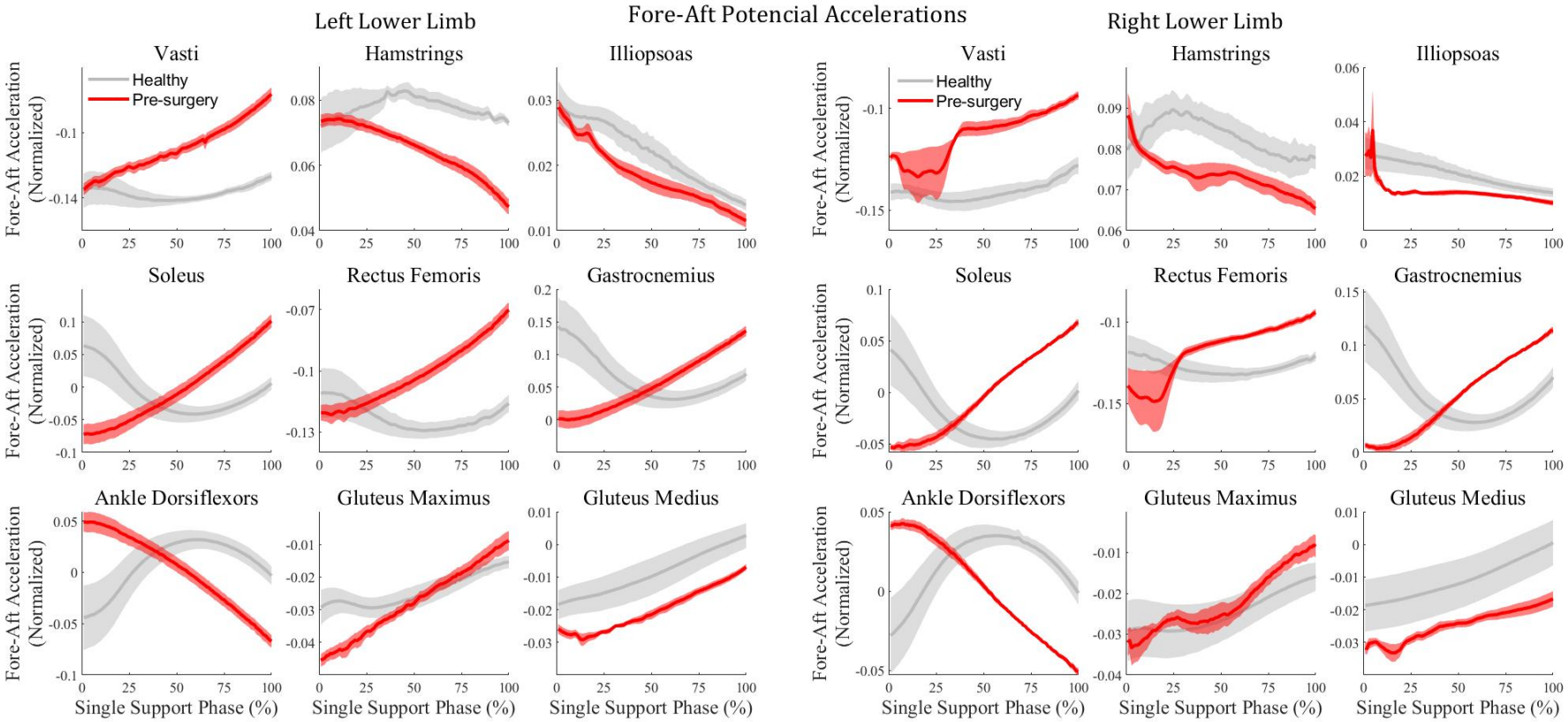

Figure A.7: Potentials of left and right lower-limb muscles to produce fore-aft COM accelerations. Normalized values calculated by dividing muscle induced accelerations (m/s^2) by the division between total muscle force (N) and subjects mass (kg) [28]. The shaded regions represent the standard error. The vertical scale is not uniform to allow for better visualization of the results.

2023

USING MUSCULOSKELETAL MODELING TO ASSESS MUSCLE FUNCTION AND GAIT ASYMMETRY AFTER A STRAYER PROCEDURE APPLIED TO A CHILD WITH CEREBRAL PALSY

Luís Cunha

NOVA SCHOOL OF
SCIENCE & TECHNOLOGY